

INTRODUCTION TO PERTURBATIVE QCD*

P. NASON

INFN, Milan, Italy

Abstract

In this lecture notes I give an introduction to perturbative QCD, that should address both theoretical and experimental physics students. I illustrate the basic features of the theory, by discussing few examples in e^+e^- physics, deep-inelastic scattering, and hard production phenomena in hadron collisions.

Contents

1	STRONG INTERACTIONS	2
2	MOTIVATIONS FOR QCD	2
2.1	Hadron Spectrum	2
2.2	Scaling	4
2.3	The QCD Lagrangian	5
2.4	Symmetries	8
2.5	Summary	9
3	AN ILLUSTRATION OF ASYMPTOTIC FREEDOM	10
3.1	Renormalization group and asymptotic freedom	12
3.2	Relation among the couplings with different number of light flavours	15
3.3	State of the art in the beta function and R	16
4	JETS IN e^+e^- ANNIHILATION	18
4.1	Sterman–Weinberg jets	22
4.2	A comparison with QED	24
4.3	Shower Monte Carlo programs	24
4.4	More jet definitions and shape variables	24
4.5	Thrust as an example	26
5	PROCESSES WITH HADRONS IN THE INITIAL STATE	30
5.1	The naive parton model formula	32
5.2	Does the Parton Model survive radiative corrections?	35
5.3	Derivation of the singular part of the cross section	36
5.4	Effects due to the emission of a collinear gluon	38
5.5	Failure of the parton model	39
5.6	The evolution equations in the general case	41
5.7	Sum rules	42

Lecture notes for the XI Jorge André Swieca Summer School, Particles and Fields, January 14-27 2001, Campos do Jordão, SP, Brazil. This notes are an updated and revised version of the lecture notes for the 1997 European School of High-Energy Physics, 25 May - 7 Jun 1997, Menstrup, Denmark, report CERN-98-03”

5.8	Scheme dependence	43
5.9	Summary	43
5.10	How solid is the Factorization Theorem?	44
6	DEEP INELASTIC SCATTERING	44
7	QCD IN HADRONIC COLLISIONS	48
7.1	The kinematic variables for hadronic collisions	49
7.2	Total cross section	50
7.3	Typical inelastic processes	50
7.4	Looking for hard processes in hadronic collisions	50
7.5	Jets at Hadron Colliders	50
7.6	Production of W , Z , and Drell-Yan pairs	55
7.7	Heavy Flavour production	56
8	CONCLUSIONS	56

1 STRONG INTERACTIONS

Strong interactions are characterized at moderate energies by the presence of a single dimensionful scale, of the order of few hundred MeV, a scale that we will call in the following Λ_S . No hint to the presence of a small parameter, in which to develop a perturbative expansion, is present in the strong interaction world. Thus, typical cross sections are of the order of 10 millibarns (corresponding roughly to $1/\Lambda_S^2$), the width of hadronic resonances is of order Λ_S , and the size of a baryon is typically of the order of $1/\Lambda_S$. This is very much different from the case of electromagnetism and of weak interaction, where all reactions can be viewed as originating from a weakly coupled point-like vertex, the fermion–fermion–photon vertex in electrodynamics, and the four fermion vertex in weak interactions. The development of a model of strong interactions has therefore followed a rather intricate path. Aside from what can be inferred from symmetry properties, S-Matrix models were developed in the 60’s, since the general feeling prevailed that it was impossible to describe strong interactions using a field theoretical framework similar to the one used for QED. Dual models, which eventually gave origin to string theories, were discovered precisely in this context, but failed to give a consistent explanation of strong interaction dynamics.

2 MOTIVATIONS FOR QCD

Today we have a satisfactory model of the strong interaction, which is given in terms of a non–Abelian gauge theory. The main motivations for this model are essentially the following.

2.1 Hadron Spectrum

The hadron spectrum can be completely classified from the following assumptions

1. Hadrons are made up of spin $\frac{1}{2}$ quarks. The charge and masses of the known quarks are given in table 1. One usually refers to u , d , s , c , b and t as “flavours”, and commonly refers to u , d and s as the light flavours, and c , b and t as heavy flavours.
2. Each quark flavour comes in 3 colours. Thus, quark fields are spinors, and carry a flavour and a colour index: $\psi_{i \leftarrow \text{colour}}^{(f) \leftarrow \text{flavour}}$.
3. The SU(3) symmetry acting on colour is an exact symmetry.

Electric Charge = $\frac{2}{3}e$ $m =$	up few MeV	charm ≈ 1.5 GeV	top ≈ 170 GeV
Electric Charge = $-\frac{1}{3}e$ $m =$	down few MeV	strange few hundred MeV	bottom ≈ 5 GeV

Table 1: Known quarks

4. Observable hadrons are neutral in colour, in the sense that they are colour singlets under the SU(3) colour group (“singlet” means invariant under the action of the group).

The SU(3) group is the group of 3×3 complex unitary matrices U with unit determinant

$$U^\dagger U = 1, \quad \det U = 1, \quad (1)$$

that act on the quark fields according to

$$\psi_i \rightarrow \sum_k U_{ik} \psi_k. \quad (2)$$

Invariants can be easily formed out of quark–antiquark states

$$\sum_i \psi_i^* \psi_i \rightarrow \sum_{ijk} U_{ij}^* \psi_j^* U_{ik} \psi_k = \sum_{kj} \left(\sum_i U_{ji}^\dagger U_{ik} \right) \psi_j^* \psi_k = \sum_k \psi_k^* \psi_k, \quad (3)$$

which gives us the possibility of forming integer spin color singlet states with a quark and an antiquark. We can form colour singlet also from three-quark states

$$\sum_{ijk} \epsilon^{ijk} \psi_i \psi_j \psi_k \rightarrow \sum_{ijk, i'j'k'} \epsilon^{ijk} U_{ii'} U_{jj'} U_{kk'} \psi_{i'} \psi_{j'} \psi_{k'} = \sum_{i'j'k'} \epsilon^{i'j'k'} \psi_{i'} \psi_{j'} \psi_{k'} \quad (4)$$

where the last equality is a consequence of the identity

$$\sum_{ijk} \epsilon^{ijk} U_{ii'} U_{jj'} U_{kk'} = \det U \epsilon^{i'j'k'} \quad (5)$$

and $\det U = 1$ for SU(3) matrices. Therefore we have the possibility of forming colour neutral, spin 1/2 hadrons out of three quarks. The most important hadron multiplets are displayed in fig. 1. Multiplets are classified according their spin, and their transformation properties under the flavour group. Each multiplet contains particles with similar properties. Observe that we need colour if we want a particle like the Δ^{++} , which is made of three up quark with the same flavours and same spin, to have similar properties to the Σ^0 , which has three different flavours. In fact, if we didn't have colour, because of the Pauli principle, the spatial wave function of the Δ^{++} should be antisymmetric, while that of the Σ^0 could very well be symmetric. With colour, instead, the colour wave-function itself is antisymmetric, and so there is no problem to have the particle of the multiplet all in a symmetric spin, flavour, and spatial wave-function.

It can be shown that in order to form an SU(3) singlet in a system with n_q quarks and $n_{\bar{q}}$ antiquark, we have the constraint

$$n_q - n_{\bar{q}} = n \times 3 \quad (6)$$

with n integer. It is a simple exercise to show that because of this condition observable hadrons must have integer charges.

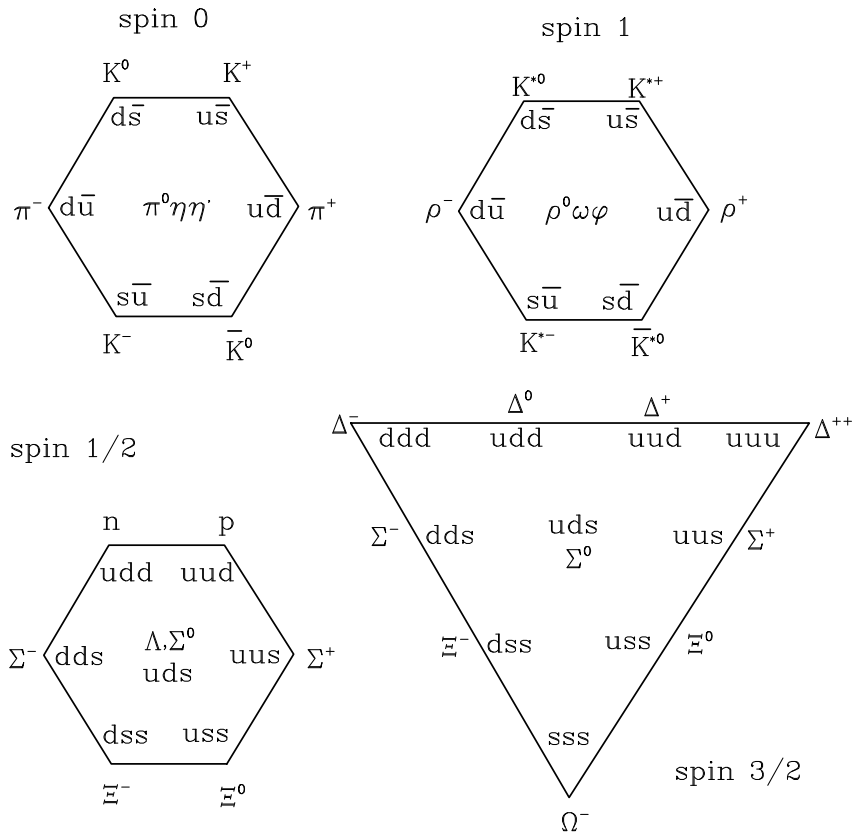


Fig. 1: Hadron spectrum.

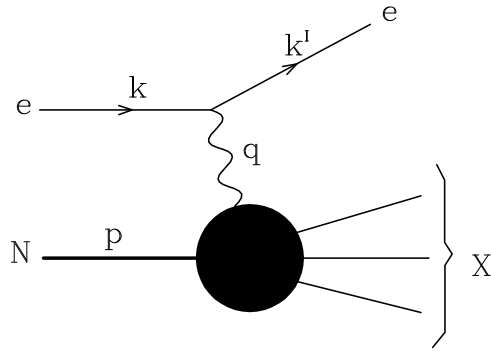


Fig. 2: Deep inelastic scattering.

2.2 Scaling

Scaling was first observed in deep inelastic scattering experiments at SLAC (Stanford Linear Accelerator Center, Stanford, California), around 1968. The deep inelastic scattering process, depicted in fig. 2, is the collision of a lepton (an electron in the SLAC case) with a nucleon target, which fragments into a high multiplicity, massive final state. The scattering process kinematics can be defined by the following dimensionless variables

$$x_{Bj} = \frac{Q^2}{2p \cdot q} \quad y = \frac{q \cdot p}{k \cdot p}. \quad (7)$$

where $Q^2 = -q^2$. The value $x_{\text{Bj}} = 1$ corresponds to elastic scattering. In fact

$$M_X^2 = (q + p)^2 = -Q^2 + m_p^2 + 2\nu = 2\nu(1 - x_{\text{Bj}}) + m_p^2. \quad (8)$$

Scaling means that the differential cross section, when expressed in terms of these dimensionless parameters, in the limit of high energy with x and y fixed, scales like the energy in the process, according to its canonical dimension

$$\frac{d\sigma}{dx dy} \propto \frac{1}{Q^2}. \quad (9)$$

This property is quite remarkable, since the right hand side does not depend upon Λ_S , like most moderate energy cross sections, and it looks more like the behaviour one may find in a renormalizable field theory with a dimensionless coupling, like electrodynamics. Even more spectacular scaling phenomena are observed in e^+e^- annihilation, where the total hadron production cross section becomes proportional to the muon pair cross section at high energies.

The discovery of scaling phenomena in deep inelastic scattering and in e^+e^- annihilation, has given a strong evidence that if a field theory was to describe strong interactions, it had to be weakly coupled at high energies, that is to say, it had to be ‘‘asymptotically free’’. The only known asymptotically free four-dimensional field theories are the non-Abelian gauge theories. It becomes therefore natural to attempt to describe the hadronic forces by using an $SU(3)$ non-Abelian gauge theory, coupled to the colour quantum number. This is also hinted by the fact that the condition of colour neutrality of the hadron spectrum must have a dynamical origin.

2.3 The QCD Lagrangian

The QCD Lagrangian reads

$$\begin{aligned} \mathcal{L} &= -\frac{1}{4}F_a^{\mu\nu}F_{\mu\nu}^a + \sum_f \bar{\psi}_i^{(f)} ((i\not{\partial} - m_f)\delta_{ij} - g_s t_{ij}^a A_a) \psi_j^{(f)} \\ F_{\mu\nu}^a &= \partial_\mu A_\nu^a - \partial_\nu A_\mu^a - g_s \sum_{b,c} f_{abc} A_\mu^b A_\nu^c. \end{aligned} \quad (10)$$

Sum over repeated Lorentz and colour indices is always assumed. The sum over different flavours is explicitly indicated. The symbols t_{ij}^a are the $SU(3)$ generators and the f_{abc} are the structure constant of the $SU(3)$ algebra. The matrices t^a form a complete basis of traceless 3×3 matrices. There are 8 such matrices, and therefore there are 8 gluons. The basis is chosen in such a way that

$$\text{Tr} \left(t^a t^b \right) = \frac{1}{2} \delta^{ab} \quad (11)$$

The symbols f are then defined by (square brackets indicate the commutator)

$$[t^a, t^b] = i f^{abc} t^c \quad (12)$$

I also give the important property (which follows from completeness, tracelessness and relation (11))

$$\sum_a t_{ij}^a t_{kl}^a = \frac{1}{2} \left(\delta_{il} \delta_{kj} - \frac{1}{3} \delta_{ij} \delta_{kl} \right). \quad (13)$$

Equation 13 is all we need to compute colour factors for feynman graphs.

The colour structure of the Lagrangian may seem complicated at first sight. One simple way to look at it, is to think of quarks as objects having 3 colour states. The gluon can be thought as carrying the combination of a colour and an anticolour, except that out of the nine possible combinations the ‘‘neutral’’ one, formed by the sum of all equal colour-anticolour pairs is subtracted away. Figure 3 shows how to

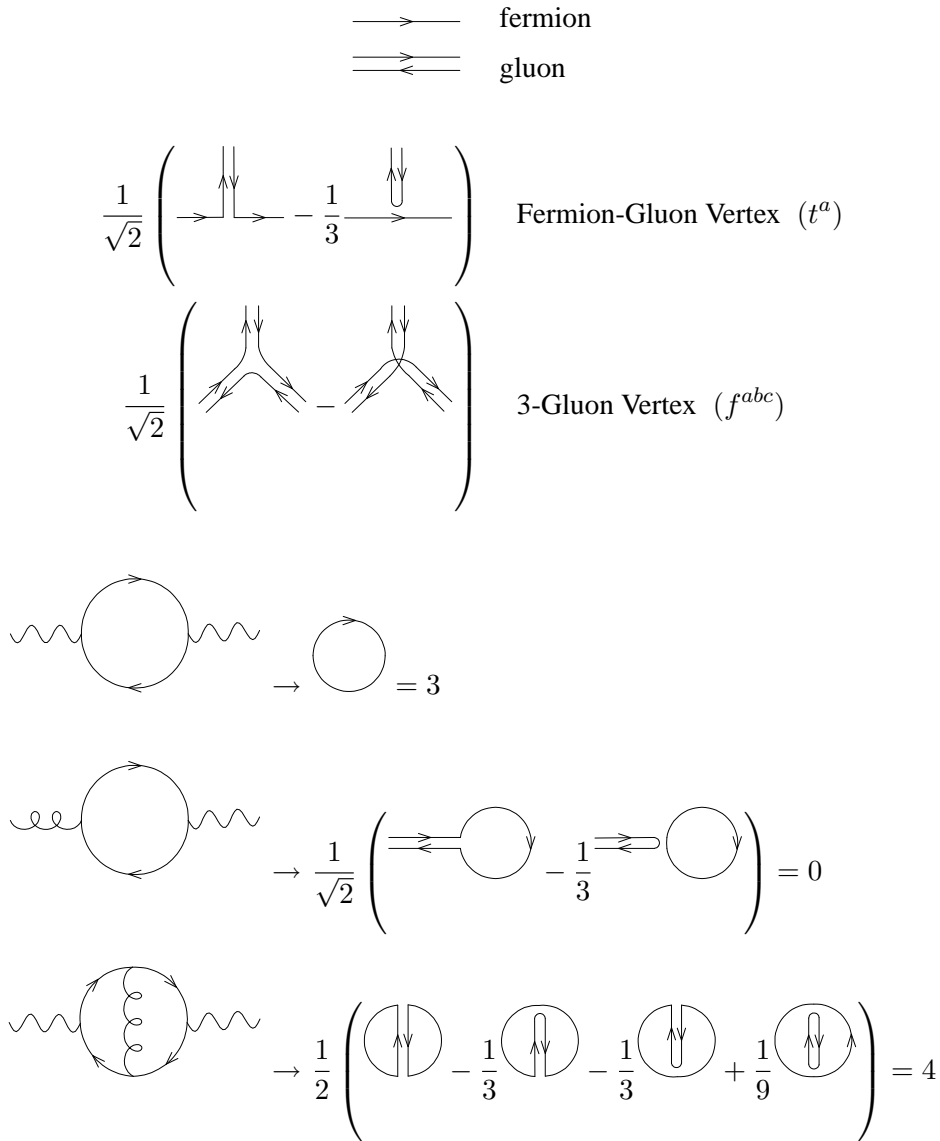


Fig. 3: Colour Feynman rules for QCD

compute colour factors by using this intuitive point of view. The Feynman rules for the QCD Lagrangian are given in fig. 4.

The QCD Lagrangian is very similar to the QED Lagrangian. The Feynman rules are also very similar. The most apparent difference is due to the fact that the fermions carry a new quantum number, the color (the indices $i, j = 1, 2, 3$ in eq. (10)). Also the gluons carry a colour related quantum number. Unlike the case of QED, therefore, the gluons are charged, and can emit other gluons.

As in the case of electrodynamics, one defines the strong coupling constant

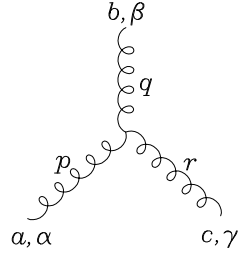
$$\alpha_S = \frac{g_S^2}{4\pi}. \tag{14}$$

As we shall see in the following, this coupling constant has a strength that depends upon the energy scale

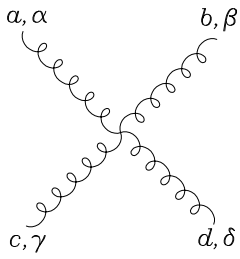
$$a, \alpha \text{---} \overset{p}{\text{---}} \text{---} b, \beta = \delta^{ab} \left[-g^{\alpha\beta} + (1-\lambda) \frac{p^\alpha p^\beta}{p^2 + i\epsilon} \right] \frac{i}{p^2 + i\epsilon}$$

$$a \text{---} \overset{p}{\text{---}} \text{---} b = \delta^{ab} \frac{i}{p^2 + i\epsilon}$$

$$i, n \xrightarrow{p} k, m = \delta^{ik} \frac{i}{\not{p} - m + i\epsilon} \Big|_{mn}$$



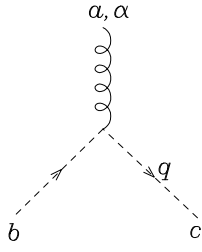
$$a, \alpha \quad b, \beta \quad c, \gamma = -g_s f^{abc} \left[g^{\alpha\beta} (p - q)^\gamma + g^{\beta\gamma} (q - r)^\alpha + g^{\gamma\alpha} (r - p)^\beta \right]$$



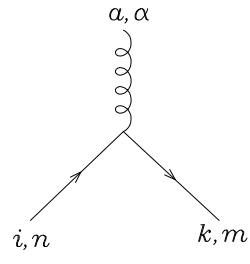
$$a, \alpha \quad b, \beta \quad c, \gamma \quad d, \delta = -ig_s^2 f^{xac} f^{xbd} (g^{\alpha\beta} g^{\gamma\delta} - g^{\alpha\delta} g^{\beta\gamma})$$

$$-ig_s^2 f^{xad} f^{xbc} (g^{\alpha\beta} g^{\gamma\delta} - g^{\alpha\gamma} g^{\beta\delta})$$

$$-ig_s^2 f^{xab} f^{xcd} (g^{\alpha\gamma} g^{\beta\delta} - g^{\alpha\delta} g^{\beta\gamma})$$



$$b \quad c = g_s f^{abc} q^\alpha$$



$$i, n \quad k, m = -ig_s t_{ki}^a \gamma_{mn}^\alpha$$

7
Fig. 4: Feynman rules for QCD

μ of the process in which enters. In leading order

$$\alpha_s = \frac{1}{b_0 \log \frac{\mu^2}{\Lambda^2}} \quad (15)$$

where

$$b_0 = \frac{11 C_A - 4 T_F n_f}{12\pi}. \quad (16)$$

where $T_F = 1/2$ and $C_A = N$ for SU(N) (3 for SU(3)) and n_f is the number of flavours. Thus Λ is the parameter that characterizes the QCD coupling constant.

2.4 Symmetries

We know that the strong interaction world has a very good symmetry property, the isospin symmetry. Particles in the same isospin multiplet, like the proton and the neutron, or the charged and neutral pions, have nearly the same mass. Furthermore, the Wigner-Eckart theorem can be used to relate decay and scattering processes which are connected by isospin transformations. This symmetry properties must be present in some way in the fundamental QCD Lagrangian, whose fermionic sector is given by

$$\mathcal{L}_F = \sum_{f,i,j} \bar{\psi}_i^{(f)} ((i\not{\partial} - m_f)\delta_{ij} - gt_{ij}^a A_a) \psi_j^{(f)}. \quad (17)$$

An isospin transformation acts on the quark field as a unitary matrix

$$\psi^{(f)} \rightarrow \sum_{f'} U^{ff'} \psi^{(f')} \quad (18)$$

where f and f' are restricted to the up and down flavours, and U is a unitary two dimensional matrix. By a simple exercise, one can verify that, in order for the fermionic Lagrangian to be invariant under the isospin transformation, we must have either $m_u = m_d$ or $m_u, m_d \rightarrow 0$. The distinction of the two possibilities is a physical one. It can be phrased as follows: if the up and down masses are of the order of the QCD scale Λ or larger, then they must be nearly equal in order for the isospin symmetry to work. Alternatively, the up and down masses must be much smaller than Λ . The first possibility is not very appealing from a theoretical point of view. From what we know from the theory of weak interactions, particles belonging to different families have different masses. It would be very hard to justify the fact that two quark flavours have equal masses while all the others are very different. In fact, there is a large body of evidence that favours the second possibility, that is to say, that the up and down quark masses are very small. This fact has a few remarkable consequences, due to the fact that, for small masses, the QCD fermionic Lagrangian has a much larger symmetry than isospin alone. In order to see this fact, let us define left and right-handed field components

$$\psi_L = \frac{1}{2}(1 - \gamma_5)\psi, \quad \psi_R = \frac{1}{2}(1 + \gamma_5)\psi \quad (19)$$

and substituting $\psi = \psi_L + \psi_R$ in the fermionic Lagrangian we have (suppressing colour indices)

$$\begin{aligned} \mathcal{L}_F = & \sum_f \left\{ \bar{\psi}_L^{(f)} (\not{\partial} - gt^a A_a) \psi_L^{(f)} + \bar{\psi}_R^{(f)} (\not{\partial} - gt^a A_a) \psi_R^{(f)} \right\} \\ & - \sum_f m_f \left(\bar{\psi}_R^{(f)} \psi_L^{(f)} + \bar{\psi}_L^{(f)} \psi_R^{(f)} \right). \end{aligned} \quad (20)$$

Terms that mix left and right components in the kinetic energy, and terms diagonal in the left and right component of the mass terms are absent because of the following elementary identities

$$\psi_L = \frac{1}{2}(1 - \gamma_5) \psi \quad \psi_R = \frac{1}{2}(1 + \gamma_5) \psi \quad (21)$$

$$\bar{\psi}_L = \bar{\psi} \frac{1}{2}(1 + \gamma_5) \quad \bar{\psi}_R = \bar{\psi} \frac{1}{2}(1 - \gamma_5) \quad (22)$$

and from the fact that γ_5 anticommutes with γ_μ . If we could neglect the fermion masses the Lagrangian would have the large symmetry

$$SU_L(N) \times SU_R(N) \times U_L(1) \times U_R(1) \quad (23)$$

where N is the number of flavours. In fact, the transformation

$$\begin{aligned} \psi_L^{(f)} &\rightarrow e^{i\phi_L} \sum_{f'} U_L^{ff'} \psi_L^{(f')} \\ \psi_R^{(f)} &\rightarrow e^{i\phi_R} \sum_{f'} U_R^{ff'} \psi_L^{(f')} \end{aligned} \quad (24)$$

where U_L and U_R are (independent) matrices of $SU(N)$, leaves the Lagrangian invariant. The phase factors constitute the two $U(1)$ groups. The isospin symmetry group is a subgroup of the above, also called the vector subgroup, characterized by equal transformation matrices for the left and right components. Besides the isospin transformations, there are other independent symmetry transformations, in which the left and right-handed component transform with matrices that are the inverse of each other. These are called axial transformations (they do not form a subgroup by themselves). In the following, I will only state what happens of all these symmetries, without giving detailed explanations

- The vector $SU(N)$ subgroup is realized in the spectrum. It is the observed isospin symmetry. The $U(1)$ vector subgroup is a phase symmetry related to baryon number conservation.
- The axial $U(1)$ symmetry does not survive quantization, because of the so-called triangle anomaly. This symmetry is simply not there in the full theory.
- The remaining axial transformations are broken symmetries. The Goldstone bosons of these broken symmetries are the pion fields.

Goldstone bosons are massless particles, while the pions are not. This is a consequence of the fact that the axial symmetries are only approximate, due to the fact that the quark masses are not strictly zero.

Thus, by assuming that the up and down quark masses are small, we explain the presence of isospin symmetry, as well as the lightness of the pions. Other dynamical predictions follow, like relations among the low energy scattering properties of the pions and the pion decay constant. The interested reader can find many good references where to study this subject [1, 2, 3].

2.5 Summary

In summary, by accepting QCD as the fundamental theory of strong interactions we can

- Explain the low energy symmetry properties, and give a justification of the observed spectrum.
- Explain scaling phenomena at high energies.
- Leave Weak interactions in peace. The QCD colour group commutes with the electroweak group $SU(2) \times U(1)$. Since the electroweak interactions are less symmetric (they break parity and CP), this guarantees that there is no mixing between electroweak and strong interactions that enhances the parity-violating effects (giving rise, for example, to parity violating interactions of size $\alpha_{ew}\alpha_S$ instead of α_{ew}/M_W^2) or flavour changing neutral current effects.
- Give a description of the hadronic forces which is similar to electroweak forces, thus opening the possibility of a uniform description of the forces in nature in terms of gauge theories (unification).

There are two common points of view among physicists, with regard to QCD.

Many believe that QCD is an extremely well established theory, much better established than the Electro-Weak theory. In fact, the Lagrangian is fully specified in term of a single parameter. Remember, in fact, that quark masses have electroweak origin, and are related to the Yukawa coupling and to the electroweak symmetry breaking. In Electroweak theories, on the other hand, we have lots of parameters and quite a few alternatives are possible for the symmetry breaking sector.

Others believe that Electro-Weak theories are much better established. In fact, we can compute every accessible phenomenon we like with great accuracy, and seek accurate comparisons with experimental results. On the other hand, in QCD, we are unable to explain rigorously even basic phenomena like colour confinement, and perturbative calculations rely upon unproven assumptions.

The first point of view can be stated by simply saying that QCD must be right because we cannot think of anything else that is even plausible as a theory of strong interaction. The second point of view is more humble, and assumes that in order to establish a physical theory one must make testable predictions, and compare them with experiments.

Thus, we find that essentially no viable alternative to QCD have been formulated so far, and yet there is a huge ongoing effort in theoretical and experimental physics aimed at testing the predictions of QCD.

At low energy, QCD is a strongly interacting theory. Besides the phenomenological results that follow from its symmetry properties, the only known way to perform calculations in this regime is by computer simulation of QCD on a lattice, that is to say on a finite and discretized model of space-time. This approach is bound to improve as time goes by, since people become more and more clever, and computers become more and more powerful.

At high energy, in many cases, standard perturbative methods can be applied. In these lectures I will deal mostly with the perturbative applications of QCD. We will see that, even at high energy, the application of perturbative techniques is not straightforward. In fact, we will be able to perform calculations only when the long distance (low energy) part of the process we examine has no or little influence upon the quantity we want to compute. In the following, I will illustrate the basics of perturbative QCD by examining the process of hadrons production via the annihilation of an e^+e^- pair at high energy. This process is particularly simple, since no strongly interacting particles appear in the initial state.

3 AN ILLUSTRATION OF ASYMPTOTIC FREEDOM

We will now introduce the basic features of QCD via the simplest process in which it can be applied, that is to say the production of hadrons in e^+e^- annihilation. By studying this process we will illustrate the remarkable property of asymptotic freedom, and its physical implications.

We are considering the process depicted in fig. 5. The production of hadrons takes place via the

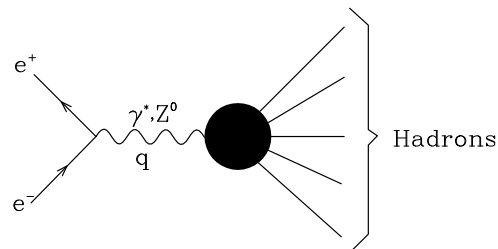


Fig. 5: Electron-positron annihilation into hadrons.

production of a virtual photon, or of a real or virtual Z boson. From the point of view of QCD, the

decay of a virtual photon, or of a W or Z boson, are very similar, and in fact strong corrections to these processes are given by essentially the same formulae. For simplicity, however, we can always think about the decay of a virtual photon. We will begin by attempting to compute the total cross section for the decay of a virtual photon, with a virtuality (q^2) much larger than typical hadronic scales. Our attempt will be extremely crude. We will simply use the QCD Lagrangian and the corresponding Feynman rules, and try to compute the cross section order by order in the strong coupling constant. The prediction at zeroth order in the strong coupling comes simply from diagram a of fig. 6. It is usually expressed in

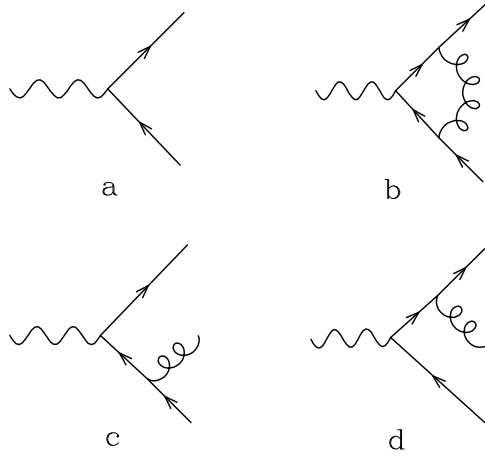


Fig. 6: Diagrams for the QCD calculation of $R(e^+e^- \rightarrow \text{Had.})$ up to the order α_s .

terms of the ratio of the hadronic cross section divided by the cross section for the production of a $\mu^+\mu^-$ pair. It is given by

$$R_0 = \frac{\sigma(\gamma^* \rightarrow \text{hadrons})}{\sigma(\gamma^* \rightarrow \mu^+\mu^-)} = 3 \sum_f c_f^2 \quad (25)$$

where f runs over the quark flavour species, and c_f is the electric charge of the quark of flavour f in units of the electron charge. The factor of 3 accounts for the fact that there are three colours for each quark. The sum extends to all the flavours that can be produced at the given energy. The formula is valid in all cases when we can neglect quark masses. Near the threshold for heavy quark production one must include a correction factor, which in the general case of a vector boson decay, yields

$$R_0 = 3 \sum_f \sqrt{1 - \frac{4m_f^2}{s}} \left(1 + \frac{2m_f^2}{s}\right) c_f^2 \quad (26)$$

Corrections of order α_s to R can be computed in a straightforward way. The relevant contributions come from the interference of the virtual diagram b with diagram a , plus the square of the real emission graphs $c + d$. There are also diagrams with self-energy on the fermion lines, not shown in the figure, that should be included with the appropriate weight. The result turns out to be completely finite. All ultraviolet divergences that arise in intermediate steps of the calculation cancel among each other. This is a consequence of the fact that the electromagnetic current is a conserved current, and therefore it is not renormalized by strong interactions. Other kind of singularities arise in intermediate steps of the calculation, namely soft and collinear singularities. They all cancel in the total. Their meaning will be discussed further on. The corrected value of R becomes

$$R = R_0 \left(1 + \frac{\alpha_s}{\pi}\right). \quad (27)$$

If we go on, and compute the corrections of order α_s^2 something new happens. We find ultraviolet divergences that do not cancel, and the result is

$$R = R_0 \left(1 + \frac{\alpha_s}{\pi} + \left[c + \pi b_0 \log \frac{M^2}{Q^2} \right] \left(\frac{\alpha_s}{\pi} \right)^2 \right) \quad (28)$$

where M is the ultraviolet cutoff (for those who are familiar with dimensional regularization, the cutoff scale in $d = 4 - 2\epsilon$ dimensions is $M = \mu \exp \frac{1}{\epsilon}$), and

$$b_0 = \frac{33 - 2n_f}{12\pi} \quad (29)$$

and n_f is the number of light flavours. The divergence is dealt with the usual prescription of renormalization. We define a renormalized charge, function of an arbitrary scale μ ,

$$\alpha_s(\mu) = \alpha_s + b_0 \log \frac{M^2}{\mu^2} \alpha_s^2 \quad (30)$$

and express the result in terms of $\alpha_s(\mu)$ instead of α_s . We obtain then

$$R = R_0 \left(1 + \frac{\alpha_s(\mu)}{\pi} + \left[c + \pi b_0 \log \frac{\mu^2}{Q^2} \right] \left(\frac{\alpha_s(\mu)}{\pi} \right)^2 \right) + \mathcal{O}(\alpha_s(\mu)^3). \quad (31)$$

The formula for R is now finite. The theory of renormalization guarantees that with this procedure we can remove the divergences from all physical quantities. This implies that the one loop divergence of any physical quantity which in lowest order has the value $A\alpha_s^n$ must have the form $nAb_0 \log M^2 \alpha_s^{n+1}$. Observe that, as a consequence of this procedure, we end up expressing our results in terms of a coupling constant which is function of a scale.

3.1 Renormalization group and asymptotic freedom

I will now give a general and abstract description of the renormalization group and asymptotic freedom. From the following discussion it should be clear that the existence of the renormalization group follows from the property of renormalizability of field theory, and that asymptotic freedom is a possible consequence of the renormalization group. I will not give any technical details on the computation of the renormalization group flow (i.e. of the so called β function), which can be found in many good textbooks.

In field theories we encounter ultraviolet divergences, which in renormalizable theories can be removed by a suitable redefinition of the coupling constants and the fields. In the simplest case of a theory characterized by a single coupling constant, renormalizability can be stated in the following way. A physical quantity G will be given in such a theory as a power expansion in the coupling α (which we will assume to be dimensionless), with possibly UV divergent coefficients. We will write:

$$G = G(\alpha, M, s_1 \dots s_n), \quad (32)$$

that is to say, G depends upon the coupling, the ultraviolet cutoff M , and some invariants $s_1 \dots s_n$ constructed out of the momenta and masses involved in the process in question. Renormalizability means that I can define a renormalized coupling α_{ren}

$$\alpha_{\text{ren}} = \alpha + c_1 \alpha^2 + c_2 \alpha^3 + \dots \quad (33)$$

with

$$c_i = c_i(M/\mu) \quad (34)$$

in such a way that

$$G(\alpha, M, s_1 \dots s_n) = \tilde{G}(\alpha_{\text{ren}}, \mu, s_1 \dots s_n). \quad (35)$$

So, the physical quantity can be expressed in term of the renormalized coupling, the finite scale μ and the invariants, in terms of a finite function. In other words, all the divergences have been reabsorbed in the renormalized coupling. The finite scale μ has to be introduced in order for the dimensionless coefficients c_i to depend upon the dimensional quantity M . We will also write

$$\alpha_{\text{ren}} = \alpha_{\text{ren}}(\alpha, M/\mu), \quad \alpha = \alpha(\alpha_{\text{ren}}, M/\mu). \quad (36)$$

and

$$G(\alpha(\alpha_{\text{ren}}, M/\mu), M, s_1 \dots s_n) = \tilde{G}(\alpha_{\text{ren}}, \mu, s_1 \dots s_n). \quad (37)$$

Therefore, renormalizability means that by a redefinition of the coupling of the form (36), eq. (37) holds for all physical quantities. The *same* redefinition of α makes *all* physical quantities independent of the cutoff.

In the redefinition of eq. (36) we are forced to introduce a scale μ . If we change μ and α_{ren} by keeping α and M fixed, the physics remains invariant, because physical quantities, to begin with, are functions of α and M only. Let us study the infinitesimal transformations $d\alpha_{\text{ren}} d\mu^2$ that leave α and M fixed. We must have

$$\frac{\partial \alpha(\alpha_{\text{ren}}, M/\mu)}{\partial \alpha_{\text{ren}}} d\alpha_{\text{ren}} + \frac{\partial \alpha(\alpha_{\text{ren}}, M/\mu)}{\partial \mu^2} d\mu^2 = 0. \quad (38)$$

Since physical quantities remain the same under this change, we must also have

$$\frac{\partial \tilde{G}(\alpha_{\text{ren}}, \mu, p_1 \dots p_n)}{\partial \alpha_{\text{ren}}} d\alpha_{\text{ren}} + \frac{\partial \tilde{G}(\alpha_{\text{ren}}, \mu, p_1 \dots p_n)}{\partial \mu^2} d\mu^2 = 0. \quad (39)$$

From equations (38) and (39) we get

$$\mu^2 \frac{d\alpha_{\text{ren}}}{d\mu^2} = -\frac{\mu^2 \frac{\partial}{\partial \mu^2} \alpha(\alpha_{\text{ren}}, M/\mu)}{\frac{\partial}{\partial \alpha_{\text{ren}}} \alpha(\alpha_{\text{ren}}, M/\mu)} = -\frac{\mu^2 \frac{\partial}{\partial \mu^2} \tilde{G}(\alpha_{\text{ren}}, \mu, s_1 \dots s_n)}{\frac{\partial}{\partial \alpha_{\text{ren}}} \tilde{G}(\alpha_{\text{ren}}, \mu, s_1 \dots s_n)} \quad (40)$$

from which it follows that

$$\mu^2 \frac{d\alpha_{\text{ren}}}{d\mu^2} = \beta(\alpha_{\text{ren}}) \quad (41)$$

where β does not depend upon $s_1 \dots s_n$, M or μ . Observe that β does not depend upon M , because M does not appear on the right hand side of the second equality of (40), it cannot depend upon $s_1 \dots s_n$ because they do not occur on the right hand side of the first equality. Finally, it could only depend upon μ . But μ is dimensionful, while β is obviously dimensionless, and so it cannot even depend upon μ .

Using the expression

$$\alpha(\alpha_{\text{ren}}, M/\mu) = \alpha_{\text{ren}} + c_1(M/\mu)\alpha_{\text{ren}}^2 + \dots \quad (42)$$

we find

$$\beta(\alpha_{\text{ren}}) = \alpha_{\text{ren}}^2 \mu^2 \frac{\partial}{\partial \mu^2} c_1(M/\mu) + \dots \quad (43)$$

Comparing this equation with eq. (30), we immediately get

$$\beta(\alpha_{\text{ren}}) = -b_0 \alpha_{\text{ren}}^2 + \dots \quad (44)$$

and therefore

$$\frac{d}{d \log \mu^2} \alpha_s(\mu) = -b_0 \alpha_{\text{ren}}^2 + \dots \quad (45)$$

which characterizes the evolution of the coupling constant as a function of the scale μ . Equation (45) can be also written, at the lowest relevant order

$$\frac{d}{d \log \mu^2} \frac{1}{\alpha_s(\mu)} = b_0 \quad (46)$$

which can be easily solved to give

$$\frac{1}{\alpha_s(\mu)} = b_0 \log \frac{\mu^2}{\mu_0^2} + \frac{1}{\alpha_s(\mu_0)}. \quad (47)$$

Without loss of generality, the solution can be written

$$\frac{1}{\alpha_s(\mu)} = b_0 \log \frac{\mu^2}{\Lambda^2} \Rightarrow \alpha_s(\mu) = \frac{1}{b_0 \log \mu^2 / \Lambda^2} \quad (48)$$

where Λ plays the role of an integration constant. In QCD, b_0 is positive, and eq. (48) makes sense only for $\mu > \Lambda$. One is tempted to infer that Λ is the value of μ at which the coupling constant becomes infinite. In fact, this identification is superficial. When the coupling constant starts to be large, we can no longer trust the perturbative expansion, and the above equation has been derived only at the lowest order in perturbation theory. It is better therefore to think of Λ as the scale parameter of the theory which defines the value of α_s at large scales. In other words, Λ is defined only through the formula for $\alpha_s(\mu)$, and this formula has a meaning only for large μ .

QED is very similar to QCD in many respects, and one may wonder why we never talk about a Λ_{QED} analogous to the Λ in QCD. In fact, the basic difference between QED and QCD is the value of b_0 . We have

$$b_0^{\text{QED}} = -\frac{4n_f}{12\pi}, \quad (49)$$

a negative value. The expression for the running coupling in QED is then

$$\frac{1}{\alpha_{\text{QED}}(\mu)} = b_0^{\text{QED}} \log \frac{\mu^2}{\Lambda_{\text{QED}}^2}. \quad (50)$$

The expression in eq. (50) makes sense only for $\mu \ll \Lambda$ (so that the right hand side is positive), while the expression in eq. (48) makes sense only if $\mu \gg \Lambda$. In other words, QCD is a weakly coupled theory at high energy, while QED is weakly coupled at low energy. This is the content of the statement that QCD is asymptotically free, while QED is not. The scale at which QED becomes strongly coupled is obtained by solving the equation

$$\frac{1}{\alpha_{\text{QED}}(m_e)} = b_0^{\text{QED}} \log \frac{m_e^2}{\Lambda_{\text{QED}}^2}. \quad (51)$$

which gives

$$\Lambda_{\text{QED}} = m_e \exp \left(-\frac{b_0^{\text{QED}}}{\alpha_{\text{QED}}(m_e)} \right). \quad (52)$$

This formula is valid only if all charged fermions have the same mass, equal to m_e , and the same charge. However, even if one does a more accurate job, the basic result is that Λ_{QED} is an astronomic scale, and this is the reason why we never talk about it. Notice that this fact indicates that QED cannot be a fundamental theory. The existence of a high scale at which the theory becomes strongly coupled makes it impossible to measure the basic vertex of QED at short distance, which is somewhat of a contradiction, since we assume that we know the local Lagrangian of the theory.

We have now discussed the evolution of the coupling constant at the leading order level. The content of the theory of renormalization is much deeper. It states that up to any order in perturbation theory, we can remove all ultraviolet divergences from a physical quantity just by a redefinition of the coupling constant. Furthermore, it states that equation (45) generalizes to all order of perturbation theory, and the right hand side of the equation is free of ultraviolet divergences. In other words

$$\frac{d\alpha_s(\mu)}{d \log \mu^2} = -b_0 \alpha_s^2(\mu) - b_1 \alpha_s^3(\mu) - b_2 \alpha_s^4(\mu) + \dots \quad (53)$$

where b_0, b_1, b_2 , etc., are ultraviolet-finite.

From eq. (30), we see that $\alpha_s = \alpha_s(M)$, that is to say that the original bare α_s was in fact the running coupling evaluated at the cutoff scale. It is not useful to try to express physical quantities in terms of α_s evaluated at a scale which differs widely from the scales involved in the physical quantities under consideration. In fact, in this case, large logarithms of the ratio of the physical scale to μ arise in the perturbative expansion, as one cannot trust the truncated (fixed order) result. In order to get a reliable result, one should instead use $\mu \approx Q$, so that no large logarithms appear in the perturbative expansion. Of course, we do not know the precise value of μ we should use. We can use $\mu = Q, \mu = 2Q, \mu = Q/2$, without the possibility of arguing what is the best choice. In practice, a difference in the value of the scale used makes a difference in the result, but this difference is of the order of the neglected terms in the perturbative expansion. This can be easily verified from formula (31) (students are encouraged to try this).

It is now tempting to formulate the first prediction of our theory. From the expression of the running coupling, eq. (48), we see that the strong coupling constant is of order 1 when the scale μ approaches Λ . It is tempting to set $\Lambda = 300$ MeV, the typical hadronic scale, and then predict that

$$R(M_Z) = R_0(M_Z) \left(1 + \frac{\alpha_s(M_Z)}{\pi} \right) = R_0(M_Z)(1 + 0.046) \quad (54)$$

in reasonable agreement with the value measured at LEP. Of course, this example is very sloppy, does not take into account the heavy flavour thresholds, higher order effects, and other important facts. It is however important to remark that, had we measured $R/R_0 = 1 + 0.08$ at LEP, this would have implied $\Lambda = 5$ GeV, a totally unacceptable value.

3.2 Relation among the couplings with different number of light flavours

Now I will spend a few words concerning the number of light flavours. In order to make the discussion clearer, let us assume that there is a top quark of 100 GeV, and that all the other quarks are massless. Intuitively, we should then be able to describe the effects of QCD, for scales much below 100 GeV, but still much above Λ , in a perturbative fashion, forgetting about the existence of the top quark. The formula for $e^+e^- \rightarrow$ hadrons contains then b_0 evaluated with $n_f = 5$. On the other hand, if the heavy top is really there, the true description of our phenomenon should be given in terms of the theory with top. While up to the order α_s a top loop never enters our Feynman graphs, at two loops we do have a top loop contribution, represented in the graphs of fig. 7. In spite of the fact that there is not enough energy

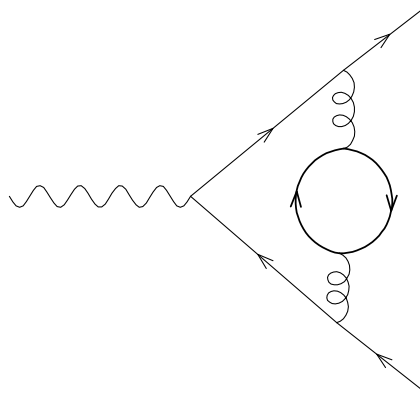


Fig. 7: Top loop contribution to $e^+e^- \rightarrow$ hadrons.

to produce the top, these graphs do contribute. They are always associated to a propagator correction.

Neglecting terms suppressed by powers of $1/m_t^2$, their effect is simply to multiply α_s by a factor $1 - \alpha_s/(6\pi)(d + \log(M^2/m_t^2))$, where d is a number which depends upon the particular renormalization scheme one uses. This result can also be guessed on the basis of the fact that the UV divergence coming from the top loop must have the same form as the UV divergence coming from any light fermion. We have then

$$R = R_0 \left(1 + \frac{\alpha'_s}{\pi} + \left[c + \pi b_0 \log \frac{M^2}{Q^2} - \frac{1}{6} \left(d + \log \frac{M^2}{m_t^2} \right) \right] \left(\frac{\alpha'_s}{\pi} \right)^2 \right). \quad (55)$$

With α'_s we indicated the true (bare) coupling, of the theory in which the heavy quark is taken into account properly, instead of the “fake” theory in which the heavy quark is ignored. The renormalization procedure for the theory including the top requires now the substitution

$$\alpha'_s(\mu) = \alpha'_s + b'_0 \log \frac{M^2}{\mu^2} \alpha_s'^2 \quad (56)$$

where $b'_0 = (33 - 2(n_f + 1))/(12\pi)$, and the renormalized formula for R becomes

$$R = R_0 \left(1 + \frac{\alpha'_s(\mu)}{\pi} + \left[c + \pi b_0 \log \frac{\mu^2}{Q^2} - \frac{1}{6} \left(d + \log \frac{\mu^2}{m_t^2} \right) \right] \left(\frac{\alpha'_s(\mu)}{\pi} \right)^2 \right) + \mathcal{O}(\alpha_s(\mu)^3). \quad (57)$$

Equation (31) and (57) must be completely equivalent, at least up the order α_s^2 . It turns out that in the commonly used $\overline{\text{MS}}$ renormalization scheme, we have $d = 0$. In this scheme, the equivalence of the two formulas imply that

$$\alpha_s(\mu) = \alpha'_s(\mu) \quad \text{for } \mu = m_t. \quad (58)$$

Therefore, in the $\overline{\text{MS}}$ scheme the relation between coupling constants defined by ignoring a heavy flavour, and the coupling with the heavy flavour included, is simply stated by saying that the two running couplings should coincide for $\mu = m_h$, where m_h is the mass of the heavy flavour. In practice, we have three useful definitions of the coupling constants. One that ignores the charm quark (and heavier flavours), which has three light flavours, and may be indicated with $\alpha_s^{(3)}$, one that ignores bottom ($\alpha_s^{(4)}$) and one that ignores top ($\alpha_s^{(5)}$).

A plot of the ratios of $\alpha_s^{(3)}/\alpha_s^{(5)}$ and $\alpha_s^{(4)}/\alpha_s^{(5)}$ is given in fig. 8. The couplings are correctly matched at the heavy flavour thresholds according to the $\overline{\text{MS}}$ prescription. From the plot, it appears that the couplings for four and five flavours are not very different. This is indeed the case. One should however be careful, because the corresponding value of Λ is in fact very different. The values used in the figure have $\Lambda_3 = 310 \text{ MeV}$, $\Lambda_4 = 260 \text{ MeV}$ and $\Lambda_5 = 170 \text{ MeV}$. A common error is, for example, to use values of Λ_4 where Λ_5 should be used. One should never forget that Λ is nothing but a parameter in the formula for α_s . If we change the formula (going for example from one to two loops) the value of Λ should be changed. Similarly, if we plug in the same value of Λ in the expression for $\alpha_s^{(3)}$ and $\alpha_s^{(4)}$, their value would be very different, even for $\mu = m_b$, while if we use the appropriate value of Λ_3 and Λ_4 in the corresponding formulas, their value will be identical at that scale.

3.3 State of the art in the beta function and R

The expression of the beta function known today has the form

$$\frac{\partial \alpha_s}{\partial \log \mu^2} = -b_0 \alpha_s^2 - b_1 \alpha_s^3 - b_2 \alpha_s^4 - b_3 \alpha_s^5 \quad (59)$$

where the term b_2 has been computed in ref. [4], and the term b_3 has been very recently computed in ref. [5]. Here I report below only the values of b_0 and b_1 , and the corresponding solution of the renor-

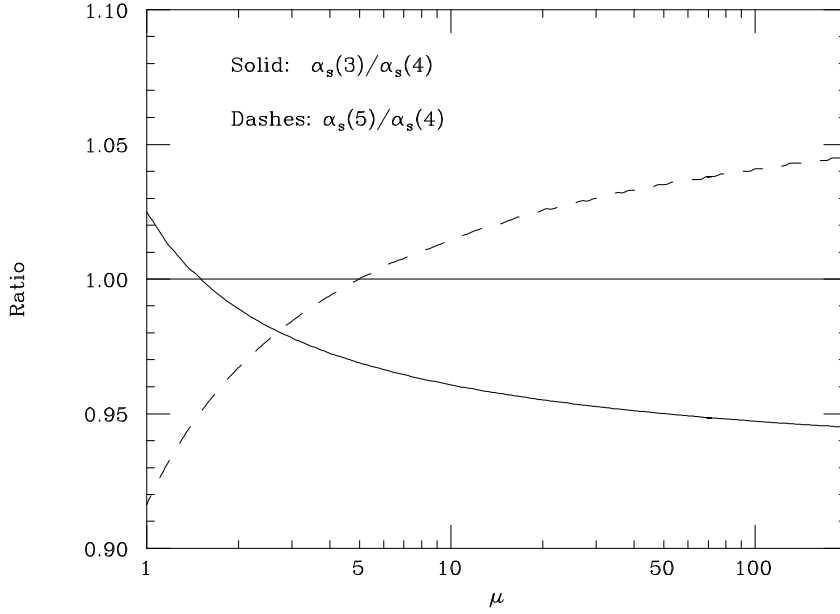


Fig. 8: Ratios of the coupling defined for different values of n_f .

malization group equation at the two loop level. This is what is commonly used in most applications.

$$\alpha_s^{(n_f)}(\mu) = \frac{1}{b_0 \log \frac{\mu}{\Lambda_{n_f}}} \left[1 - \frac{b_1}{b_0^2} \frac{\log \log \frac{\mu^2}{\Lambda_5^2}}{\log \frac{\mu^2}{\Lambda_5^2}} \right] \quad (60)$$

$$b_0 = \frac{33 - 2n_f}{12\pi} \quad (61)$$

$$b_1 = \frac{153 - 19n_f}{24\pi^2}. \quad (62)$$

The reader can verify that the eq. (60) satisfies equation (59) up to terms of order α_s^3 .

The accuracy of the β function that is required in phenomenological applications depends upon the accuracy of the calculations one is using. The rule of thumb is the following:

- if only the leading strong interaction effect is included (LO calculation), one needs one-loop evolution;
- if terms subleading by one power of α_s are included (NLO calculation), one needs two-loop evolution;
- if terms subleading by two powers of α_s are included (NNLO), one needs two-loop evolution;
- ...

Thus, for example, if we use the $\mathcal{O}(\alpha_s)$ formula for R , that is to say $R = R_0(1 + \alpha_s/\pi)$, we need to include 1-loop evolution. Similarly, if we have a process that starts at order α_s^2 (like four-jet production in e^+e^- annihilation), we need 1-loop evolution. If we include the $\mathcal{O}(\alpha_s^2)$ term in R , we need to use 2-loop evolution. Notice that the accuracy in the β function that we want is always higher than the accuracy in the calculation by one unit. So, the leading term in the β function is of order two, but it is needed to maintain the accuracy of the result for R , which seems strange: if R is known at order α_s , why should its derivative needed at order α_s^2 ? The answer is that for a large evolution span, an error of order α_s^2 in

the derivative can become of order α_s , because a large evolution logarithm $\log \mu_f/\mu_i$ can compensate a power of $\alpha_s \propto 1/\log \mu/\Lambda$. Consider the case when the final evolution scale is such that $\mu_f/\mu_i \approx \mu_i/\Lambda$. From the 1-loop renormalization group equation we get:

$$\alpha_s(\mu_f) - \alpha_s(\mu_i) = -b_0 \int_{\mu_i}^{\mu_f} \alpha_s(\mu)^2 d \log \mu^2 \approx \mathcal{O} \left(\alpha_s^2(\mu) \log \frac{\mu_f^2}{\mu_i^2} \right) \approx \mathcal{O}(\alpha_s), \quad (63)$$

consistently with the fact that in this case $\alpha_s(\mu_f) \approx \alpha_s(\mu_i/2)$.

If the evolution span is small (i.e. if the scale changes by a factor of order one), one does not need an extra power of α_s in the β function to match the accuracy of the calculation.

Evolution must also be properly adjusted when crossing a flavour threshold. When one uses the 1-loop β function, the condition $\alpha^{(\text{nf}+1)}(\mu) = \alpha^{(\text{nf})}(\mu)$ for $\mu = 2m$, or $\mu = m/2$ are accurate enough. In other words, the matching is done at a scale of the order of the flavour mass. The difference of choosing, for example, $\mu = 2m$ or $\mu = m/2$, is simply

$$\alpha(2\mu) = \alpha(\mu/2) - 2b_0\alpha_s^2 \log(4) \quad (64)$$

and is thus a NLO effect. When using a 2-loop β function in the context of an NLO calculation, one must use a matching condition which is accurate up to terms of order α_s^3 . In the $\overline{\text{MS}}$ scheme, this is

$$\alpha^{(\text{nf}+1)}(\mu) = \alpha^{(\text{nf})}(\mu) + \mathcal{O}(\alpha_s^3) \quad \text{for } \mu = m \quad (65)$$

where we no longer have the freedom of a factor of order 1. Matching conditions appropriate for a 3-loop β function in the context of a NNLO calculation are given in ref. [6], and consist in a correction of order α_s^3 to equation 65.

The radiative corrections to R have been computed up to the order α_s^3 in ref. [7, 8, 9], a rather remarkable achievement. The result for $n_f = 5$, expressed in the $\overline{\text{MS}}$ scheme reads

$$R = R_0 \left\{ 1 + \frac{\alpha_s}{\pi} (1 + 0.448\alpha_s - 1.30\alpha_s^2) \right\} \quad (66)$$

where $\alpha_s = \alpha_s^{(5)}(Q)$, Q is the annihilation energy. Besides finding applications in e^+e^- annihilation physics, this formula has found recently a very interesting application to the determination of α_s from the hadronic decay of the τ lepton [10]. After what we have learned in this section about the ratio R , it should be easy for us to compute the ratio between the hadronic and the leptonic branching ratios of the τ , at zeroth order in the strong coupling constant. This is depicted symbolically in fig. 9. From the figure, it is clear that the top and bottom processes only differ by the number of possible final states. Thus, the top graph has a factor of 3, because of the three colours. Only an up-anti-down, or up-antistrange pair can be produced, since phase space forbids the production of charmed final states. Neglecting the mass difference between the down and the strange, one can see that the Cabibbo angle is irrelevant in this case. Thus, the ratio of the hadronic width to the (for example) electron width is 3 at zeroth order in the coupling constant. As in the case of R , this ratio will receive strong corrections, and the displacement of this ratio from 3 can be used to attempt a determination of the strong coupling constant from τ decays. Observe that the value of α_s at the scale of the τ mass is quite large, around 0.35. At LEP1 energy this value is around 0.12. In table 2 (taken from ref. [11]) the experimental determinations of α_s coming from R below the Z peak, R on the Z peak, and tau decays, are reported. All determinations are performed at the relevant scale of the process (thus, for example, the τ determination is performed in terms of $\alpha_s(M_\tau)$), and then evolved at the Z mass for comparison. Notice the rather remarkable agreements among the different determinations.

4 JETS IN e^+e^- ANNIHILATION

In the discussion of the previous section, we have left aside a few important issues, that can be summarized in the following questions:

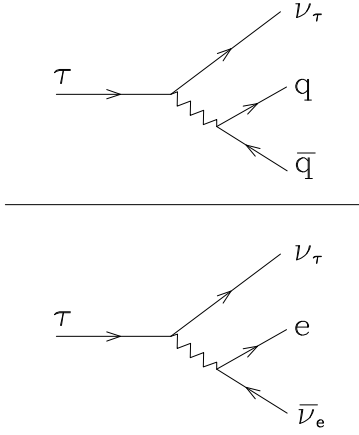


Fig. 9: The ratio between the τ hadronic and leptonic width.

Measurements	Q (GeV)	$\alpha_s(Q)$	$\alpha_s(m_Z)$
R_τ	1.777	$0.323 \pm 0.005(\text{exp.}) \pm 0.030(\text{th.})$	$0.1181 \pm 0.0007(\text{exp.}) \pm 0.0030(\text{th.})$
Re^+e^- ($20 < \sqrt{s} < 60$ GeV)	42	0.175 ± 0.028	0.126 ± 0.022
Z peak	91.2		$0.124 \pm 0.004 \pm 0.002(M_t, M_H) \begin{smallmatrix} +0.003 \\ -0.001 \end{smallmatrix} \text{QCD}$

Table 2: Determinations of α_s from inclusive hadronic decays, taken from ref. [11]. In the Z_{peak} determination, the error due to uncertainties in the Higgs and top mass, and the error due to QCD uncertainties, are separately specified.

1. How can we identify a cross section for producing quarks and gluons with a cross section for producing hadrons?
2. Given the fact that free quarks are not observed, why is the computed Born cross section so good?
3. Are there any other calculable quantities besides the total cross section?

We will see in the following that question 1 and 2, although unanswerable in QCD, imply no contradiction. We will also see that, under the same assumptions that make 1 and 2 work, also question 3 has an affirmative answer.

Looking at the lowest order formula, we immediately wonder why a formula describing the production of quarks in the final state should also be able to describe the production of hadrons, since we never observe free quarks in the final state. The structure of the perturbative expansion by itself give us a hint of how this may happen. Consider in fact the corrections of order α_s to the total cross section. They are given by diagrams in which a real gluon is emitted into the final state, and diagrams in which a virtual gluon is exchanged (interfered with a Born graph) as depicted in fig. 10. In the previous section I have just stated that the total of the corrections of order α_s is finite, and equals α_s/π . I will now show that the individual real contributions (those with a gluon in the final state) are individually infinite. As a consequence of the finiteness of the total, also the virtual ones (those with only the quark-antiquark pair in the final state) must be infinite, with the opposite sign. Let us therefore compute the diagram of fig. 10. We will perform the calculation under the simplifying assumption that the gluon energy is much smaller than the total available energy. It turns out that in this approximation the computation will require very little effort, and the approximation itself contains all the interesting features of the result. It is easy to convince oneself that the colour factors for all contributing diagrams (after squaring and taking the colour traces) are one factor of $C_F = 4/3$ relative to the Born term (which has a colour factor of 3, equal to the number of colours that can flow in the loop), a result which is illustrated in the last equality

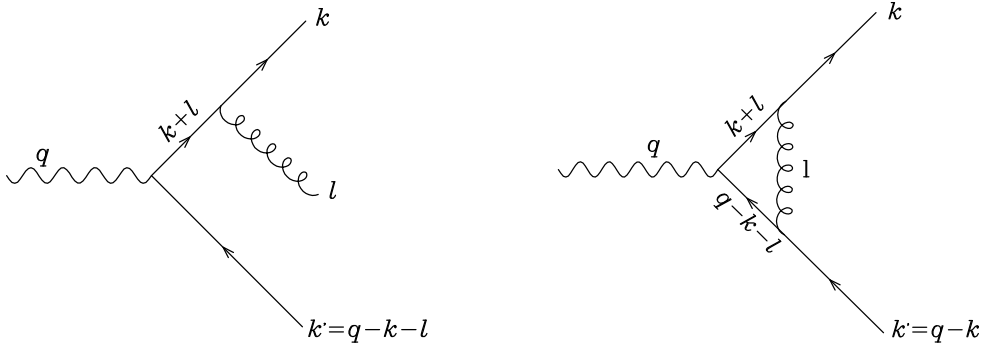


Fig. 10: Soft gluon emission (left graph) and virtual gluon exchange in e^+e^- annihilation.

of fig. 3. The amplitude for the Born process is

$$\mathcal{M} = \bar{u}(k)\epsilon^\mu\gamma_\mu v(k') \quad (67)$$

where ϵ is the virtual photon polarization, q is the incoming four momentum, k is the momentum of the outgoing fermion and $k' = q - k$ is the momentum of the outgoing antifermion. Defining

$$\mathcal{N} = \epsilon^\mu\gamma_\mu v(k') \quad (68)$$

we have

$$\mathcal{M} = \bar{u}(k)\mathcal{N}. \quad (69)$$

Consider now the diagram of fig. 10, in which the gluon is emitted from the outgoing fermion. The amplitude is given by

$$\mathcal{M}_1 = \bar{u}(k)(-i)\gamma_\alpha i \frac{\not{k} + \not{l}}{(k+l)^2} \mathcal{N}. \quad (70)$$

Actually we should have also substituted $k' = q - k - l$ in \mathcal{N} , but we are assuming that l is small. Fermion masses are also being neglected, since we assume we are considering a high energy process. Neglecting l in the numerator, and using the identity $\bar{u}(k)\not{k} = 0$, and expanding the denominator (recall that $l^2 = 0$, $k^2 = 0$) we obtain

$$\mathcal{M}_1 = \bar{u}(k) \frac{\gamma_\alpha \not{k} + \not{l} \gamma_\alpha}{(k+l)^2} \mathcal{N} = \bar{u}(k) \frac{2k_\alpha}{2k \cdot l} \mathcal{N} = \frac{k_\alpha}{k \cdot l} \mathcal{M}. \quad (71)$$

Analogously, for the amplitude with the gluon emitted from the outgoing antiquark, we obtain

$$\mathcal{M}_2 = -\frac{k'_\alpha}{k' \cdot l} \mathcal{M} \quad (72)$$

and the total is

$$\mathcal{M}_{q\bar{q}g} = \mathcal{M}_1 + \mathcal{M}_2 = \left(\frac{k_\alpha}{k \cdot l} - \frac{k'_\alpha}{k' \cdot l} \right) \mathcal{M} \quad (73)$$

which vanishes when contracted with l^α , as gauge invariance requires. Taking the square (with the extra minus for the gluon projector)

$$\mathcal{M}_{q\bar{q}g}^2 = 2 \frac{k \cdot k'}{(k \cdot l)(k' \cdot l)} \mathcal{M}^2. \quad (74)$$

From the amplitude square we turn to the cross section by supplying the phase space factor for the gluon

$$\sigma_{q\bar{q}g} = C_F g_s^2 \sigma_{q\bar{q}}^{\text{Born}} \cdot \int \frac{d^3l}{2l^0 (2\pi)^3} 2 \frac{k \cdot k'}{(k \cdot l)(k' \cdot l)}. \quad (75)$$

At this stage I have also included the coupling constant and the appropriate colour factor. Let us now consider the process in the rest frame of the incoming virtual photon, with $q = (q^0, 0, 0, 0)$, and $\vec{k} = -\vec{k}'$. Let us call θ the angle that the gluon makes with the fermion direction. We have then

$$2 \frac{k \cdot k'}{(k \cdot l)(k' \cdot l)} = \frac{4}{l_0^2(1 - \cos \theta)(1 + \cos \theta)} \quad (76)$$

so that (using $\alpha_S = g_S^2/(4\pi)$)

$$\sigma_{q\bar{q}g} = C_F \frac{\alpha_S}{2\pi} \sigma_{q\bar{q}}^{\text{Born}} \int d\cos \theta \frac{dl^0}{l^0} \frac{4}{(1 - \cos \theta)(1 + \cos \theta)}. \quad (77)$$

The cross section for producing an extra gluon is therefore divergent in three regions:

- when the emitted gluon is in the direction of the outgoing quark ($\theta = 0$)
- when the emitted gluon is in the direction of the outgoing antiquark ($\theta = \pi$)
- when the emitted gluon is soft ($l^0 \rightarrow 0$).

The first two kind of divergences are called collinear divergences, while the last one is called a soft divergence. Both divergences are of infrared (IR from now on) type, that is to say, they involve long distances. In fact, because of the uncertainty principle, we need an infinite time in order to specify accurately the particle momenta, and therefore their directions. Unlike UV divergences, there is nothing like renormalization for the IR divergences. Their meaning is the following: the cross section is sensitive to the long distance effects, like the fermion masses, the hadronization mechanisms, and so on. In fact, if we give a fictitious mass to the gluon, the result becomes convergent, but it will be sensitive to the value of the gluon mass.

It was stated in the previous section that the total of the corrections of order α_S to the production of hadrons in e^+e^- annihilation is finite, and equals $\frac{\alpha_S}{\pi}$. It follows that also the virtual corrections must have the same kind of infinities, with opposite sign. If we cutoff these divergences with some method (like dimensional regularization, or by giving a mass to the gluon), and then sum up real and virtual contributions, the divergences cancel, and the left-over is finite and equal to α_S/π times the Born cross section, independent of the method we used to regularize the diagrams. This cancellation is a consequence of the Kinoshita-Lee-Nauenberg theorem [12, 13]. Roughly speaking, this theorem deals with divergences that arise because of degeneracy in the final state. For example, the final state with an extra soft gluon is nearly degenerate with the state with no gluons at all, and the state with a quark split up into a quark plus a gluon, with parallel momenta, is degenerate with the state with no radiation at all. The theorem states that the cross section obtained by summing up over degenerate states are not divergent.

We are now ready to show, as promised, that point 1 and 2 imply no contradiction. We have in fact shown that if we attempt to compute the cross section for the production of a pair of quark–antiquark alone, while the zeroth order term (the Born term) is finite, the term of order α_S is infinite, being collinear and soft divergent. This means that a perturbative expansion for this quantity does not work, since the coefficients of the expansion are large (actually infinite). Therefore, even the Born term alone cannot represent the cross section for producing a quark–antiquark pair. Thus, the fact that a final state with a quark–antiquark pair and nothing else is not observed is not in contradiction with perturbation theory, since we have shown that there is no valid perturbative expansion for this quantity. On the contrary, the cross section for producing strongly interacting particles (no matter how many quarks or gluons) remains finite even after perturbative corrections are added. One can show that in fact it remains finite order by order in perturbation theory. Its lowest order approximation is in fact the Born cross section. So, the Born cross section is the lowest order term in a well defined perturbative expansion with infrared finite

coefficients, which is just the cross section for producing strongly interacting particles (no matter how many and which types). This is why the Born cross section represents quite accurately the total hadronic cross section. We are now also in the position to answer the third question. We will show that there are quantities which characterize the hadronic final state, that are infrared finite in perturbation theory, and therefore should be calculable in perturbative QCD.

4.1 Serman–Weinberg jets

Serman and Weinberg [14] first realized that one can define a cross section which is calculable and finite in perturbation theory, and characterizes in some way the hadronic final state. The definition goes as follows.

We define the production of a pair of Serman–Weinberg jets, depending on the parameters ϵ and δ , in the following way. A hadronic event in e^+e^- annihilation, with centre-of-mass energy E , contributes to the Serman–Weinberg jets cross section if we can find two cones of opening angle δ that contain more than a fraction $1 - \epsilon$ of the total energy E . In other words ϵE is the maximum energy allowed outside of the cones. An example of Serman–Weinberg jet event is illustrated in fig. 11. We

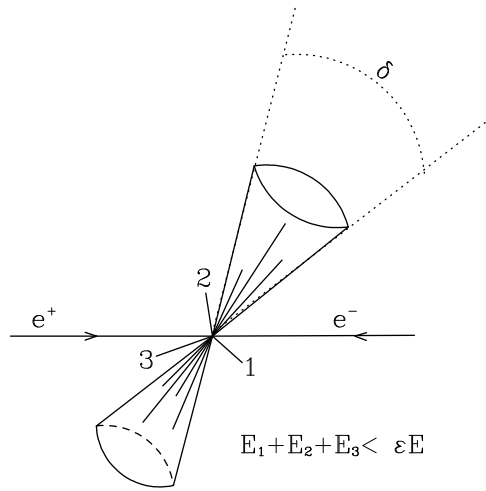


Fig. 11: Serman–Weinberg jets.

will now show that the computation of the cross section for the production of Serman–Weinberg jets, in the approximation introduced in the previous chapter, is infrared finite. The various contributions to the cross section (illustrated in fig. 12) are as follows

- All the Born cross section contributes to the Serman–Weinberg cross section, for any ϵ and δ (fig. 12a).
- All the virtual cross section contributes to the Serman–Weinberg cross section, for any ϵ and δ (fig. 12b).
- The real cross section, with one gluon emission, when the energy of the emitted gluon l^0 is limited by $l^0 < \epsilon E$ (fig. 12c), contributes to the Serman–Weinberg cross section.
- The real cross section, when $l^0 > \epsilon E$, when the emission angle with respect to the quark (or antiquark) is less than δ (fig. 12d), contributes to the Serman–Weinberg cross section.

The various contributions are given formally by

$$\text{Born} = \sigma_0 \tag{78}$$

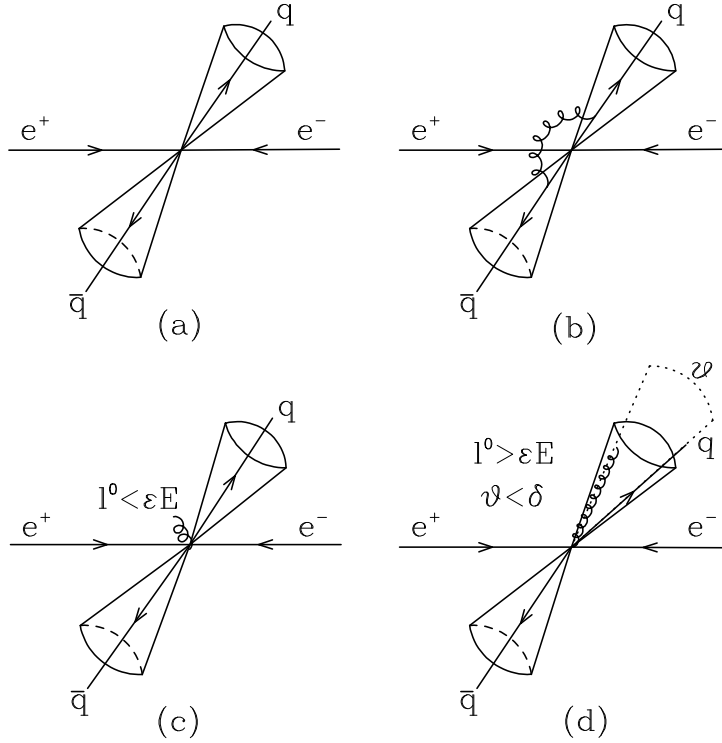


Fig. 12: Contributions to the Serman–Weinberg cross–section. Born: (a), virtual: (b), real emission: (c) and (d).

$$\text{Virtual} = -\sigma_0 \frac{4\alpha_S C_F}{2\pi} \int_0^E \frac{dl^0}{l^0} \int_{\theta=0}^{\pi} \frac{d \cos \theta}{1 - \cos^2 \theta} \quad (79)$$

$$\text{Real (c)} = \sigma_0 \frac{4\alpha_S C_F}{2\pi} \int_0^{\epsilon E} \frac{dl^0}{l^0} \int_{\theta=0}^{\pi} \frac{d \cos \theta}{1 - \cos^2 \theta} \quad (80)$$

$$\text{Real (d)} = \sigma_0 \frac{4\alpha_S C_F}{2\pi} \int_{\epsilon E}^E \frac{dl^0}{l^0} \left[\int_{\theta=0}^{\delta} \frac{d \cos \theta}{1 - \cos^2 \theta} + \int_{\theta=\pi-\delta}^{\pi} \frac{d \cos \theta}{1 - \cos^2 \theta} \right]. \quad (81)$$

Observe that the expression of the virtual term is fixed by the fact that it has to cancel the total of the real contribution. Since we are looking only at divergent terms, and since the virtual term is independent of δ and ϵ , the expression (79) is fully adequate for our purposes. Summing all terms we get

$$\begin{aligned} \text{Born} + \text{Virtual} + \text{Real (a)} + \text{Real (b)} &= \sigma_0 - \sigma_0 \frac{4\alpha_S C_F}{2\pi} \int_{\epsilon E}^E \frac{dl^0}{l^0} \int_{\theta=\delta}^{\pi-\delta} \frac{d \cos \theta}{1 - \cos^2 \theta} \\ &= \sigma_0 \left(1 - \frac{4\alpha_S C_F}{2\pi} \log \epsilon \log \delta^2 \right) \end{aligned} \quad (82)$$

which is finite, as long as ϵ and δ are finite. Furthermore, as long as ϵ and δ are not too small, we find that the fraction of events with two Serman-Weinberg jets is 1, up to a correction of order α_S .

Now we are ready to perform a qualitative step: we interpret the Serman-Weinberg cross section, computed using the language of quarks and gluons, as a cross section for producing hadrons. Thanks to this qualitative step, we make the following prediction: at high energy, most events have a large fraction of the energy contained in opposite cones, that is to say, *most events are two jet events*. As the energy becomes larger α_S becomes smaller. Therefore we can use smaller values of ϵ and δ to define our jets. Thus, at higher energies jets become thinner.

It should be clear now to the reader that, by the same reasoning, we could show that the angular distribution of the jets will be very close, at high energy, to the angular distribution one computes using

the Born cross section, that is to say, the typical $1 + \cos^2 \theta$ distribution. These predictions have been confirmed experimentally since a long time.

4.2 A comparison with QED

The alert reader will have probably realized that the discussion given in this section should also apply to electrodynamics. In fact, the Feynman diagrams we have considered are present also in electrodynamic processes, like $e^+e^- \rightarrow \mu^+\mu^-$, and they differ from the QCD graphs only by the color factor. Thus, from the previous discussion, we would infer that Serman-Weinberg jets in electrodynamic processes at high energy do not depend upon long distance features of the theory. For example, they become independent from the μ mass when $E \gg \mu$. Also in electrodynamics, the cross section for producing a $\mu^+\mu^-$ pair plus a photon is divergent, as is divergent the cross section for producing the pair without any photon. In many books on quantum electrodynamics these divergences are discussed, and it is shown that a resolution parameter for the minimum energy of a photon is needed in order to have finite cross section order by order in perturbation theory. In electrodynamics, we can go even farther, and prove that by resumming the whole tower of divergent graphs, the infinite negative virtual correction to the production of a $\mu^+\mu^-$ pair with no photons exponentiates, and gives a zero cross section. In other words, as it is well known, it is impossible to produce charged pairs without producing arbitrarily soft photons. What is then the difference with QCD? Why cannot we prove similar results in QCD? The difference arises because of the different asymptotic properties of QCD and QED. In QED the coupling becomes smaller at low energy, while in QCD it grows. Thus, when the scale of an emission process approaches a few hundred MeV the coupling constant becomes of order one, and perturbation theory becomes inapplicable. So, the infrared problem in QCD is tightly untangled with the confinement problem, and it seems to be unanswerable in the context of perturbation theory alone. In this sense perturbative QCD is an incomplete theoretical framework. In order to make predictions we need to assume that the soft phenomena characterized by scales of the order of few hundred MeV do not spoil completely the computation of the high energy part of the process. This assumption is consistent with perturbation theory; it is however an assumption, and it cannot be proven using perturbation theory alone.

4.3 Shower Monte Carlo programs

Perturbation theory can be used to compute radiation processes as long as the energies involved are safely above the typical hadronic scales. It is then possible to construct event generator programs that implement the properties of QCD Feynman diagrams for the splitting of partons into more partons, as long as the splitting involves large transverse momentum, and then use some plausible model for last step of the splitting process, in which the partons become hadrons. These programs are generally called shower Monte Carlo event generators [15, 16, 17], and are an invaluable tool for experimental physicists. They essentially sum a large class of Feynman graphs, precisely the most collinear and (in some cases) soft-singular ones. In the attempt to describe the full final state, they give up the accuracy that can be obtained in perturbation theory. They are (until now) compatible with QCD only at the leading order in the strong coupling. While the QCD part is quite similar in all of them, for the last step of the final state formation, that is to say the hadronization, they differ widely, since they have to rely on models, like the so called Lund string model or the Herwig cluster model. Hadronization models are tuned to data. Nevertheless, one should not forget that there is very little predictivity in these models, since they are only qualitatively based upon the theory. One can expect in general that the hadronization properties for which the Monte Carlo has been tuned for will be well reproduced by it, but not much more than this.

4.4 More jet definitions and shape variables

The key property of the Serman-Weinberg jets, that makes them calculable in perturbation theory, is the insensitivity of the jet definition to radiation of soft particles, and to the collinear splitting of an particle

into two particles that share its momentum. This insensitivity is necessary to guarantee the cancellation of effects that depend strongly upon long distance phenomena, that is to say, those effects that are infrared divergent when computed in perturbation theory.

After the paper of Serman and Weinberg, it was soon realized that it is not difficult to build a whole class of final state observables that do have the same property of soft and collinear insensitivity, and can thus be computed in perturbation theory, and compared with experimental measurements: thrust, oblateness, the C parameter, jet clusters, the mass of the heaviest hemispheres, etc.. The important thing which is assumed in these definitions is that *the same definition must be applied to the final state hadrons by the experimenter that measures this quantity, and by the theorist that computes this quantity in terms of quark and gluons*. Only if this condition is satisfied, one can assume that in the high energy limit the computed quantity will agree with the measured one, up to corrections that are suppressed by some inverse power of the energy.

One of the first of these infrared safe shape variables is thrust. It is defined by the equation

$$t = \max_{\vec{v}} \frac{\sum_i |\vec{p}_i \cdot \vec{v}|}{\sum_i |\vec{p}_i|}. \quad (83)$$

In words, one takes an arbitrary vector (in the centre-of-mass frame of the colliding electron-positron pair) and sums the absolute values of the projection of the momenta of all final state particles onto that vector, normalized to the sum of all absolute values of the hadron momenta. The vector is rotated until a maximum is found. The maximum direction is called the thrust axis, and the value at the maximum the thrust of the event. The maximum value of thrust is one, for a final state of two massless particles in the back-to-back direction. It is easy to check that thrust is an infrared safe shape variables. In fact, a soft emission does not alter the thrust abruptly, since all emitted particles enter weighted by their momenta. Also collinear splitting does not alter the thrust of an event, as one can easily verify. An example of a quantity which is not infrared safe is the total number of particles in the final state, which changes by one unit in case of soft emission. Examples of a quantities which are sensitive to collinear splitting are the axis of the tensor

$$S^{ij} = \sum_l p_l^i p_l^j \quad (84)$$

which were actually used in the past to classify the “jettiness” of an event.

A modern, and very clever way to define jets is by clustering [18]. For a given events, one forms the invariant mass of all pairs of particles in the final state. The pair with the smallest mass is merged into a single pseudoparticles, and then the procedure is continued with the pseudoparticles, and it is stopped when the smallest mass of a pair exceeds a given cutoff $y \times S$. One ends up with a definite number of clusters, and one can thus define the cross section for producing two, three, four or more clusters for a given y cut. It is easy to convince oneself that these cross section definitions are infrared safe. Since the computation of these cross sections (in terms of partons) should in first approximation give the correct answer, we see that in perturbative QCD we roughly expect (for not too extreme values of y) that most events will be made up by two clusters, a fraction of order α_S will be made up by three clusters, and a fraction of order α_S^2 will be made by four clusters. Analogously, we expect thrust to be near one, and its departure from one to be of order α_S . We also expect that a fraction of events of order α_S will have thrust well below one.

Because of the obvious interest in the determination of α_S from jet shape variables, a lot of effort has gone in the study of jet and shape variables that are directly proportional to α_S , which we may call “three-jet sensitive”, like the thrust distribution, and the fraction of events with three clusters. There are tens of variables of these kind that have been studied at e^+e^- machines.

The present state of the art for jet studies in e^+e^- machines mainly relies on the calculation of Ellis, Ross and Terrano (ERT) [19, 20], which allows to compute any infrared safe 3–jet shape variable up to the order α_S^2 . Various computer programs for the computations of these quantities are available, and

many of these quantities have been tabulated [21]. Heavy quark mass effects have also been included in the 3-jets calculation [22, 23, 24]. Three-jet quantities have been intensively studied at e^+e^- machines, The results of LEP1 and SLD have given a quite remarkable contribution to the tests of QCD, and considerably reinforced our confidence in perturbative QCD.

Recently, the NLO correction to 4-jet partons production have been computed [25, 26, 27, 28], allowing thus the computation of any 4-jets shape variable in the form $\alpha_s^2(\mu^2)C + \alpha_s^3(\mu^2)D(\mu^2/Q^2) + \dots$. Phenomenological applications have begun to appear recently [29] [30].

Fixed order calculations of shape variables distributions are sometimes supplemented with all-order resummation of effects that are enhanced in the limit of thin jets. An example of these effects is visible in eq. 82; when δ and ϵ become small, the $\mathcal{O}\alpha_s$ correction becomes large, because of the large collinear and soft logarithms. These logarithms, called ‘‘Sudakov logarithms’’, are a general phenomenon that happens in QCD and QED when we force a process into a region of phase space where radiation is inhibited. Since soft radiation is infrared divergent, and its divergence cancels against virtual contributions, when we suppress soft radiation the cancellation becomes unbalanced, and large logarithms appear at all orders in the perturbative expansion. In some cases, these logarithms can be organized and resummed [31, 32, 33]

Hadronization and power corrections are believed to be suppressed as $1/Q$, but they are still important at LEP energies. They are usually estimated using Monte Carlo hadronization models. The renormalon inspired model of ref. [34] provides an alternative method [35].

4.5 Thrust as an example

Let us focus upon the case of thrust as an example. The thrust distribution has the perturbative expansion

$$\frac{1}{\sigma_0} \frac{d\sigma}{dt} = \delta(1-t) + \frac{\alpha_s(\mu)}{2\pi} A(t) + \left(\frac{\alpha_s(\mu)}{2\pi} \right)^2 \left[A(t) 2\pi b_0 \log \frac{\mu^2}{Q^2} + B(t) \right] + \mathcal{O}(\alpha_s^3). \quad (85)$$

The first term, proportional to a delta function, is the Born contribution, which corresponds to the production of two back-to-back massless partons. The functions $A(t)$ and $B(t)$ can be computed from the ERT results (they are tabulated in ref. [21]). The renormalization scale μ is explicitly indicated in the formula. As in the total cross section formula, the explicit scale dependence of the term of order α_s^2 is related to the coefficient of the term of order α_s . Again, using the renormalization group equation at 1 loop (i.e., $\partial\alpha_s/\partial\log\mu^2 = -b_0\alpha_s^2$), one can prove that the scale dependence of the above equation cancels up to the order α_s^2 . Of course, if the whole perturbative expansion was included in the right hand side, no scale dependence would survive, since the left hand side is scale independent. However, only terms up to the order α_s^2 are included, and thus one expects a residual scale dependence at order α_s^3 .

Radiative corrections are generally quite large. For example

$$\begin{aligned} \langle 1-t \rangle &= \frac{1.05}{\pi} \alpha_s(Q) (1 + 3\alpha_s) \\ \langle o \rangle &= 1.29 \alpha_s(Q) (1 - 4.3\alpha_s) \\ \langle M_{D,t}^2 \rangle &= \frac{1.05}{\pi} \alpha_s(Q) (1 - 0.025\alpha_s) \end{aligned} \quad (86)$$

where the second quantity is oblateness (for a precise definition, see ref. [21]), and the third quantity is the difference of the square of the masses of the heavy hemisphere with respect to the light hemisphere, with the hemisphere defined according to the thrust axis. Thus, corrections can be as large as 40% even at LEP1 energies. Because of this, it is mandatory that corrections of even higher orders (α_s^3 and higher) should be at least estimated and included in the theoretical error. There is no universal method to estimate the theoretical error in this case. A commonly used method is to look at the scale dependence of the result. Since the remaining terms of the perturbative expansion should compensate the scale dependence, they

Table 3: A summary of measurements of α_s from shape variables.

Process	Q [GeV]	$\alpha_s(Q)$	$\alpha_s(M_{Z^0})$	$\Delta\alpha_s(M_{Z^0})$	
				exp.	theor.
e^+e^-	22	$0.161^{+0.016}_{-0.011}$	$0.124^{+0.009}_{-0.006}$	0.005	$+0.008$ -0.003
e^+e^-	35	$0.145^{+0.012}_{-0.007}$	$0.123^{+0.008}_{-0.006}$	0.002	$+0.008$ -0.005
e^+e^-	44	0.132 ± 0.008	0.123 ± 0.007	0.003	0.007
Z^0	91.2	0.121 ± 0.006	0.121 ± 0.006	0.001	0.006
e^+e^-	133	0.113 ± 0.008	0.120 ± 0.007	0.003	0.006
e^+e^-	161	0.109 ± 0.007	0.118 ± 0.008	0.005	0.006
e^+e^-	172	0.104 ± 0.007	0.114 ± 0.008	0.005	0.006
e^+e^-	183	0.109 ± 0.005	0.121 ± 0.006	0.002	0.005
e^+e^-	189	0.110 ± 0.004	0.123 ± 0.005	0.001	0.005

must be at least as large as the scale variation of the truncated result. The scale should be varied in a range around the typical scale of the process. It should not be chosen neither much higher of this typical scale, nor much smaller, since in these cases the perturbative expansion is not well behaved. A common choice is $m_Z/4 < \mu < m_Z$, which accounts for the fact that the typical scale of the process is somewhat below the Z mass.

Hadronization effects should also be estimated, and included in the theoretical error. For the observable $\langle 1 - t \rangle$, for example, we can make a naive estimate in the following way. Let us assume that the emission of an extra soft pion in the final state has a probability of order one. This emission takes away from the thrust a value of few hundred MeV (the transverse mass of a soft pion) divided by the total available energy. To fix the numbers, let us say that at LEP we have $\delta_t = 0.5/90 \approx 0.0055$, assuming a 500 MeV average transverse mass for the pion. The perturbative value of $\langle 1 - t \rangle$ is roughly $\alpha_s/\pi \approx .04$, increased by the α_s^2 correction to roughly 0.055. Thus $\delta_t/\langle 1 - t \rangle = 0.1$. This means that we can expect that hadronization effects may have a 10% effect in the determination of α_s from $\langle 1 - t \rangle$.

An instructive example of a QCD study at LEP can be found in ref. [36]. Estimates of hadronization corrections are used there to correct the raw data. Their typical value is around 10%. Hadronization corrections are estimated by running a shower Monte Carlo with or without the hadronization stage. The corrections are determined by looking at the difference between the two runs, and are then applied to the data. The error on the hadronization corrections are estimated by using different Monte Carlo programs with different hadronization models. It is quite clear that this procedure is quite risky. The QCD stage is in fact similar in all shower Monte Carlo. The hadronization step is different, but it is in all cases tuned to fit the data. This may generate a bias towards determining the same value of α_s used in the Monte Carlo. The size of the radiative correction is reported in ref. [36], and thus, the pessimistic reader may use the whole hadronization correction as an error on the determination, if he wishes to do so.

Table 3 (from ref. [11]) summarizes the determinations of α_s from event shape variables. In all determinations, NLO calculations are used, together with resummation of soft gluon effects. Power corrections are estimated using Monte Carlo programs.

Alternative models for the power suppressed corrections have recently appeared, and have been introduced in phenomenological analysis. In ref. [35], several shape variables have been examined in the energy range of $\sqrt{S} = 14$ to 189 GeV. QCD NLO prediction, together with the power correction model of ref. [34] are used to fit the data. I will not try to describe here the features of the model; it is enough to know that power corrections to shape variables depend upon a universal parameter α_0 in this model. A summary of the results of this analysis is displayed in figs. 13 and table 4.5. We observe

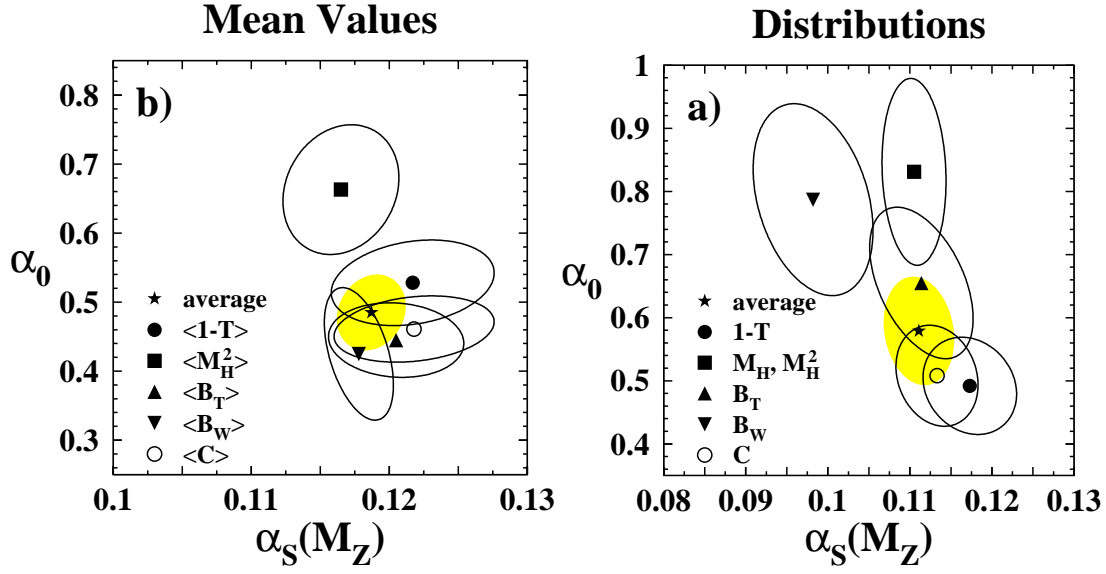


Fig. 13: Simultaneous fits to α_S and α_0 using mean values of shape variables (left) and distributions (right).

			fit	syst.	Th.
means	α_S	0.1187	± 0.0014	± 0.0001	$+0.0028$ -0.0015
	α_0	0.485	± 0.013	± 0.001	$+0.065$ -0.043
distr.	α_S	0.1111	± 0.0004	± 0.0020	$+0.0044$ -0.0031
	α_0	0.579	± 0.005	± 0.011	$+0.099$ -0.071
Comb.	α_S	0.1171		$+0.0032$ -0.0020	
	α_0	0.513		$+0.066$ -0.045	

Table 4: Results of the fits to $\alpha_S(M_Z)$ and $\alpha_0(2 \text{ GeV})$ from ref. [35].

that the final value is well in agreement with other determinations [11]. Also, to some extent the data supports the universality of the non-perturbative parameter. On the other hand, the value determined from distributions is considerably lower than the value obtained with standard methods (i.e. hadronization corrections with Monte Carlo models). Furthermore, for some shape variables the consistency of the determination is quite poor. Thus, as far as power suppressed corrections are concerned, we can certainly say that they are very poorly understood.

Even if we assume a pessimistic attitude with regard to power corrections, one must recognize that LEP results do show a remarkable consistency with perturbative QCD results. In figure 14 I try to give an unbiased illustration of the comparison of LEP data with perturbative QCD results. In the figure,

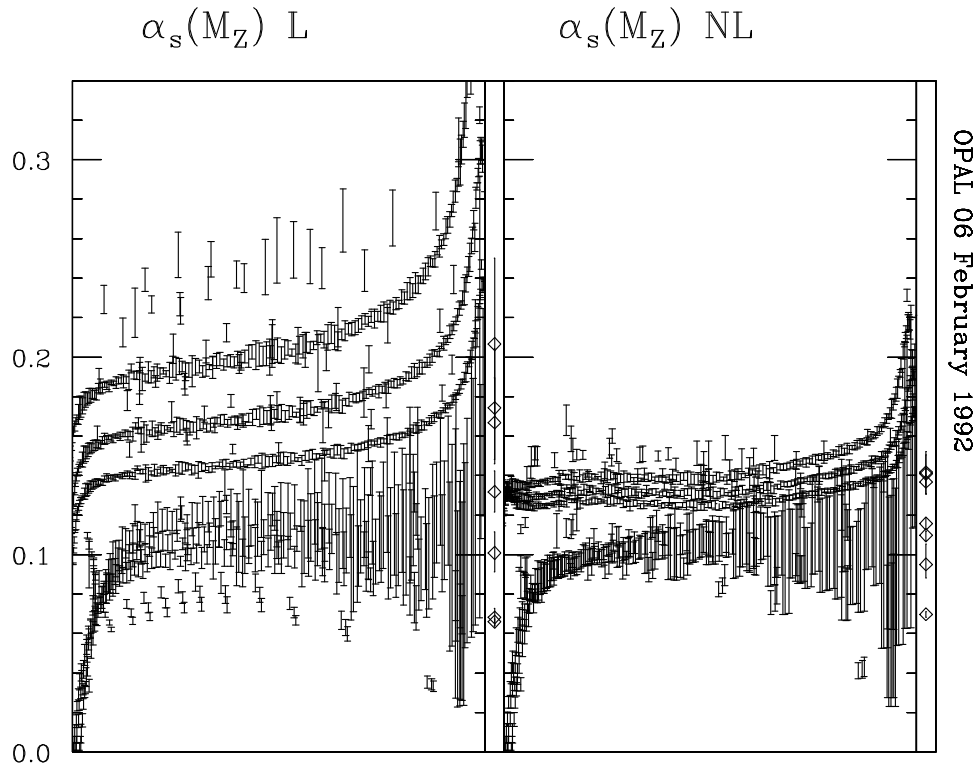


Fig. 14: Bin-by-bin determination of α_s for several different shape variables.

a determination of α_s is performed for several shape variables. The determination was performed first using a leading order formula (left plot), and then the full $\mathcal{O}(\alpha_s^2)$ formula. No hadronization correction was applied to the data. Three values of the renormalization scale were chosen for each variable: $\mu = m_Z/4, m_Z/2,$ and m_Z . In the figure, parallel bands correspond to these three choices. The errors on the various point are experimental errors. If we had a perfect QCD calculation, e.g. all orders in perturbation theory, and hadronization corrections were truly negligible, we should expect that all experimental point lie (within errors) on a constant line. If we only have a leading order calculation, we expect instead large differences among the various points, that should become smaller and smaller as we include higher order corrections. In the plot, of course, we can only represent the leading and next-to-leading result, since an $\mathcal{O}(\alpha_s^3)$ calculation has never been performed. It is quite striking to see how, by including the next-to-leading corrections, the various determinations become much closer to each other. It is left to our fantasy to imagine what would happen if we could include the $\mathcal{O}(as^3)$ effects.

5 PROCESSES WITH HADRONS IN THE INITIAL STATE

We will now turn to describe the application of perturbative QCD to processes in which hadrons are present also in the initial state, like Deep-Inelastic Scattering (DIS), or the production of some objects of high invariant mass in hadronic collisions. It turns out that cross sections for these processes can be computed and related to each other. In general the cross section for the production of some final state with high invariant mass (which could be made of a heavy weak vector boson, a lepton-antilepton pair, heavy quarks, jets, and the like) will be expressed by the so called *improved parton model formula*

$$\sigma_{H_1, H_2}(p_1, p_2) = \sum_{i, j} \int dx_1 dx_2 f_i^{(H_1)}(x_1, \mu) f_j^{(H_2)}(x_2, \mu) \hat{\sigma}_{ij}(x_1 p_1, x_2 p_2, \alpha_S(\mu), \mu) . \quad (87)$$

A pictorial representation of formula 87 is given in fig. 15.

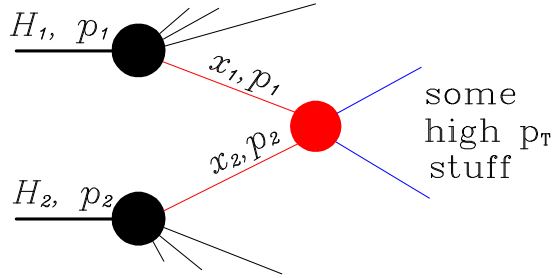


Fig. 15: A graphic representation of the improved parton model formula.

For processes with a single incoming the improved parton model formula is even simpler. For example, in DIS

$$\sigma_H(p) = \sum_i \int dx f_i^{(H)}(x, \mu) \hat{\sigma}_i(x, \mu) , \quad (88)$$

Formulae (87) and (88) are applicable to inclusive hard processes. By inclusive, we mean that no detailed

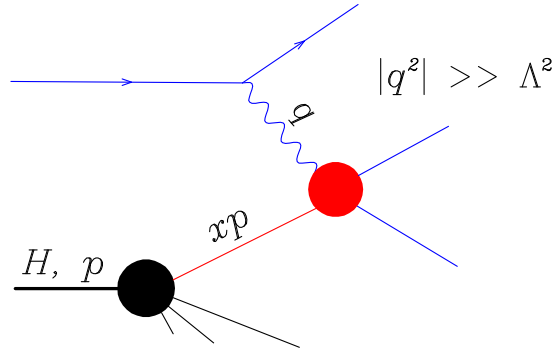


Fig. 16: The improved parton model formula for DIS.

question on the distribution of the final state hadrons is asked in order to measure the cross section. The generic concept of a hard process is better illustrated by examples. We may, for example, require that a very large invariant-mass lepton-antilepton pair (the so called Drell-Yan process) is present in the final state. Or that jets (for example, of the Serman-Weinberg kind) with large transverse momentum are observed. In the case of DIS, we simply require $|q^2|$ to be very large.

The recipe for the improved parton model formulae can be summarized in the following points:

- An incoming beam made of hadrons of type H is equivalent to a beam of constituents (also called *partons*), that is to say of quark and gluons, with a longitudinal momentum distribution characterized by the parton density functions (pdf's from now on) $f_i^{(H)}(x, \mu)$. More specifically, given the hadron H with momentum p , the probability to find in H the parton i with momentum between xp and $(x + dx)p$ is precisely $dx f_i^{(H)}(x, \mu)$. The pdf's are universal, that is to say, they do not depend upon the particular process considered.
- The short distance cross section $\hat{\sigma}$ is calculable as a perturbative expansion in α_s

$$\hat{\sigma}_{ij}(x_1 p_1, x_2 p_2, \alpha_s(\mu), \mu) = \sum_l \hat{\sigma}_{ij}^{(l)}(x_1 p_1, x_2 p_2, \mu) \alpha_s^l(\mu). \quad (89)$$

The lowest order term of this expansion is precisely the cross section one would compute naively at lowest order. For the computation of higher order, a more complex prescription is specified.

- The pdf's have a mild dependence upon the scale μ , determined by the Dokshitzer-Gribov-Lipatov-Altarelli-Parisi equation [37]

$$\frac{\partial}{\partial \log \mu^2} f_i^{(H)}(x, \mu) = \int_x^1 \frac{dz}{z} \sum_j P_{ij}(\alpha_s(\mu), z) f_j^{(H)}(x/z, \mu). \quad (90)$$

Using the above equations, given the pdf's at a specified value of μ , we can compute them at any other value. The functions P are called splitting function, and have a perturbative expansion in powers of $\alpha_s(\mu)$

$$P_{ij}(\alpha_s(\mu), z) = \frac{\alpha_s(\mu)}{2\pi} P_{ij}^{(0)}(z) + \left(\frac{\alpha_s(\mu)}{2\pi} \right)^2 P_{ij}^{(1)}(z) + \mathcal{O}(\alpha_s^3). \quad (91)$$

The functions $P^{(0)}$ are given in [37], and the functions $P^{(1)}$ are given in [38, 39]. The scale μ is arbitrary. The μ dependence in the pdf's is compensated by the μ dependence in the short distance cross section. As in the case of $e^+e^- \rightarrow$ hadrons, the scale μ is taken to be of the order of the typical scales in the process, in order to avoid the appearance of large logarithms to all orders in the short distance cross section. In this way, a truncated expression for the short distance cross section may be used safely.

The approach described above gives the cross section in terms of a power expansion in $\alpha_s(\mu)$. Since $\alpha_s(\mu) \approx 1/\log \mu/\Lambda$, this means that by increasing the perturbative order at which the computation is performed, one adds corrections which are suppressed by one more inverse power of $\log \mu/\Lambda$. Corrections which are suppressed by powers of Λ/μ are not included in this approach. Thus, for example, the pdf's describe the longitudinal momentum distribution of the partons. Since the partons are confined in a hadron, one knows that they must also have a transverse momentum of the order of the inverse of a typical hadron size, that is to say $1/\Lambda$. This transverse momentum is neglected, since it would give rise to power suppressed corrections.

In the following I will try to illustrate and justify the improved parton model approach. I will do this in three steps.

I will first give a naive argument to show that a somewhat simplified version of formula (87), called the (naive) parton model formula (i.e., not yet improved), should work. The simplifications consist in the absence of the scale μ in the pdf's and in $\hat{\sigma}$. Such formula can be used to compute, for example, DIS cross section, or Drell-Yan pair production cross section. The parton model formula predicts correctly the existence of scaling in DIS.

In the second step will try to compute QCD corrections in the context of the parton model formula. I will show that this approach does not survive when radiative corrections are included.

In the third step we will find a modification of the parton model formula that is consistent with radiative corrections. The main consequence of this improved approach is the appearance of a scale dependence in the pdf's. This scale dependence is at the origin of scaling violation phenomena in DIS.

5.1 The naive parton model formula

The basic parton model ideas are based upon a very commonly used intuitive picture of inclusive high energy scattering of composite systems, when we require a very large momentum transfer. Suppose, for example, that we collide to hydrogen beams, and require that in the final state we find a pair of electrons with large transverse momenta. It is clear that the most likely mechanism for producing such an event is the collision of two electron from the two incoming hydrogen atoms. If the transverse momenta of the electrons are much higher than the hydrogen binding energy, we may think that, to a good approximation, the cross section may be computed from the elementary electron-electron cross section, applied to a beam of incoming free electron. The fact that we want to observe a high transverse momentum scattering implies that the binding of the electrons to the nuclei cannot have an important effect in this case. In other words, the electrons behave as free particles in the collision. Observe that the inclusive character of the reaction, and the presence of high momentum transfer, are both necessary conditions for this approach to be valid. Inclusiveness is needed, because after the two electron collide, the remaining constituent of the original atoms (i.e., the protons in the case of hydrogen) are also found in the final state. The high momentum transfer is instead needed for the reaction to take place in a very short transverse distance. If this was not the case, like, for example, in the case when we look for small angle scattering, the atoms may interact coherently. Or, more simply, if the momentum transfer was of the same size as the typical momentum of the electron in the atom, the binding properties of the system could no longer be neglected.

Assuming now that we have ultra-relativistic monochromatic beams of hydrogen atoms of energy E , in order to compute the above cross section we would assume that these beams are equivalent to electron beams with energy $E_e = E \times m_e/m_p$. In reality, even if the atom beams were perfectly monochromatic, the electron beam would not be perfectly monochromatic. The electrons are moving inside the atom, with a typical velocity of the order of the electromagnetic coupling $v \approx \alpha_{em}$. A simple exercise in relativistic transformations would show that its energy spread would be of the order vE_e . In fact, the electron energy could be characterized by a pdf $f_e(x)$, peaked around the value $x = m_e/m_p$, and a width of order vx . Also the transverse momentum of the electron would be of order vm_e . However, while the transverse momentum remains invariant under boost, and thus becomes truly negligible at high energy, the spread in longitudinal momentum is amplified by the boost, and it thus scales with the energy. This discussion applies to a boosted, non-relativistic system. We can now try to guess what happens for a relativistic system, in which all constituents have velocities of order 1, and comparable energies. The transverse momenta still remain fixed at high energies. Their pdf's, however, will no longer be peaked around a particular value. Their spread would be of order 1.

Knowing that the basic building blocks of our hadronic world are quarks and gluons, we thus expect that for a proton projectile, we will have structure functions for quarks, antiquarks and gluons. We also naively expect the momentum sum rule

$$\int_0^1 dx \sum_i x f_i^{(p)}(x) = 1 , \quad (92)$$

because the total momentum of the incoming projectile must be conserved. We also expect that the proton flavour is conserved. Thus, for example

$$\int_0^1 dx \left(f_u^{(p)}(x) - f_{\bar{u}}^{(p)}(x) \right) = 2 . \quad (93)$$

Since we know that the proton is a relativistic system, we expect that a good fraction of its energy should be carried by the binding force, that is to say, by the gluons. Thus, the gluon pdf should be sizeable.

Based upon these assumptions, we can now compute various high energy processes involving hadrons in the initial state. The rules are simple: compute the cross section you are considering for colliding partons, and then assume that your hadron beam is a beam of partons, with momenta distributed according to the pdf's. Always neglect the transverse momenta of the partons, and their masses.

Let us now apply this model to Deep-Inelastic scattering. There we collide an electron with a proton. The kinematical variables of the process are usually defined as

$$q = k - k', \quad Q^2 = -q^2, \quad S = (k + p)^2, \quad x_{\text{Bj}} = \frac{Q^2}{2p \cdot q}, \quad y = \frac{p \cdot q}{k \cdot p}. \quad (94)$$

Experimentally, one measures S , y and x_{Bj} . One only needs to observe the outgoing electron to obtain these quantities. The process is an inclusive one, that is to say, no conditions are imposed on the hadronic final state. The variable y has a simple interpretation in the laboratory frame of a fixed target experiment: it is the fractional energy loss of the electron.

The corresponding partonic process is the scattering of a charged parton, that is to say a quark or an antiquark, with the electron. The cross section for this process is easily computed, by using the

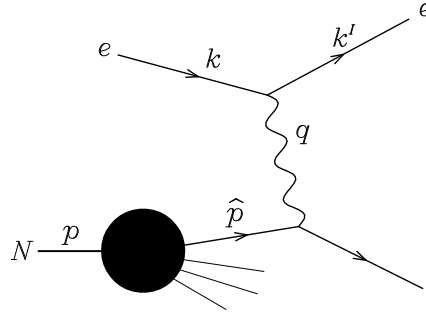


Fig. 17: DIS in the parton model.

standard Feynman rules of electrodynamics

$$\frac{d\hat{\sigma}_l}{d\hat{y}} = c_l^2 \frac{\hat{s}}{Q^4} 2\pi\alpha_{\text{em}}^2 (1 + (1 - \hat{y})^2) \quad (95)$$

where l runs over all quarks and antiquarks, and c_l is the corresponding electric charge. The kinematics is given by

$$\hat{p} = xp \quad \hat{s} = (k + \hat{p})^2 = 2k \cdot \hat{p}, \quad \hat{y} = \frac{\hat{p} \cdot q}{k \cdot \hat{p}}, \quad (\hat{p} + q)^2 = 2\hat{p} \cdot q - Q^2 = 0. \quad (96)$$

Observe that eq. 95 is a full cross section, properly normalized, divided by the appropriate flux factors. Now we write, according to the parton model, the hadronic cross section

$$\frac{d\sigma}{d\hat{y}} = \int dx \sum_l f_l(x) \frac{d\hat{\sigma}_l}{d\hat{y}}. \quad (97)$$

In order to obtain formula (97) we have only used the composition of probabilities, and the fact that cross sections are invariant for longitudinal boosts. We now observe that

$$y = \frac{p \cdot q}{k \cdot p} = \frac{\hat{p} \cdot q}{k \cdot \hat{p}} = \hat{y}, \quad x_{\text{Bj}} = \frac{Q^2}{2p \cdot q} = x \frac{Q^2}{2\hat{p} \cdot q} = x, \quad (98)$$

and thus we have

$$\frac{d\sigma}{dy dx_{\text{Bj}}} = \sum_l f_l(x) \frac{d\hat{\sigma}_l}{d\hat{y}} = \frac{2\pi\alpha_{\text{em}}^2 S x_{\text{Bj}}}{Q^4} (1 + (1-y)^2) \sum_l c_l^2 f_l(x_{\text{Bj}}). \quad (99)$$

Observe that y has a simple interpretation also in the centre-of-mass of the electron-quark system, where it is given by $y = (1 - \cos \theta_{\text{el}})/2$, and θ_{el} is the scattering angle of the electron in this frame.

In its simplicity, the parton model makes rather striking predictions. First of all, it shows that the DIS cross section scales with energy at fixed x_{Bj} and y . Furthermore, the y dependence of the cross section is fully predicted. As we will discuss further on, this y dependence is typical of vector interaction with fermions, and is thus direct evidence of the fact that charged partons are fermions (this is formally expressed by the so called Callan-Gross relation, as we will see in subsequent chapters).

The same type of reasoning can be applied also to other processes. For example, in a collision of two hadrons, a quark from one hadron may annihilate with an antiquark from the other hadron, and produce a lepton-antilepton pair, provided there are enough antiquarks in the projectile, like in pion-nucleon collisions, or in proton-antiproton collisions. This is the so-called Drell-Yan process. Its parton

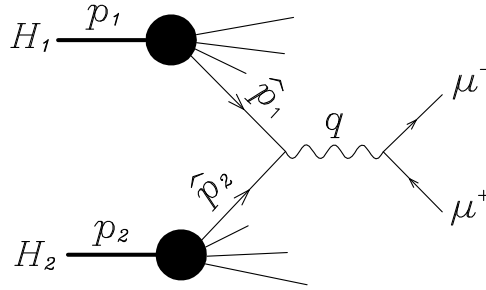


Fig. 18: Drell-Yan pair production in the parton model.

model interpretation is illustrated in fig. 18. As before, we define the partonic variables:

$$\hat{p}_1 = x_1 p_1, \quad \hat{p}_2 = x_2 p_2, \quad S = (p_1 + p_2)^2 = 2 p_1 p_2, \quad Q^2 = q^2 = 2 x_1 x_2 S. \quad (100)$$

The partonic cross section is given by

$$\hat{\sigma}_l^{(\text{DY})} = c_l^2 \frac{4\pi\alpha_{\text{em}}}{9Q^2}, \quad (101)$$

which is very similar to the cross section for $e^+e^- \rightarrow \mu^+\mu^-$, except for an extra factor of $1/3$ ¹. According to the parton model interpretation, the hadronic cross section is

$$\sigma^{(\text{DY})} = \sum_l \int dx_1 dx_2 \left(f_l^{(H_1)}(x_1) f_{\bar{l}}^{(H_2)}(x_2) + (l \leftrightarrow \bar{l}) \right) c_l^2 \frac{4\pi\alpha_{\text{em}}}{9Q^2}, \quad (102)$$

for $Q^2 = \hat{s} = x_1 x_2 S$. The validity of the above formula is restricted to the range where Q^2 is large. It is therefore usually written as

$$\frac{d\sigma^{(\text{DY})}}{dQ^2} = \sum_l \int dx_1 dx_2 \left(f_l^{(H_1)}(x_1) f_{\bar{l}}^{(H_2)}(x_2) + (l \leftrightarrow \bar{l}) \right) \delta(x_1 x_2 S - Q^2) c_l^2 \frac{4\pi\alpha_{\text{em}}}{9Q^2}. \quad (103)$$

¹This comes from the colour average for the initial state quark. Its physical meaning is that, in the average, the probability for the colour of the initial quark to match that of the antiquark is $1/3$.

Pushing further our parton model interpretation of hard scattering processes, we can go on and compute the cross section for producing high transverse momentum jets, of heavy $b\bar{b}$ pairs, of $t\bar{t}$ pairs, and so on. In these processes, also gluons could enter in the initial state.

Not all hadronic processes can be computed in this way. For example, Drell-Yan cross sections, for Q^2 approaching typical hadronic scales, cannot be computed. The rule of thumb for deciding if a process is a hard process or not, in the context of the parton model, is to ask whether it is insensitive to the initial transverse momentum of the partons, which is of the order of typical hadronic scales. The parton densities do not carry any information about this quantity.

5.2 Does the Parton Model survive radiative corrections?

We will now try to add perturbative QCD corrections to the Parton Model. As in the case of $e^+e^- \rightarrow$ hadrons, we will find soft and collinear singularities associated to radiation of gluons from final state partons, which we expect to cancel for appropriately defined final states. This is the case, for example, in fully inclusive hadronic final states, like in DIS or in Drell-Yan pair production, or in the production of Serman-Weinberg jets.

A new element that can arise in the case of reactions initiated by hadrons, is the appearance of initial state soft and collinear singularities. We will show that initial state collinear singularities cannot possibly cancel, and thus spoil the Parton Model interpretation of hard processes. Let us thus consider a generic hard process initiated by a hadron, and its parton cross section, which we assume for simplicity to be initiated by a quark



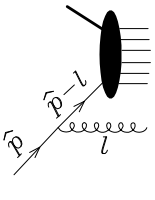
$$= \mathcal{M}(\hat{p})u(\hat{p}) . \quad (104)$$

Here \mathcal{M} indicates the amplitude for the process, and u is the Dirac spinor. All the complexity of the process is hidden in \mathcal{M} , and we don't care about it for the moment. The cross section is obtained by squaring the amplitude, averaging over the initial state spin and colors, and dividing by the appropriate flux factors

$$\sigma^{(0)}(\hat{p}) = \frac{N}{\hat{p}^0} \mathcal{M}(\hat{p}) \frac{1}{2} \sum u(\hat{p})\bar{u}(\hat{p}) \mathcal{M}^\dagger(\hat{p}) = \frac{N}{\hat{p}^0} \mathcal{M}(\hat{p}) \frac{\not{\hat{p}}}{2} \mathcal{M}^\dagger(\hat{p}) \quad (105)$$

where N is whatever normalization factor arises from the rest of the amplitude.

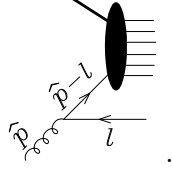
We want to focus upon the initial state corrections



$$= g_s \mathcal{M}(\hat{p}-l) \frac{\not{\hat{p}}-\not{l}}{(\hat{p}-l)^2} \gamma^\mu u(\hat{p}) \epsilon_\mu(l) , \quad (106)$$

where $\epsilon_\mu(l)$ is the polarization vector of the final gluon. We also observe that this may not be the only

correction of order α_s . One may also have a process in which an initial gluon splits into a quark-antiquark pair, and the generated quark gives rise to the reaction



We will assume that this complication does not occur. For example, we may assume that the hard cross section measures some effect due to the difference of the quark content for two different flavours. Since the gluon produces equal number of quarks for all flavours, it could not contribute in this case. In these cases, one says that the cross section is only sensitive to the *non-singlet* component of the parton densities. We thus concentrate on the non-singlet case now. Further on we will describe how to treat the general case.

Experience with the e^+e^- case tells us that as l becomes parallel to \hat{p} we will have a collinear singularity. It is convenient thus to write l in the following way

$$l = (1 - z)\hat{p} + l_{\perp} + \xi\eta \quad (107)$$

where η is an arbitrary vector such that $\eta^2 = 0$ and $\eta \cdot \hat{p} \neq 0$. For example, in the centre-of-mass frame of the collision process we can choose

$$\hat{p} = (\hat{p}^0, 0_{\perp}, \hat{p}^0), \eta = (1, 0_{\perp}, -1). \quad (108)$$

The phase space for the emission of the gluon is

$$\begin{aligned} \frac{d^3l}{2l^0(2\pi)^3} &= \frac{d^4l}{(2\pi)^4} 2\pi \delta(l^2) = \frac{\hat{p} \cdot \eta d\xi dz d^2l_{\perp}}{(2\pi)^3} \delta(2\hat{p} \cdot \eta(1 - z)\xi - |l_{\perp}^2|) \\ &= \frac{d^2l_{\perp}}{2(2\pi)^3} \frac{dz}{1 - z}. \end{aligned} \quad (109)$$

which yields, from the on-shell condition for the gluon,

$$\xi = \frac{|l_{\perp}^2|}{2\hat{p} \cdot \eta(1 - z)} \quad \text{and} \quad (\hat{p} - l)^2 = -\frac{|l_{\perp}^2|}{1 - z}. \quad (110)$$

The most singular part of this cross section can be obtained similarly with what was done in the case of e^+e^- annihilation. It does not make much sense, in this case, to assume that l is small, and thus the derivation is a little bit more involved. It is nevertheless instructive, so I will report it in the next subsection. People who are willing to accept the result without discussion, can skip it.

5.3 Derivation of the singular part of the cross section

The amplitude in eq. (106), using our kinematic definitions, can be written as

$$g_s \mathcal{M}(\hat{p} - l) \frac{\not{\hat{p}} - \not{l}}{-|l_{\perp}^2|/(1 - z)} \gamma^{\mu} u(\hat{p}) \epsilon_{\mu}(l). \quad (111)$$

When squared, it seems to give rise to terms of order $1/l_{\perp}^4$. We will see that these terms, however, cancel. The trick is to make careful use the relation $l^{\mu} \epsilon_{\mu}^{(i)}(l) = 0$. The singular region is the one when l is collinear to \hat{p} , that is to say when l_{\perp} vanishes. In this region $l \approx (1 - z)p$, and thus $p \approx l/(1 - z)$, up

to small corrections. Inserting this expression for p in eq. (111) will lead to simple Dirac algebra, since by anticommuting l with γ^μ we get l^μ , which vanishes when dotted into the polarization. We thus write

$$p = \frac{l - l_\perp - \xi\eta}{1 - z} \quad (112)$$

and replace it in eq. (111). The term in ξ kills the singularity, and we drop it, since we are only interested in the singular part. We obtain

$$g_s \mathcal{M}(\hat{p} - l) \frac{z\not{l} - \not{l}_\perp}{-|l_\perp^2|} \gamma^\mu u(\hat{p}) \epsilon_\mu(l), \quad (113)$$

which becomes

$$\begin{aligned} & g_s \mathcal{M}(\hat{p} - l) \frac{-z\gamma_\mu \not{l} - \not{l}_\perp \gamma_\mu}{-|l_\perp^2|} u(\hat{p}) \epsilon_\mu(l) \\ &= g_s \mathcal{M}(\hat{p} - l) \frac{-z\gamma_\mu [(1-z)\not{p} + \not{l}_\perp] - \not{l}_\perp \gamma_\mu}{-|l_\perp^2|} u(\hat{p}) \epsilon_\mu(l) \end{aligned} \quad (114)$$

$$\begin{aligned} &= g_s \mathcal{M}(\hat{p} - l) \frac{-z\gamma_\mu \not{l}_\perp - \not{l}_\perp \gamma_\mu}{-|l_\perp^2|} u(\hat{p}) \epsilon_\mu(l), \\ &= g_s \mathcal{M}(\hat{p} - l) \frac{-2z l_\perp^\mu - (1-z)\not{l}_\perp \gamma_\mu}{-|l_\perp^2|} u(\hat{p}) \epsilon_\mu(l), \end{aligned} \quad (115)$$

where the first step is obtained by anticommuting \not{l} and γ^μ , which we can do as explained before. Then we rewrite l in terms of p . Next, we drop the \not{p} term, since it is in front of the spinor $u(\hat{p})$, and thus gives zero, according to the Dirac equation. Finally, we use the anticommutation relation $\gamma_\mu \not{l}_\perp = -\not{l}_\perp \gamma_\mu + 2l_\perp^\mu$. In this last form, the singularity appears to be at most of order $1/|l_\perp|$, so that the amplitude squared will give at most a $1/|l_\perp^2|$ singularity. The rest is simple algebra. We square eq. (115), replace the gluon spin sum with the transverse projector $-g_{\mu\nu}^\perp$, replace the fermion spin averaged product $u(\hat{p})\bar{u}(\hat{p})$ with $\hat{p}/2$, and obtain

$$\begin{aligned} & g_s^2 \frac{1}{l_\perp^4} \mathcal{M}(\hat{p} - l) (-2z l_\perp^\mu - (1-z)\not{l}_\perp \gamma^\mu) \frac{\not{p}}{2} (-2z l_\perp^\nu - (1-z)\gamma^\nu \not{l}_\perp) (-g_{\mu\nu}^\perp) \mathcal{M}^\dagger(\hat{p} - l) \\ &= g_s^2 \frac{1}{l_\perp^4} \mathcal{M}(\hat{p} - l) \frac{\not{p}}{2} (4z^2 |l_\perp^2| + 4z(1-z) |l_\perp^2| + 2(1-z)^2 |l_\perp^2|) \mathcal{M}^\dagger(\hat{p} - l) \\ &= g_s^2 \frac{2}{|l_\perp^2|} (1+z^2) \mathcal{M}(\hat{p} - l) \frac{\not{p}}{2} \mathcal{M}^\dagger(\hat{p} - l). \end{aligned} \quad (116)$$

To get the cross section, we should multiply the above expression by N/\hat{p}^2 , and integrate over the phase space. We obtain

$$\sigma^{(1)} = \frac{\alpha_s C_F}{2\pi} \int \sigma^{(0)}(zp) \frac{1+z^2}{1-z} \frac{dl_\perp^2}{l_\perp^2} dz. \quad (117)$$

where

$$\sigma^{(0)}(zp) = N \mathcal{M}(\hat{p} - l) \frac{\not{p} - \not{l}}{2(\hat{p} - l)^0} \mathcal{M}^\dagger(\hat{p} - l) = N \mathcal{M}(\hat{p} - l) \frac{\not{p}}{2(\hat{p})^0} \mathcal{M}^\dagger(\hat{p} - l). \quad (118)$$

where we have made use of the relation $g_s^2 = 4\pi\alpha_s$. The factor $C_F = 4/3$ arises from the colour algebra. It can be obtained according to the colour Feynman rules of fig. 3, as illustrated in the graphic equation

$$\frac{1}{2} \left(\begin{array}{c} \text{diagram 1} \\ \text{diagram 2} \end{array} \right). \quad (119)$$

There we see a factor of 3 arising in the first term, because of the sum over the colour entering the Born amplitude, and a factor of 3 in the second because of the colour loop, the net effect being $(3 + 1/3)/2 = 4/3$.

The result obtained so far arises from the real emission of a gluon. Virtual corrections are also present, i.e. a gluon can be emitted and reabsorbed by the same line.

5.4 Effects due to the emission of a collinear gluon

The final result is

$$\sigma^{(1)} = \frac{\alpha_S C_F}{2\pi} \int \left[\sigma^{(0)}(z\hat{p}) - \sigma^{(0)}(\hat{p}) \right] \frac{1+z^2}{1-z} \frac{dl_{\perp}^2}{l_{\perp}^2} dz, \quad (120)$$

where the second term in squared parenthesis is due to the virtual corrections. We see that there is a singularity at $z = 1$ which cancels between real and virtual corrections. The region $z \rightarrow 1$ corresponds to soft gluon emission. Thus, soft singularities cancel. There are also collinear singularities, associated to the small l_{\perp} region. These do not cancel.

We first make the following remark. In the initial amplitudes, the presence of a denominator of the form $1/l_{\perp}^2$ may seem to give rise to divergences like d^2l_{\perp}/l_{\perp}^4 . The singularity we find at the end is instead weaker, of order d^2l_{\perp}/l_{\perp}^2 , because of an l_{\perp}^2 we find from the numerator algebra. We can easily convince ourselves that this is a consequence of angular momentum conservation. Vector interaction, in fact, do not change the helicity of a particle. Thus the helicity of the incoming quark must be equal to the that of the outgoing quark. On the other hand, physical gluons have ± 1 helicity. Thus, in the collinear limit, the total angular momentum contributed by spin is not conserved. This gives rise to the extra l_{\perp}^2 suppression in the cross section. Also, by dimensional analysis, we see that we cannot expect divergences stronger than d^2l_{\perp}/l_{\perp}^2 in theories with dimensionless coupling constants.

In the case of $e^+e^- \rightarrow$ hadrons, we made the approximation that $z \approx 1$, for simplicity. If we had been more careful, instead of formula (75), we would have obtained a formula similar to eq. (120). There would be, however, a very important difference: in the Born cross section for the real emission, under the integral sign, we would have $\sigma^{(0)}(\hat{p})$ instead of $\sigma^{(0)}(z\hat{p})$. This property is characteristic of splitting processes taking place in the final state, rather than in the initial state. Figure 19 illustrate this fact. This

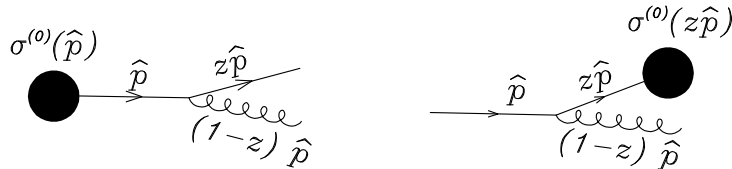


Fig. 19: Collinear processes in the final and in the initial state.

is the reason why collinear singularities cancel in the $e^+e^- \rightarrow$ hadrons case, and do not cancel in this case.

Equation (120) exhibit a rather intuitive property of collinear emission. Since the singularities are due to the fact that the intermediate propagator goes near its mass shell, the intermediate particle travels for a relatively long time and distance. Thus, when it initiates the interaction, it behaves essentially like an on-shell particle, and the phenomenon can be described in probabilistic terms. In other words, the total amplitude squared for the splitting process and the hard scattering, becomes the product of the square of the amplitude for the splitting process, times the square of the amplitude for the hard scattering (i.e., the cross section).

The l_{\perp}^2 integral is divergent in the lower limit. Its upper limit is instead some scale, of the order of the typical momenta involved in the hard process, which we now call Q . Equation (120) can then be

interpreted intuitively in the following way. In a hard process, taking place in a time of order $1/Q$ (by the Heisenberg indeterminacy principle), an incoming parton is also probed for a time of order $1/Q$. In a short period of time, a quantum state may fluctuate into states to which it couples, even if they have energies that differ by an amount of order Q or less. This is what happens to our incoming quark. This also explain why the larger is Q , the more likely is the splitting to take place.

5.5 Failure of the parton model

The presence of collinear divergences tells us that there must be something wrong with the parton model. Of course, we know that divergences, in the real physical world, are never there. In our case, for example, if we introduce the mass of the quark, the divergence goes away. Or, we may use the known fact that at low scale confinement effects take place, and thus put a lower cutoff of order Λ in the transverse momentum integral. Or again, we may remember that the parton is off-shell in the incoming nucleon, by an amount of order Λ . This also would act as a cut-off. However, neither of these remedies would really solve the problem. Our cross section would become strongly dependent upon low energy details, like the quark mass, the off-shellness in the nucleon, or confinement effects, while the Parton Model assumes that these details do not count. Furthermore, the physics of these details is low scale physics, and is thus uncalculable in perturbative QCD.

We will now show that, in spite of the collinear divergences, the Parton Model can be rescued, provided we accept to make some modifications to the original concept.

We begin by introducing some notation. First of all we define

$$P_{qq}^{(0)}(z) = C_F \left(\frac{1+z^2}{1-z} \right)_+ \quad (121)$$

where the notation with the $+$ suffix is called the *plus prescription*. It specifies that the expression in parenthesis is to be interpreted as a distribution, and its integral against a smooth function $f(z)$ is given by

$$\int_0^1 \left(\frac{1+z^2}{1-z} \right) f(z) dz = \int_0^1 \frac{1+z^2}{1-z} (f(z) - f(1)) . \quad (122)$$

We then introduce an infrared cutoff λ , and rewrite formula 120 as

$$\sigma^{(1)} = \frac{\alpha_S}{2\pi} \log \frac{Q^2}{\lambda^2} \int dz P_{qq}^{(0)}(z) \sigma^{(0)}(z\hat{p}) , \quad (123)$$

where Q is a characteristic scale in the process. Since The corrected partonic cross section can be written as

$$\sigma(\hat{p}) = \sigma^{(0)}(\hat{p}) + \sigma^{(1)}(\hat{p}) = \int dz \Gamma_{qq}(z, Q^2) \sigma^{(0)}(z\hat{p}) \quad (124)$$

where

$$\Gamma_{qq}(z, Q^2) = \delta(1-z) + \frac{\alpha_S}{2\pi} \log \frac{Q^2}{\lambda^2} P_{qq}^{(0)}(z) . \quad (125)$$

The form of equation (124) hints to a possible way to resque the parton model approach. In fact, it has the form of the parton model cross section, except for the Q^2 dependence. It is telling us that we should consider a parton as having a structure, that depends upon the scale at which we are probing it. This becomes even more apparent if we insert the corrected formula in the parton model formula for the hadronic cross section. We just replace $\hat{p} = yp$, multiply by the parton density $f_q(y)$ and integrate in y :

$$\sigma(p) = \int dy dz f_q(y) \Gamma_{qq}(z, Q^2) \sigma^{(0)}(zyp) . \quad (126)$$

This formula represents the probability to find parton q in the hadron, with a fraction y of its momentum, times the probability to find parton q in parton q with a fraction z of its momentum times the cross

section for the final parton, with momentum yzp . It is natural to think that if we have an object that can be represented as a beam of constituents, and the constituents can be represented as a beam of subconstituents, the same object can be represented as a beam of subconstituents. Mathematically this works as follows. We insert the identity $\int dx \delta(x - yz)$ in equation 126, and obtain

$$\sigma(p) = \int dx \tilde{f}_q(x, Q^2) \sigma^{(0)}(xp) . \quad (127)$$

where we have defined

$$\tilde{f}_q(x, Q^2) = \int dy dz f_q(y) \Gamma_{qq}(z, Q^2) \delta(x - zy) . \quad (128)$$

We are getting closer and closer to the improved parton model formula. In fact, if instead of using the process scale Q we introduce an intermediate scale μ , the connection becomes even clearer. We can write

$$\sigma(p) = \int dx \tilde{f}_q(x, \mu^2) \hat{\sigma}(xp, \mu^2) , \quad (129)$$

where

$$\hat{\sigma}(\hat{p}) = \sigma^{(0)}(\hat{p}) + \frac{\alpha_s}{2\pi} \log \frac{Q^2}{\mu^2} \int dz P_{qq}^0(z) \sigma^{(0)}(z\hat{p}) . \quad (130)$$

Equation (129) is easily verified by expanding the product of \tilde{f} and $\hat{\sigma}$, neglecting terms of order α_s^2 , and combining the logarithms according to the equation $\log \mu^2/\lambda^2 + \log Q^2/\mu^2 = \log Q^2/\lambda^2$. It is the QCD-improved parton model formula we were seeking, and it forms the basis for the application of perturbative QCD to phenomena initiated by hadrons. A considerable difference with the “naive” Parton Model formula is the appearance of a scale μ in the parton densities.

Let us summarize we have done so far. We have attempted to compute radiative corrections to a parton process. We have found that these corrections are large, and depend upon unknown low scale dynamics, which is represented here by the cutoff λ . However, we have found that these large corrections can be absorbed into a redefinition of the parton densities. The parton densities redefinition does not depend upon the hard process in question: it is universal. The physical cross section can then be defined in terms of these new parton densities. Instead of the partonic cross section, in the QCD-improved parton model formula we have a so called *short distance* cross section $\hat{\sigma}$. This is obtained by subtracting the infrared sensitive (or *long distance*) part from the partonic cross section. Thus, the short-distance cross section is controlled by high momenta, and is thus calculable in perturbation theory. It is important to choose the scale μ of the order of the scale Q of the hard process, in order to avoid the appearance of large logarithms in the perturbative expansion.

Of course, our argument was only carried out at leading order in perturbation theory. There is a variety of more complex arguments that show that formula (87) actually holds to all order in perturbation theory. This is called the *Factorization Theorem* [40]. We will comment later on its present status. For now, we will assume that the procedure outlined above can in fact be carried out to all orders in the coupling constant. Thus, the short-distance cross section can be given as a power expansion in α_s . If the scale at which α_s is evaluated is near the typical scale of the hard process, no large logarithms can appear in the coefficients of the expansion, since all the scales entering in the coefficients are of the same order. Thus, one can improve the accuracy of the short distance cross section by computing higher and higher orders in perturbation theory. The scale μ introduced in this context is called the factorization scale. The scale at which α_s is evaluated is the renormalization scale, and should be of the same order as the factorization scale. In principle, they can be taken to be different. Here, for simplicity, I will always assume that the renormalization and factorization scales are taken equal.

The new pdf $\tilde{f}(\mu)$ contains uncalculable long distance effects. It has to be measured, by using formula (87) with some reference hard process, which is typically chosen to be DIS. One then extracts

$f(\mu)$ at a given scale μ . Its μ dependence is however calculable. In fact, taking the derivative of eq. (128) we get

$$\begin{aligned} \frac{\partial}{\partial \log \mu^2} \tilde{f}_q(x, \mu^2) &= \int dy dz f_q(y) \frac{d\Gamma_{qq}(z, \mu^2)}{d \log \mu^2} \delta(x - zy) \\ &= \frac{\alpha_s}{2\pi} \int dy dz f_q(y) P_{qq}^0(z) \delta(x - zy) \\ &= \frac{\alpha_s}{2\pi} \int dy dz \tilde{f}_q(y, \mu^2) P_{qq}^0(z) \delta(x - zy) + \mathcal{O}(\alpha_s^2), \end{aligned} \quad (131)$$

where we have used eq. 125, and dropped higher order terms in α_s in order to identify f with \tilde{f} in the last step.

Equation (131) is the Altarelli–Parisi (AP) equation (or Dokshitzer–Gribov–Lipatov–Altarelli–Parisi equation) for the non-singlet case. It is also commonly written in the form

$$\frac{\partial}{\partial \log \mu^2} f_q(x, \mu^2) = \frac{\alpha_s}{2\pi} \int_x^1 \frac{dy}{y} f_q(y, \mu^2) P_{qq}^0(x/y), \quad (132)$$

where we have dropped the tilde sign, since the “naive” parton density disappears in the improved parton model approach.

The AP equation allows us to compute the parton densities at any scale, once we have measured them at an initial scale. Thus, in the improved parton model, predictivity is not lost. As before, the measurement of the pdf’s in one process (at one scale) allows one to extend the computation to any scale.

5.6 The evolution equations in the general case

We introduce the following symbolic notation for the AP equation

$$\mu^2 \frac{\partial}{\partial \mu^2} f_i(\mu) = \sum_j P_{ij} \otimes f_j(\mu), \quad (133)$$

where the \otimes product is defined as

$$f_1 \otimes f_2 \otimes \dots \otimes f_n(x) = \int_0^1 dx_1 dx_2 \dots dx_n f_1(x_1) f_2(x_2) \dots f_n(x_n) \delta(x - x_1 x_2 \dots x_n). \quad (134)$$

We have

$$P_{ij}(y) = \frac{\alpha_s(\mu)}{2\pi} P_{ij}^{(0)}(y) + \left(\frac{\alpha_s(\mu)}{2\pi} \right)^2 P_{ij}^{(1)}(y) + \dots \quad (135)$$

where the $P_{ij}^{(0)}(y)$ are given in ref. [37], and the $P_{ij}^{(1)}(y)$ in [38, 39]. The terms of order α_s^3 are not yet known exactly, although recently approximate expressions have become available [41], based upon some partial results [42] [43]. Work on an exact calculation is under way [44].

We report below the formulae for the $P_{ij}^{(0)}(y)$. Its only non-vanishing components are

$$P_{qq}^{(0)}(x) = P_{\bar{q}\bar{q}}^{(0)}(x) = C_F \left(\frac{1+x^2}{1-x} \right)_+, \quad (136)$$

$$P_{qg}^{(0)}(x) = P_{\bar{q}g}^{(0)}(x) = T_F (x^2 + (1-x)^2), \quad (137)$$

$$P_{gq}^{(0)}(x) = P_{g\bar{q}}^{(0)}(x) = C_F \frac{1+(1-x)^2}{x}, \quad (138)$$

$$P_{gg}^{(0)}(x) = 2C_A \left[z \left(\frac{1}{1-z} \right)_+ + \frac{1-z}{z} + z(1-z) + \left(\frac{11}{12} - \frac{n_f}{6C_A} \right) \delta(1-x) \right] \quad (139)$$

For a derivation of the above formulae similar to the one given in subsection 5.3, the reader can look in Appendix B of ref. [45]. For a more intuitive (although less conventional) derivation, the reader can look directly in the original Altarelli-Parisi paper [37].

We do not report here the higher order $P_{ij}^{(1)}(y)$ functions. Observe, however, that at higher orders the components $P_{q_i q_j}$ for $i \neq j$ and $P_{q_i \bar{q}_j}$ (for any i and j) do arise. Here we limit our discussion, for simplicity, to leading order evolution only.

We begin by taking the difference of eq. (133) with itself, for two different quark or antiquark flavour labels i and j . We find

$$\mu^2 \frac{\partial}{\partial \mu^2} (f_i(\mu) - f_j(\mu)) = \sum_k (P_{ik} \otimes f_k(\mu) - P_{jk} \otimes f_k(\mu)) . \quad (140)$$

As discussed earlier, if i is a quark (or antiquark), then k can only be the same quark (or antiquark) or a gluon. The gluon contribution cancels among the two terms in parenthesis, and one gets

$$\mu^2 \frac{\partial}{\partial \mu^2} (f_i(\mu) - f_j(\mu)) = P_{qq} \otimes (f_i(\mu) - f_j(\mu)) . \quad (141)$$

Thus, if we have n_f light flavours, there are $2n_f - 1$ independent combinations of the parton densities that evolve independently from each others. They are called non-singlet components. Next, we take the sum of eq. (133) for all quark flavours and antiflavours. We get

$$\begin{aligned} \sum_{i \neq g} \frac{\partial}{\partial \mu^2} f_i(\mu) &= \sum_{i \neq g} P_{ik} \otimes f_k(\mu) = \sum_{i \neq g} \sum_{k \neq g} P_{ik} \otimes f_k(\mu) + \sum_{i \neq g} P_{ig} \otimes f_g(\mu) \\ &= P_{qq} \otimes \sum_{i \neq g} f_i(\mu) + 2n_f P_{ig} \otimes f_g(\mu) . \end{aligned} \quad (142)$$

On the other hand, eq. (133) for the gluon reads

$$\frac{\partial}{\partial \mu^2} f_g(\mu) = \sum_i P_{gi} \otimes f_i(\mu) = \sum_{i \neq g} P_{gi} \otimes f_i(\mu) + P_{gg} \otimes f_g(\mu) . \quad (143)$$

Thus, defining

$$S(\mu) = \sum_{i \neq g} f_i(\mu) , \quad (144)$$

we get the system of equations

$$\begin{aligned} \mu^2 \frac{\partial}{\partial \mu^2} f_g(\mu) &= P_{gq} \otimes S(\mu) + P_{gg} \otimes f_g(\mu) \\ \mu^2 \frac{\partial}{\partial \mu^2} S(\mu) &= P_{qq} \otimes S(\mu) + 2n_f P_{ig} \otimes f_g(\mu) , \end{aligned} \quad (145)$$

which define the evolution of the so called *singlet* component S and the gluon. Thus, while the non-singlet components evolve independently, the singlet component mixes with the gluon density in its evolution.

5.7 Sum rules

We said earlier that we expect our parton densities to satisfy certain sum rules. Thus, for example

$$\int dx \left[f_u^{(p)}(x) - f_{\bar{u}}^{(p)}(x) \right] = 2 . \quad (146)$$

We must make sure that evolution equations do not spoil the sum rules. Since the difference of the quark and antiquark parton densities is a non-singlet component, we have

$$\begin{aligned} \mu^2 \frac{\partial}{\partial \mu^2} \int dx \left[f_u^{(p)}(x) - f_{\bar{u}}^{(p)}(x) \right] &= \int dx \frac{\alpha_S}{2\pi} P_{qq}(y) \left[f_u^{(p)}(z) - f_{\bar{u}}^{(p)}(z) \right] \delta(x - yz) dy dz \\ &= \frac{\alpha_S}{2\pi} \left[\int P_{qq}(y) dy \right] \int dz \left[f_u^{(p)}(z) - f_{\bar{u}}^{(p)}(z) \right] = 0 \end{aligned} \quad (147)$$

because $\int P_{qq}(y) dy = 0$. Similarly, one can show that the momentum sum rule is also preserved by evolution.

5.8 Scheme dependence

There is some ambiguity in the way one defines the parton densities, This ambiguity is best seen as an ambiguity in the type of infrared cutoff one uses. For example, one could give a mass to the quark, or assume it is slightly off-shell. By doing this, the large logarithm does not change, but different finite pieces can arise in the calculation. In the present context we have only looked at the divergent parts. When doing next-to-leading QCD calculation, however, one would like to compute precisely the finite pieces. The reader can find interesting examples in ref. [46, 47] and [48]. There the same processes are computed (the Deep-Inelastic and the Drell-Yan cross section), but with different infrared cutoffs. Thus, the finite terms in the various cross sections turn out to be different. However, when expressing the DY cross section in terms of the DI cross section, both approaches yield the same formula. Thus, to some extent, the definition of the parton density is a matter of convention, like the definition of α_S . It has to be specified together with a procedure for the computation of short distance cross section. Today, the so called $\overline{\text{MS}}$ scheme is widely used, and most parton densities are given in the $\overline{\text{MS}}$ scheme.

5.9 Summary

We summarize what we have learned in this chapter.

First of all, by intuitive reasoning, we derived cross sections for high energy inclusive processes, assuming that the transverse momentum of constituents in hadrons was limited to typical hadronic scales.

We tried to compute radiative corrections to these formulae, and we found inconsistencies, i.e. uncancelled collinear divergences.

With a procedure very similar to renormalization, we showed that the collinear divergences can be factorized into the parton densities.

Let us discuss how is the procedure of factorization similar to renormalization. In renormalization, we hide our ignorance of UV effects into a redefinition of the strong coupling constant. Here, we hide our inability to compute IR effects into a redefinition of the parton densities.

As a result of this procedure, we find that the parton densities are actually scale dependent. We may think of a hard process as a probe of transverse dimensions and time of order $1/Q$. When we probe a constituent at higher and higher values of Q , that is to say for shorter and shorter time, because of the uncertainty principle, we may find it fluctuating into a virtual pair of constituents off the energy shell by an amount of order Q . The larger is Q the larger is the phase space for virtual particles. This is why parton densities evolve with the scale at which they are measured.

The original assumption of limited transverse momenta fails in the parton model. We have seen, in fact, that because of initial state radiation, integrals of the form $d^2 l_{\perp} / l_{\perp}^2$ arise. Roughly, we expect

$$\langle l_{\perp}^2 \rangle \approx \alpha_S \int \frac{d^2 l_{\perp}}{l_{\perp}^2} l_{\perp}^2 \approx \alpha_S Q^2 . \quad (148)$$

Thus the transverse momentum is not limited, but it is ‘‘perturbatively’’ small, i.e. it is suppressed by a coupling constant factor.

5.10 How solid is the Factorization Theorem?

The argument given in this chapter does not certainly pretend to be fully convincing. Thus, we would like to have a more solid proof of this theorem.

In the case of the DIS process, such proof exists. It relies upon a clever analytic continuation property of the DIS cross section, that can be used to apply the powerful language of the operator-product expansion (O.P.E.) to the problem.

For production processes in hadronic collisions, things are much more difficult. Even in the simplest case, the Drell-Yan process, the factorization theorem has a long controversial history, which was finally settled by the calculation of Lindsay, Ross and Sachrajda [49, 50, 51]. All-order arguments for factorization have been given in ref. [52]. Today, the factorization theorem is widely accepted in the high energy physics community.

6 DEEP INELASTIC SCATTERING

Deep-Inelastic Scattering (DIS) is the next-to-simplest QCD process after e^+e^- annihilation into hadrons. It is experimentally quite simple, since in order to define the DIS cross section one does not need to introduce jet definitions. It is enough to measure the momentum of the outgoing lepton in order to characterize the final state.

Deep-Inelastic scattering is also the best place where to measure structure functions, as can be seen from eq. (99). Thus, QCD predictions for hadronic collisions rely upon the experimental determination of structure functions performed at DIS experiments.

From a theoretical point of view, DIS (like $R_{e^+e^-}$) has also a privileged status. There are in fact good reasons to believe that power corrections in DIS processes behave like $1/Q^2$. This is unlike (for example) jets in e^+e^- annihilation, where one expects corrections of the order of $1/Q$. Thus, DIS is a good place where to measure α_s .

The most general form of the DIS cross section for electromagnetic processes is given by

$$\frac{d\sigma}{dx dy} = \frac{4\pi\alpha_{\text{em}}^2(S-M)^2}{Q^4} \left[\left(1 - y - \frac{xyM^2}{S-M^2} \right) F_2(x, Q^2) + y^2 x F_1(x, Q^2) \right], \quad (149)$$

where F_2 and F_1 are called the structure functions for DIS, y corresponds to the variables defined previously, M is the mass of the target nucleon and $x = x_{\text{Bj}}$. I will not illustrate the derivation of this formula, which is found in many textbooks. It is a simple consequence of electrodynamics at the lowest order in α_{em} , and of Lorentz invariance. It does not, therefore, contain any dynamical consequence of strong interactions, aside from its symmetry properties. From formula (99), and after what we have said in the previous chapter with regard to the factorization theorem, we can now write down the leading order, QCD-improved parton model formula for DIS

$$\frac{d\sigma}{dy dx} = \frac{2\pi\alpha_{\text{em}}^2 S x_{\text{Bj}}}{Q^4} (1 + (1-y)^2) \sum_l c_l^2 f_l(x, Q). \quad (150)$$

In order to have leading order accuracy, it is sufficient to choose $\mu \approx Q$. For simplicity, I have chosen $\mu = Q$. From eqs. (149) and (150), neglecting mass effects, we find

$$F_2(x, Q) = 2xF_1(x, Q), \quad (151)$$

which is the so-called Callan-Gross relation, and

$$F_2(x, Q) = x \sum_l c_l^2 f_l(x, Q). \quad (152)$$

The Callan–Gross relation is a prediction of the parton model, and it is a consequence of the fact that the only charged partons are fermions. It is however only a leading order prediction. When radiative corrections are included, it is violated. One defines $F_L = F_2 - 2xF_1$.

It is useful to focus now upon the y dependence of the parton model formula. We have

$$y = \frac{\hat{p} \cdot q}{\hat{p} \cdot k} = 1 - \frac{\hat{p} \cdot k'}{\hat{p} \cdot k} = \frac{1 - \cos \theta}{2}, \quad (153)$$

and thus y is related to the electron scattering angle θ in the CM frame of the electron-parton collision (sometimes called the partonic CM frame).

The scattering of the lepton on a quark of the same helicity, gives rise to a y dependence proportional to 1, while in the case of a quark of different helicity, the y dependence is $(1 - y)^2$. Thus, in the case of spin-averaged cross sections in electromagnetism, the y dependence is $1 + (1 - y)^2$. The verification of these properties is a simple exercise with Feynman graphs.

The vanishing of the cross section in the backward limit (i.e. $y = 1$) for the quarks and lepton with opposite helicity has a simple intuitive explanation. The spins of the lepton and the quark are aligned, since their helicities are opposite, and their momenta are opposite. Thus, they have a total angular momentum 1 in the collision direction. Vector interactions conserve helicities. Thus, the quark and lepton will have the same helicity after the interaction. In the case of backward scattering, however, they have opposite momentum, and thus they have opposite total spin. Thus, conservation of angular momentum imposes the vanishing of the backward cross section, which is what the $(1 - y)^2$ dependence predicts.

Parity violating processes contribute anti-symmetrically in the exchange of the helicity of the incoming lepton. We expect a $(1 - (1 - y)^2) = 2(y - y^2/2)$ dependence to be present in this case. Thus, a third structure function appears. For example, in neutrino charged current DIS (i.e. $\nu_\mu N \rightarrow \mu^- X$ or $\bar{\nu}_\mu N \rightarrow \mu^+ X$) we have

$$\begin{aligned} \frac{d\sigma}{dx dy} = & \frac{G_F^2(S - M^2)}{2\pi} \frac{M_W^2}{(Q^2 + M_W^2)^2} \left[\left(1 - y - \frac{xyM^2}{S - M^2}\right) F_2^{cc}(x, Q^2) \right. \\ & \left. + y^2 x F_1^{cc}(x, Q^2) \pm (y - y^2/2) x F_3^{cc} \right], \end{aligned} \quad (154)$$

where the sign in front of F_3 is chosen positive for ν , and negative for $\bar{\nu}$ interactions. The parton cross section is given by

$$\frac{d\sigma}{dy} = \frac{G_F^2 \hat{s}}{\pi} \frac{M_W^2}{(Q^2 + M_W^2)^2} \begin{cases} 1 & \text{same helicities} \\ (1 - y)^2 & \text{opposite helicities} \end{cases}. \quad (155)$$

The neutrino is left handed, and charged current interactions involve left-handed quarks and their antiparticles, which are right-handed. Thus, when the neutrino scatters off a quarks, we get the constant y dependence; when it scatters off an antiquarks, we get the $(1 - y)^2$ dependence. Because of charge conservation (i.e., the neutrino goes into an electron, and thus gives one unit of positive charge to the quark) only negatively charged quarks or antiquarks can be involved. Thus, for example, for $\nu_\mu p \rightarrow \mu^- X$, neglecting for the moment a possible charm or bottom parton density in the proton we have

$$\frac{d\sigma}{dx dy} = \frac{G_F^2 S x}{\pi} \frac{M_W^2}{(Q^2 + M_W^2)^2} [(d(x, Q) + s(x, Q)) + (1 - y)^2 \bar{u}(x, Q)], \quad (156)$$

Here we introduce the notation

$$u(x, Q) = f_u^{(p)}(x, Q), \quad d(x, Q) = f_d^{(p)}(x, Q), \quad \text{etc.} \quad (157)$$

for the quark densities in the proton. The corresponding densities in the neutron are obtain from isospin symmetry

$$f_u^{(n)}(x, Q) = d(x, Q), \quad f_d^{(n)}(x, Q) = u(x, Q), \quad \text{etc.} \quad (158)$$

Thus

$$F_2^{\text{cc}}(x, Q) = 2xF_1^{\text{cc}}(x, Q) = 2x(d(x, Q) + s(x, Q) + \bar{u}(x, Q)) \quad (159)$$

$$F_3^{\text{cc}}(x, Q) = 2(d(x, Q) + s(x, Q) - \bar{u}(x, Q)) . \quad (160)$$

Similarly, for $\bar{\nu}p \rightarrow e^+ X$

$$F_2^{\text{cc}}(x, Q) = 2(u(x, Q) + s(x, Q) + \bar{d}(x, Q)) \quad (161)$$

$$F_3^{\text{cc}}(x, Q) = 2(-\bar{d}(x, Q) - \bar{s}(x, Q) + u(x, Q)) . \quad (162)$$

One gets the sum rule

$$\int_0^1 dx [F_3^{\bar{\nu}p}(x, Q) + F_3^{\nu p}(x, Q)] = \quad (163)$$

$$2 \int_0^1 dx [u(x, Q) - \bar{u}(x, Q) + d(x, Q) - \bar{d}(x, Q) + s(x, Q) - \bar{s}(x, Q) + \dots] = 6$$

which is called Gross–Llewellyn Smith sum rule, and expresses the fact that there are three quarks in a proton.

The phenomenology of DIS scattering is quite complex, and it is really impossible to review it in a satisfactory way in the context of these lectures. Several complications of experimental nature arise, and have to be dealt with properly. When extracting the structure functions F_1 or F_2 from data, it is usually assumed that F_1 and F_2 are related on the basis of the Callan–Gross relation

$$2xF_1(x, Q) = F_2(x, Q) \times \frac{1 + 4M^2x^2/Q^2}{1 + R(x, Q^2)} \quad (164)$$

where, if the Callan–Gross relation was satisfied exactly, one would have $R = 0$. Different experiments are performed on different targets. The structure functions for a nucleon embedded in a nucleus are distorted (EMC effect). Finally, the size of power suppressed effects (the so called *higher twist effects*) should be assessed, especially for low Q^2 experiments. In the present context I will not try to explain how to deal with these complications. I will instead try to give a rough idea of how the strong coupling constant and the parton densities are extracted from data.

The strong coupling constant can be extracted from DIS data using sum rules, like the Gross–Llewellyn Smith sum rule. Sum rules are in fact calculable in perturbative QCD, and the difference from their parton model value can be used to extract α_S . For the Gross–Llewellyn Smith sum rule

$$\int_0^1 dx [F_3^{\bar{\nu}p}(x, Q) + F_3^{\nu p}(x, Q)] = \quad (165)$$

$$6 \left[1 - \frac{\alpha_S}{\pi} \times \left(1 + 3.58 \frac{\alpha_S}{\pi} + 19 \left(\frac{\alpha_S}{\pi} \right)^2 \right) + \mathcal{O}(\alpha_S^4) - \Delta_{\text{HT}} \right] .$$

A recent CCFR determination [53] obtains

$$\alpha_S(1.73\text{GeV}) = 0.280_{-0.068}^{+0.070} \rightarrow \alpha_S(M_Z) = 0.114_{-0.012}^{+0.009} . \quad (166)$$

These determinations have the advantage that these quantities have been computed at very high order in perturbation theory [54], and thus the theoretical error are reduced. Since, however, they are performed at a rather low scale, some estimate of higher twist effects (the Δ_{HT}) are necessary.

Measurements	Q (GeV)	$\alpha_s(Q)$	$\alpha_s(m_Z)$	$\Delta\alpha_s(M_Z)$		Theory
				exp.	theor.	
DIS, GLS-sr	1.73	$0.280^{+0.070}_{-0.068}$	$0.114^{+0.009}_{-0.012}$	$+0.008$ -0.010	± 0.005	NNLO
DIS, ν ; $x F_3$	5	0.214 ± 0.021	0.118 ± 0.006	± 0.005	± 0.003	NNLO
DIS, e/μ ; F_2	2.96	0.252 ± 0.011	0.1172 ± 0.0024	± 0.0017	± 0.0017	NNLO

Table 5: Determinations of α_s from DIS data, taken from ref. [11]. GLS-sr stands for Gross-Llewellyn Smith sum rule.

The standard method to measure α_s in DIS is based upon the fact that the speed of evolution is proportional to α_s . The logarithmic derivative of the structure functions with respect to Q^2 are found therefore to have a strong sensitivity to the value of α_s . It is convenient to use a non-singlet structure function, in order to avoid uncertainties due to the poor knowledge of the gluon density. Thus, for example, one can use F_3 in neutrino scattering [55]. Alternatively, one can use structure functions at very large x . Since gluons are not valence particles, their density is quite soft, that is to say, concentrated at small values of x . In general, there is little gluon content in the hadrons for $x > 0.2$. Using this fact, one can also use muon data to determine α_s . A summary of α_s measurements from DIS is reported in table 5 from ref. [11]. The table deserves some comments. First of all, notice that all these determinations are performed at the NNLO level. This has become possible because of recent progress in the computation of moments of the splitting functions at order α_s^3 [42] [43]. This has allowed NNLO analysis of DIS data [56] [57]. The theoretical precision of these analysis matches that of R_{e+e-} . Comparing tables 5 and 2 we see a remarkable consistency in two different determinations, performed with completely different experimental setups, and at very different scales.

Neutrino scattering allows independent access to the quark and antiquark content of nucleons. It is generally carried out on heavy, approximately isosinglet targets. F_2 measurements in electromagnetic and charged current experiments give access to the combinations reported in the table 6. In principle,

F_2^{ep}/x	$\frac{4}{9}(u + \bar{u}) + \frac{1}{9}(d + \bar{d} + s + \bar{s})$
F_2^{ed}/x	$\frac{5}{9}(u + \bar{u} + d + \bar{d}) + \frac{2}{9}(s + \bar{s})$
$F_2^{\nu d}$	$2(u + \bar{u} + d + \bar{d} + 2s)$
$F_2^{\nu \bar{d}}$	$2(u + \bar{u} + d + \bar{d} + 2\bar{s})$
$F_3^{\nu d}$	$2(u - \bar{u} + d - \bar{d} + 2s)$
$F_3^{\nu \bar{d}}$	$2(u - \bar{u} + d - \bar{d} - 2\bar{s})$

Table 6: F_2 in various experimental configurations of interest.

strange and anti-strange content could be extracted from neutrino and antineutrino data on isosinglet targets. Or, assuming $s = \bar{s}$, we can use the combination $5/6 F_2^{\nu d} - 3 F_2^{ed} = x 2s$. In practice, the strange content is better constrained by looking at charm production in neutrino DIS. The corresponding signal, in the case of ν_μ scattering, is given by an unlike sign muon pair, one arising from the charged current scattering, and the other from charm decay.

Assuming that we have measured the strange content, we have access to the combinations $u + \bar{u}$, $d + \bar{d}$, $u + d$ and $\bar{u} + \bar{d}$. These quantities are not independent, since the sum of the first two equals the sum of the last two. Thus, one more input is needed. It was usually assumed that $\bar{u} = \bar{d}$. This assumption, supplemented with sum-rule restrictions, is however in conflict with data. In fact, using the flavour sum rules

$$\int dx [u(x, Q) - \bar{u}(x, Q)] = 2, \quad \int dx [d(x, Q) - \bar{d}(x, Q)] = 1, \quad , \quad (167)$$

we obtain

$$\int_0^1 \frac{dx}{x} \left[F_2^{(p)}(x, Q) - F_2^{(n)}(x, Q) \right]$$

$$\begin{aligned}
&= \int_0^1 dx \frac{1}{3} [u(x, Q) + \bar{u}(x, Q) - d(x, Q) - \bar{d}(x, Q)] \\
&= \frac{1}{3} + \frac{2}{3} \int_0^1 dx [\bar{u}(x, Q) - \bar{d}(x, Q)]
\end{aligned} \tag{168}$$

which, if $\bar{u} = \bar{d}$ gives the so called Gottfried sum rule. Experimental measurements of the Gottfried sum favour a negative contribution from the $\bar{u} - \bar{d}$ difference.

In order to access the $\bar{u} - \bar{d}$ difference as a function of x , one has to use different experiments. Drell-Yan pair production in proton-proton collisions is one example.

The x integrals of F_2 are proportional to a combination of the momentum fraction carried by the quarks and antiquarks. In particular, for example, the integral of $F_2^{\nu d}$ gives the total momentum fraction carried by quarks. This quantity is measured to be roughly 0.5. Thus, one expects that a large fraction of the hadron momentum is carried by gluons. This poses a valuable constraint on the gluon density $g(x, Q)$. From DIS, the traditional way to determine $g(x, Q)$ is from its influence upon the evolution of the singlet structure functions. This is viable at relatively small values of x , where the gluon density is not small. At large x , however, one needs to rely upon direct methods, since the gluon density is too small there to influence evolution. Direct photon production is one such process.

Today's tendency for structure function studies is to perform global fits to a large variety of data samples. One recent description of structure functions fits is given in ref. [58], where many aspects are discussed in detail. The result of these fits is shown in fig. 20.

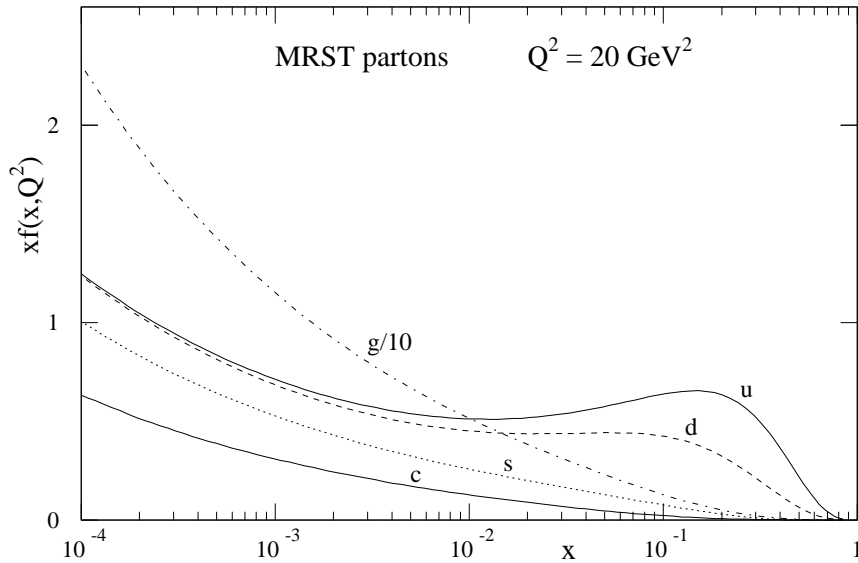


Fig. 20: Parton distributions by the MRST group.

7 QCD IN HADRONIC COLLISIONS

Perturbative QCD applications in hadronic collisions is extremely important, due to the impact it has had in the recent past for the discovery of new particles, and the impact it is going to have in the future for the search of new physics at the LHC. Thus there are essentially two main points of study for QCD at hadron colliders, and they clearly go hand in hand

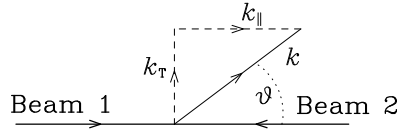
- QCD tests in hard processes

- Modeling of particle production processes (computing cross sections for top, higgs, etc.) and computing backgrounds.

Unlike the case of e^+e^- annihilation into hadrons, where each event is a hard process, in hadronic collisions most events are soft, even if the CM energy is very high. This is because, even if the colliding energy is high, the momentum transfer involved is not large. However, in the production of very massive particles, or in processes in which particles at high transverse momentum appear, hard momenta are actually present, and we can apply perturbative QCD. As a rule of thumb, when we try to compute a process using the parton model formula, and find that it is dominated by small momenta, this means that we can no longer neglect low energy details, like the off-shellness of the partons inside the colliding hadrons, or their mass. In this case, the process is controlled by long distance dynamics, and cannot be computed using perturbative QCD.

7.1 The kinematic variables for hadronic collisions

Given the two colliding hadron beams, one defines the kinematical variables of any outgoing particles according to the figure below



Thus, the transverse momentum k_{\perp} is the projection of the particle momentum into the transverse plane (the plane orthogonal to the collision axis). The azimuthal angle ϕ is defined with respect to the collision axis. One usually defines

$$\begin{aligned} \text{Transverse energy} &= E_T = \sin \theta E \\ \text{Transverse mass} &= m_T = \sqrt{k_{\perp}^2 + m^2} \\ \text{Rapidity} &= y = \frac{1}{2} \log \frac{k^0 + k^{\parallel}}{k^0 - k^{\parallel}} . \end{aligned}$$

The rapidity has the nice property that under a longitudinal boost it is simply translated by the boost angle: $y \rightarrow y + \log \gamma$. The transverse momentum, and thus the transverse mass, are simply invariant under longitudinal boosts. Thus, these variables are particularly useful to study hard processes, since in general the parton centre-of-mass system for the process will be translated with respect to the hadron CM. For particles of small mass, we have

$$y \approx \frac{1}{2} \log \frac{1 + \cos \theta}{1 - \cos \theta} = -\log \tan \frac{\theta}{2} , \quad (169)$$

and thus one defines the pseudorapidity

$$\eta = -\log \tan \frac{\theta}{2} . \quad (170)$$

It is useful to remember the following formula for the single particle phase space

$$\frac{d^3k}{2k^0(2\pi)^3} = \frac{1}{2(2\pi)^3} d^2k_{\perp} dy . \quad (171)$$

Thus, the single particle phase space is uniform in transverse momentum and rapidity.

7.2 Total cross section

The total hadronic cross section is in the range of several 10mb range, and it grows logarithmically with S . This is roughly the inverse of few hundred MeV squared, the characteristic scale of strong interactions. We cannot compute the total cross section using perturbative QCD. Phenomenological models based upon Regge theory are usually employed to describe the data.

If we attempted to estimate the total cross section using parton model concept, we would end up computing a parton production cross section integrated over the transverse momentum of the parton. On dimensional ground, this cross section would be divergent at small transverse momenta

$$\frac{d\sigma}{dk_T^2} \approx \frac{1}{k_T^4} \Rightarrow \sigma \approx \int \frac{dk_T^2}{k_T^4} \approx \frac{1}{\Lambda^2} \quad (172)$$

where the last step follows from the fact that some non-perturbative hadronic scale (for example, the off-shellness of the incoming partons) should act as a lower cutoff of the integral. Thus, perturbation theory, although incapable to give a definite answer, fails precisely at the point when the cross section becomes of the order of the total cross section.

7.3 Typical inelastic processes

The typical inelastic events in hadronic collisions are quite complex. Several hadrons are produced, the average charged multiplicity $\langle n_{\text{ch}} \rangle$ being typically of the order of 30 to 40 per event for $E_{\text{cm}} = 600$ to 1800 GeV, and it grows logarithmically with energy. Fluctuations in multiplicity are large, of the order of 100%, a typical feature of cascade processes. The transverse momentum distribution of the produced hadrons are characterized by an average transverse mass of the order of few hundred MeV, growing slowly with energy. The produced particles are distributed uniformly in rapidity, the distribution dropping smoothly to zero when approaching the maximum rapidity.

7.4 Looking for hard processes in hadronic collisions

Hadron collider physics is complicated by the fact that interesting events are rare with respect to the common low p_T inelastic events. This is immediately understood if we estimate the cross section for the production of a 100 GeV object to be of the order of 10^{-4} GeV^{-2} , while the typical inelastic cross section is of the order of 10^{-4} MeV^{-2} . We expect roughly 1 hard event every 10^6 soft ones, and this estimate ignores eventual suppression due to the coupling constant.

Furthermore, soft events may look like hard ones, because of fluctuations. Thus, with a multiplicity of 30 and an average p_T of few hundred MeV, the average total transverse energy can very well be of the order of tens of GeV. Fluctuations may favour occasionally even larger transverse momenta.

7.5 Jets at Hadron Colliders

Thus, unlike the e^+e^- case, where above a certain energy all events look like jet events, in hadronic collisions establishing the existence of jets has required the use of an appropriate trigger. In fact, one has to look only at events with a large total transverse energy. If the total transverse energy is larger than the typical value for a soft event, the events show the presence of jets. This was the method followed by the UA2 and UA1 experiments at the CERN $S\bar{p}pS$ collider, to establish the existence of jets in hadronic collisions. It was found there that requiring a transverse energy larger than 70 GeV, most events look like jet events.

The description of jet production in QCD follows the lines of the QCD-improved parton model. At the leading order level, in order to compute jet cross section we only need the Born cross sections for parton parton scattering, reported in table 7. The 2-jet inclusive cross section can then be obtained from

Process	$\frac{d\hat{\sigma}}{d\Phi_2}$
$qq' \rightarrow qq'$	$\frac{1}{2\hat{s}} \frac{4}{9} \frac{\hat{s}^2 + \hat{u}^2}{\hat{t}^2}$
$qq \rightarrow qq$	$\frac{1}{2} \frac{1}{2\hat{s}} \left[\frac{4}{9} \left(\frac{\hat{s}^2 + \hat{u}^2}{\hat{t}^2} + \frac{\hat{s}^2 + \hat{t}^2}{\hat{u}^2} \right) - \frac{8}{27} \frac{\hat{s}^2}{\hat{u}\hat{t}} \right]$
$q\bar{q} \rightarrow q'\bar{q}'$	$\frac{1}{2\hat{s}} \frac{4}{9} \frac{\hat{t}^2 + \hat{u}^2}{\hat{s}^2}$
$q\bar{q} \rightarrow q\bar{q}$	$\frac{1}{2\hat{s}} \left[\frac{4}{9} \left(\frac{\hat{s}^2 + \hat{u}^2}{\hat{t}^2} + \frac{\hat{t}^2 + \hat{u}^2}{\hat{s}^2} \right) - \frac{8}{27} \frac{\hat{u}^2}{\hat{s}\hat{t}} \right]$
$q\bar{q} \rightarrow gg$	$\frac{1}{2} \frac{1}{2\hat{s}} \left[\frac{32}{27} \frac{\hat{t}^2 + \hat{u}^2}{\hat{t}\hat{u}} - \frac{8}{3} \frac{\hat{t}^2 + \hat{u}^2}{\hat{s}^2} \right]$
$gg \rightarrow q\bar{q}$	$\frac{1}{2\hat{s}} \left[\frac{1}{6} \frac{\hat{t}^2 + \hat{u}^2}{\hat{t}\hat{u}} - \frac{3}{8} \frac{\hat{t}^2 + \hat{u}^2}{\hat{s}^2} \right]$
$gq \rightarrow gq$	$\frac{1}{2\hat{s}} \left[-\frac{4}{9} \frac{\hat{s}^2 + \hat{u}^2}{\hat{s}\hat{u}} + \frac{\hat{u}^2 + \hat{s}^2}{\hat{t}^2} \right]$
$gg \rightarrow gg$	$\frac{1}{2} \frac{1}{2\hat{s}} \frac{9}{2} \left(3 - \frac{\hat{t}\hat{u}}{\hat{s}^2} - \frac{\hat{s}\hat{u}}{\hat{t}^2} - \frac{\hat{s}\hat{t}}{\hat{u}^2} \right)$

Table 7: Cross sections for light parton scattering. The notation is $p_1 p_2 \rightarrow kl$, $\hat{s} = (p_1 + p_2)^2$, $\hat{t} = (p_1 - k)^2$, $\hat{u} = (p_1 - l)^2$.

the formula

$$d\sigma = \sum_{ijkl} dx_1 dx_2 f_i^{(H_1)}(x_1, \mu) f_j^{(H_2)}(x_2, \mu) \frac{d\hat{\sigma}_{ij \rightarrow k+l}}{d\Phi_2} d\Phi_2 \quad (173)$$

that has to be expressed in term of the rapidity and transverse momentum of the quarks (or jets), in order to make contact with physical reality. The two particle phase space is given by

$$d\Phi_2 = \frac{d^3k}{2k^0(2\pi)^3} 2\pi \delta((p_1 + p_2 - k)^2), \quad (174)$$

and using eq. (171), in the CM of the colliding partons, we get

$$d\Phi_2 = \frac{1}{2(2\pi)^2} d^2k_{\text{T}} dy 2 \delta(\hat{s} - 4(k^0)^2). \quad (175)$$

Here y is the rapidity of the produced parton in the parton CM frame. It is given by

$$y = \frac{y_1 - y_2}{2} \quad (176)$$

where y_1 and y_2 are the rapidities of the produced partons in the laboratory frame (in fact, in any frame). One also introduces

$$y_0 = \frac{y_1 + y_2}{2} = \frac{1}{2} \log \frac{x_1}{x_2}, \quad \tau = \frac{\hat{s}}{s} = x_1 x_2. \quad (177)$$

We have

$$dx_1 dx_2 = dy_0 d\tau. \quad (178)$$

We obtain

$$d\sigma = \sum_{ijkl} dy_0 \frac{1}{s} f_i^{(H_1)}(x_1, \mu) f_j^{(H_2)}(x_2, \mu) \frac{d\hat{\sigma}_{ij \rightarrow k+l}}{d\Phi_2} \frac{1}{2(2\pi)^2} 2 dy d^2k_{\text{T}} \quad (179)$$

which can also be written as

$$\frac{d\sigma}{dy_1 dy_2 d^2k_{\text{T}}} = \frac{1}{s 2(2\pi)^2} \sum_{ijkl} f_i^{(H_1)}(x_1, \mu) f_j^{(H_2)}(x_2, \mu) \frac{d\hat{\sigma}_{ij \rightarrow k+l}}{d\Phi_2}. \quad (180)$$

The variables x_1, x_2 can be obtained from y_1, y_2 and p_T from the equations

$$y_0 = \frac{y_1 + y_2}{2} \quad (181)$$

$$y = \frac{y_1 - y_2}{2} \quad (182)$$

$$x_T = \frac{2p_T}{\sqrt{s}} \quad (183)$$

$$x_1 = x_T e^{y_0} \cosh y \quad (184)$$

$$x_2 = x_T e^{-y_0} \cosh y. \quad (185)$$

For the partonic variables, we need $\hat{s} = s x_1 x_2$ and the scattering angle in the parton CM frame θ , since

$$t = -\frac{s}{2} (1 - \cos \theta), \quad u = -\frac{s}{2} (1 + \cos \theta). \quad (186)$$

Since we are neglecting parton masses, rapidity and pseudorapidity are identical, so that the equation

$$y = -\log \tan \frac{\theta}{2} \quad (187)$$

gives us θ .

The Born cross section formulae given here predict the production of back-to-back jets, with opposite transverse momenta. Details of the jet distributions depend upon the knowledge of the structure functions. However, it has been observed that, to a good approximation, scattering processes with gluon exchange in the t channel dominate, and that they are roughly proportional to each other. More specifically, the $gg \rightarrow gg$, $qg \rightarrow qg$ and $qq' \rightarrow qq'$ processes are in the ratio 3×3 , $3 \times 4/3$ and $4/3 \times 4/3$ respectively. This property is exact in the small angle scattering limit, but holds to a good approximation also at large angles. It can be obtained from Table 7, by keeping only the most enhanced terms when $t \rightarrow 0$ (and $u \rightarrow -s$) or when $u \rightarrow 0$ (and $t \rightarrow -s$). The processes with identical particles in the final state have an extra factor of $1/2$, but on the other hand have enhanced terms when $t \rightarrow 0$ and when $u \rightarrow 0$, while those with different particles in the final state have only the t singularity. Thus, at the end, the $qg \rightarrow qg$ process at small angle gives the same contribution as the $qq' \rightarrow qq'$ process.

Using this property the jet cross section simplifies

$$\frac{d\sigma}{dy_1 dy_2 d^2k_T} \approx \frac{1}{s 2(2\pi)^2} F^{(H_1)}(x_1, \mu) F^{(H_2)}(x_2, \mu) \frac{d\hat{\sigma}_{gg \rightarrow gg}}{d\Phi_2}. \quad (188)$$

with

$$F^{(H)}(x, \mu) = f_g^{(H)}(x, \mu) + \frac{4}{9} \sum_{i \neq g} f_i^{(H)}(x, \mu). \quad (189)$$

Equation (188) gives a definite prediction for the angular dependence of jet production. It can also be written, more explicitly, in terms of x_1, x_2 and $\cos \theta$, where θ is the scattering angle in the rest frame of the partons.

$$\frac{d\sigma}{dx_1 dx_2 d\cos \theta} = F^{(H_1)}(x_1, \mu) F^{(H_2)}(x_2, \mu) \frac{d\hat{\sigma}_{gg \rightarrow gg}}{d\cos \theta}. \quad (190)$$

Early studies of the UA1 and UA2 experiments have confirmed this behaviour [59].

Modern studies of jet physics at colliders are performed at the next-to-leading level in QCD. Calculations of jets cross sections at next-to-leading level have been available for quite a long time. Comparisons between data and calculation require agreement on a jet definition to be used. Such a definition should be of the Serman-Weinberg type, that is to say, it should be infrared and collinear safe. Several algorithms have been proposed to define jets. For the purpose of this lectures, it will be enough

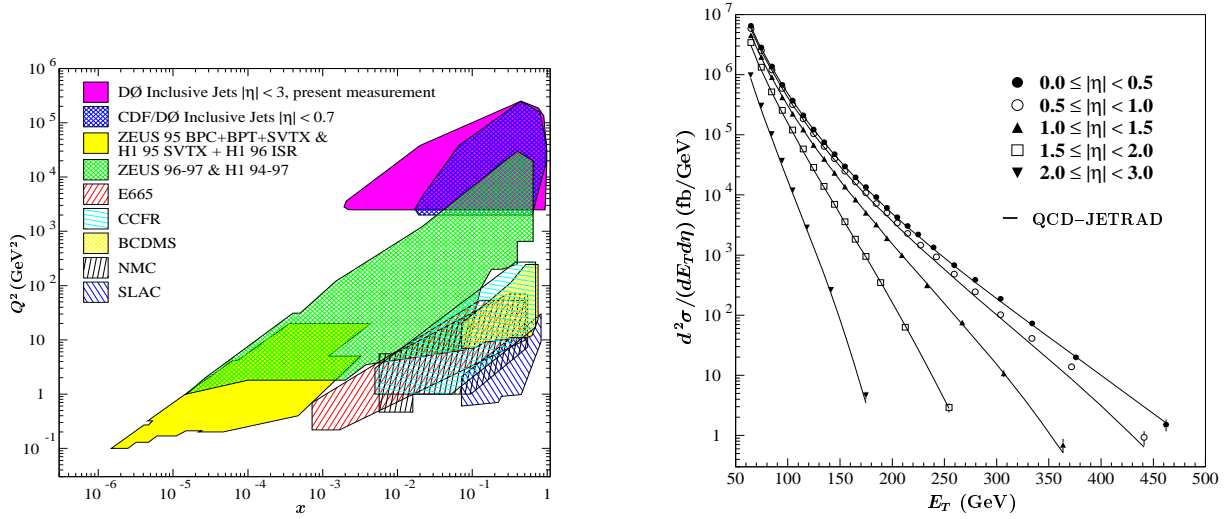


Fig. 21: The reach of the D0 inclusive jet analysis in the Q^2, x plane for the parton densities (left plot), and the Inclusive jet cross section as a function of E_T , in various rapidity bins, versus theoretical predictions (right plot).

to know that the most commonly used definitions make use of a circle of a given radius R in the $\phi\theta$ plane. The circle is moved in the plane until one finds a maximum of the transverse energy deposition inside the circle, and a jet of the given $\phi\eta$ and E_T values is associated with this point. The single inclusive distribution of jets found in this way, as a function of E_T , is compared with QCD NLO calculation.

An example of a recent measurement of the inclusive jet cross section is given in ref. [60], from the D0 collaboration. The inclusive jet cross section is measured in a wide rapidity range. By exploring the high rapidity region, one extends toward smaller values of x the region in the Q^2, x plane where parton densities are probed, as shown in the left plot of fig. 21. Jets are defined with the $\eta\phi$ cone algorithm, with a radius $R = 0.7$. The D0 results, together with a NLO QCD predictions, are shown in the right plot of fig. 21, showing a remarkable agreement. A more detailed comparison is shown in fig. 22, where the ratio (data – theory)/theory is plotted. Theoretical results are obtained with the program JETRAD [61], using the CTEQ4 [62] (left figure) and MRST [58] (right figure) structure functions. The shaded band corresponds to one standard deviation on the systematic error. One expects a comparable band for the theoretical error. The data is therefore in good agreement with theoretical predictions, showing a preference for the CTEQ4 sets.

Double-inclusive jet cross section (i.e., dijet production) studies at the NLO have also become to appear. CDF has performed a study of dijet production [63]. They look at the E_T of one central jet ($0.1 < \eta_1 < 0.7$), while the second jet lies in several different pseudorapidity intervals. In this way, the sensitivity to the parton densities at large x is enhanced. Qualitatively the theory gives a good description of data, as can be seen from fig 23. A closer look reveals problems at the quantitative level. Looking at the (data – theory)/theory ratio in the right plot of fig. 23, one sees that no parton density functions set fits the data satisfactorily, especially in the high E_T region.

We recall that jet studies at the Tevatron is at the frontier of our knowledge on the parton density functions. In fact, the single inclusive jet cross section [64] was found initially to be higher than QCD predictions. Further studies have shown that the excess over perturbative predictions is within the current flexibility in our parametrization of the parton density. It is however interesting to recall the value of studies of this kind. Since the QCD jets parton cross sections drop with the square of the transverse energy, a contact, 4-fermion interaction (similar, therefore, to weak interactions at low energies) would stick out at sufficiently high E_T . In particular, a 4-fermion interaction with a coupling constant G , would give rise to corrections to the cross section due to the interference terms with the standard QCD amplitude. On purely dimensional ground, such corrections would be of order G , and would thus overcome the

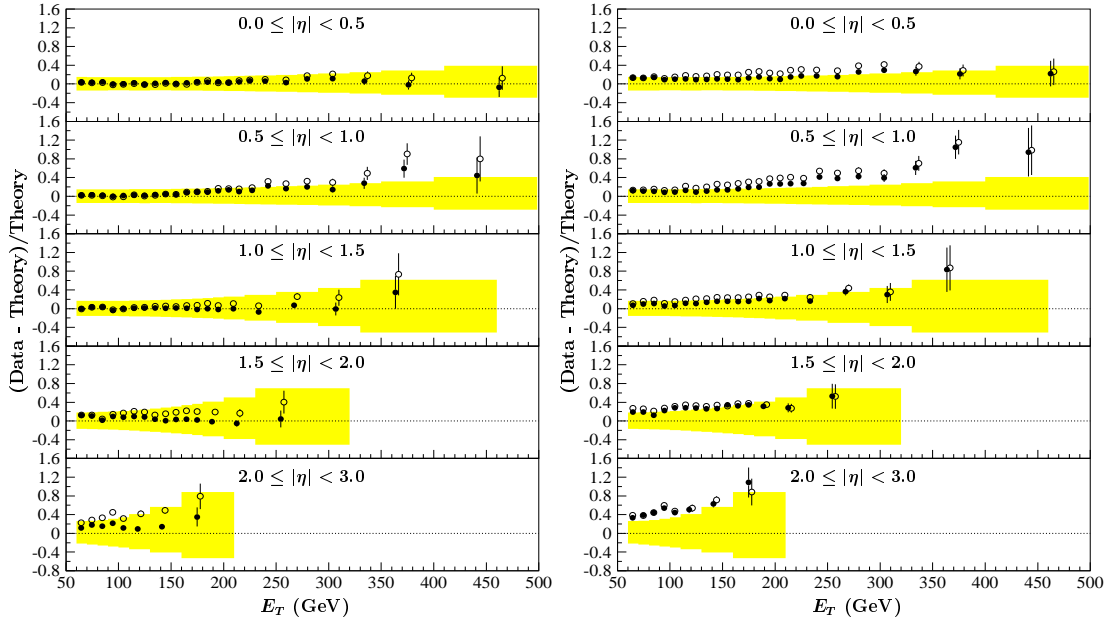


Fig. 22: Comparison of experimental measurements versus theoretical predictions: CTEQ4HJ (●) and CTEQ4M (○) (left figure); MRSTg† (●) and MRST (○) (right figure).

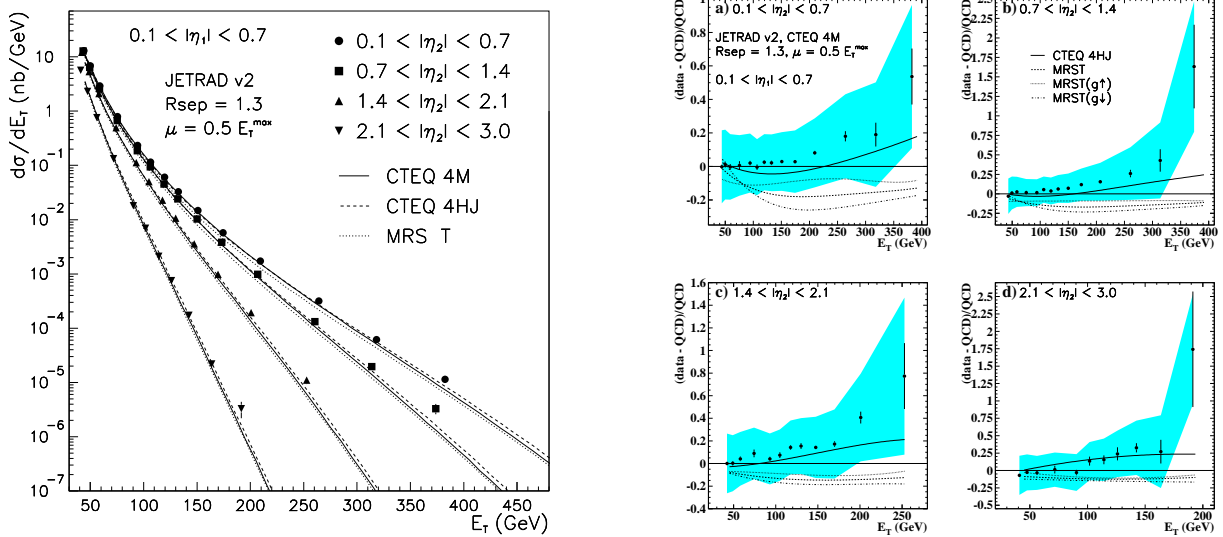


Fig. 23: Dijet cross sections from CDF; E_T distribution of one central jet, for the recoiling jet in different rapidity bins (left plot). A comparison if the dijet cross section to theoretical predictions is shown in the right plot. The error bars represent the statistical errors, while the shaded band represents the correlated systematic error.

strong interaction at some E_T . Thus, high transverse momentum jets studies can be used to put bounds on these kind of interactions. Sometimes, these bounds are called, somewhat improperly, compositeness bounds, since these kinds of 4-fermion interactions would naturally arise in composite models, due to the exchange of heavy composite particles.

7.6 Production of W , Z , and Drell-Yan pairs

From the point of view of perturbative QCD, the production of W , Z and Drell-Yan pairs are very similar processes. Some graphs contributing at leading, next-to-leading, and next-to-next-to-leading order in the strong coupling are shown in fig. 24. The corrections of order α_s have been given a long time ago in

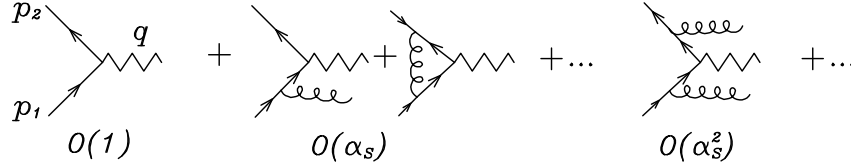


Fig. 24: Some graphs contributing to the Drell-Yan partonic cross section in QCD.

refs. [46, 47, 48], while the α_s^2 corrections have been computed in ref. [65, 66]. In order to get acquainted with the kinematics, let us compute the parton cross section for the production of a hypothetic massive vector meson. The amplitude is

$$\mathcal{M} = g \bar{v}(p_2) \gamma^\mu u(p_1) \quad (191)$$

and the partonic cross section is

$$\hat{\sigma} = \frac{1}{2\hat{s}} \frac{1}{4} \frac{1}{9} \int d\Phi_1 \sum_{\text{spin,col.}} |\mathcal{M}|^2, \quad (192)$$

where we have included a factor of $1/4$ for the initial spin average, $1/9$ for the initial colour average, $1/2\hat{s}$ to go from an amplitude squared to a cross section, and the one-particle phase space $d\Phi_1$. We have

$$\sum_{\text{spin,col.}} |\mathcal{M}|^2 = 3g^2 \text{Tr}[p_1 \gamma^\mu (-p_2) \gamma_\mu] = 12g^2 \hat{s}, \quad (193)$$

and

$$d\Phi_1 = \int \frac{d^3 q}{2q^0 (2\pi)^3} (2\pi)^4 \delta^4(p_1 + p_2 - q) = 2\pi \delta((p_1 + p_2)^2 - M_V^2) \quad (194)$$

so that at the end we get

$$\hat{\sigma} = \frac{4\pi^2}{3} \alpha \delta(\hat{s} - M_V^2), \quad (195)$$

with $\alpha = g^2/(4\pi)$. For W^\pm production, the coupling is $g = g_{\text{em}}/(\sqrt{2} \sin \theta_w)$, and only left handed quarks, and right handed antiquarks, can contribute. We get

$$\hat{\sigma}_W = \frac{\pi^2 \alpha_{\text{em}}}{3} \sin^{-2} \theta_w \delta(\hat{s} - M_W^2). \quad (196)$$

The full hadronic cross section is then

$$\begin{aligned} \sigma_W &= \int dx_1 dx_2 \left[\left(f_u^{(H_1)}(x_1) f_{\bar{d}}^{(H_2)}(x_2) + f_{\bar{d}}^{(H_1)}(x_1) f_u^{(H_2)}(x_2) \right) \cos^2 \theta_c + \dots \right] \\ &\times \frac{\pi^2 \alpha_{\text{em}}}{3 \sin^2 \theta_w} \delta(s x_1 x_2 - M_W^2) \end{aligned} \quad (197)$$

where one should not forget the appropriate CKM factors. A recent summary of W/Z cross section studies at the Tevatron is given in ref. [67].

From the measured ratio

$$R = \frac{\sigma_W \cdot B(W \rightarrow e\nu)}{\sigma_Z \cdot B(Z \rightarrow ee)}, \quad (198)$$

assuming that the ratio of the production cross section is accurately calculable, one can extract $B(W \rightarrow e\bar{\nu})$, and from it Γ_W ,

$$\Gamma_W = \frac{\Gamma(W \rightarrow e\bar{\nu})}{B(W \rightarrow e\bar{\nu})}, \quad (199)$$

assuming that the $e\nu$ width is correctly given by the standard model.

7.7 Heavy Flavour production

The production of heavy flavour in hadronic collisions involves strong interactions directly. Furthermore, in many cases of interest, the gluon densities play an important role. This is unlike the case of W/Z production, in which the main production mechanism does not involve the strong coupling constant. The search and discovery of the top quark has therefore relied on the whole machinery of perturbative QCD, factorization, and structure function physics.

The leading order process is proportional to the square of the strong coupling constant. Next-to-leading (order α_s^3) calculations for the production of heavy flavour production have been available for a long time. Furthermore, a large amount of work has been performed on resummation of effects enhanced in particular kinematic regions [68].

Since the top is very heavy, one expects that perturbative QCD should work well in this case. In fig. 25, taken from ref. [69], I show a comparison of theoretical predictions with the CDF and D0 measurements.

CDF data for bottom production has always shown a tendency to be higher than the theoretical predictions, as one can see from fig. 26, a problem that is being actively investigated. A large body of data is available for charm production. Theoretical calculations are, however, not very reliable in these cases, since the charm mass is only moderately heavy, and thus one cannot safely rely upon perturbation theory. Some results are shown in fig. 27. A recent review of heavy flavour production is given in [68].

8 CONCLUSIONS

In these lectures I have given an overview of perturbative QCD. As we have seen, the application of perturbation theory in strong interactions is not straightforward, unlike the case of weak interactions and electrodynamics. Nevertheless, a consistent and testable framework for the application of perturbation theory in strong interactions can be defined. This framework has been severely tested in e^+e^- , ep , and hadron-collision physics. It is perhaps true that, after the very extensive work performed at LEP1 and at the SLD, our confidence in perturbative QCD has become quite solid. Testing QCD remains however an important activity, due to the large number of applications that heavily depend upon it. The near future in particle physics research is in hadron collider physics, where the application of QCD is more complex. We should not forget, for example, that Higgs production at hadronic colliders is essentially a strong-interaction phenomenon, driven by gluons. Thus, it is important to build more confidence upon our ability to compute hadronic processes.

REFERENCES

- [1] M. E. Peskin, ., Lectures presented at the Summer School on Recent Developments in Quantum Field Theory and Statistical Mechanics, Les Houches, France, Aug 2 - Sep 10, 1982.

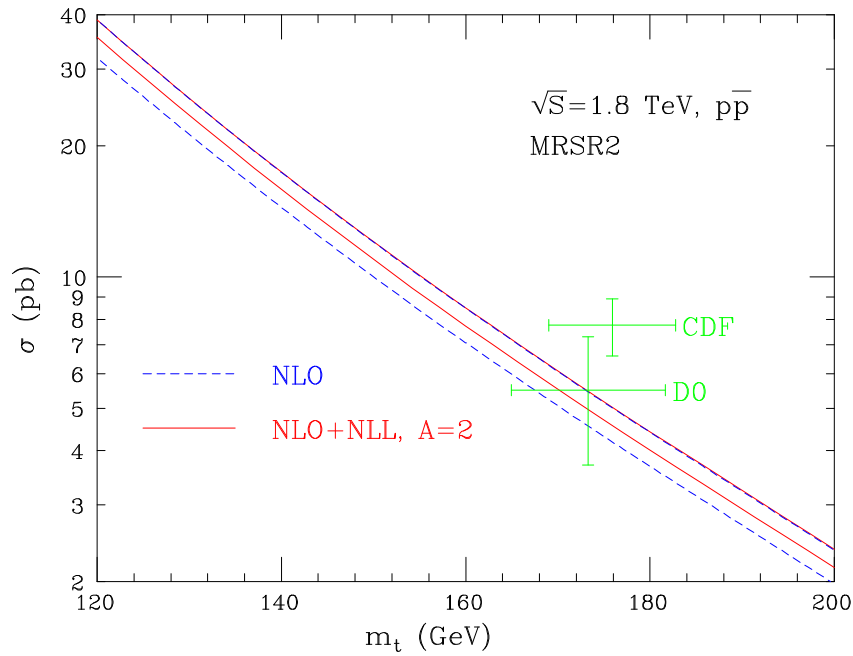


Fig. 25: Top production cross section versus the mass, compared to CDF and D0 measurements. The dashed band correspond to an $\mathcal{O}(\alpha_s^3)$ calculation, while the solid band includes also soft gluon resummation effects to the subleading logarithmic level.

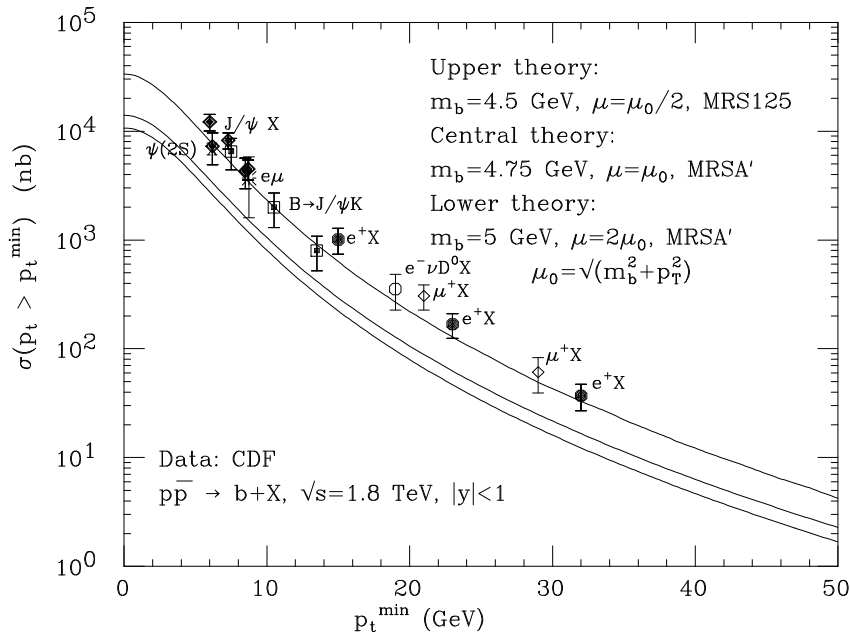


Fig. 26: Comparison of bottom cross section calculations versus CDF measurement.

- [2] H. Leutwyler, „ Lectures given at 30th Int. Universitätswochen für Kernphysik, Schladming, Austria, Feb 27 - Mar 8, 1991 and at Advanced Theoretical Study Inst. in Elementary Particle Physics, Boulder, CO, Jun 2-28, 1991.
- [3] G. Ecker, „ To be published in the proceedings of 4th Hellenic School on Elementary Particle Physics, Corfu, Greece, 2-20 Sep 1992 and Lectures given at Cargese Summer School on

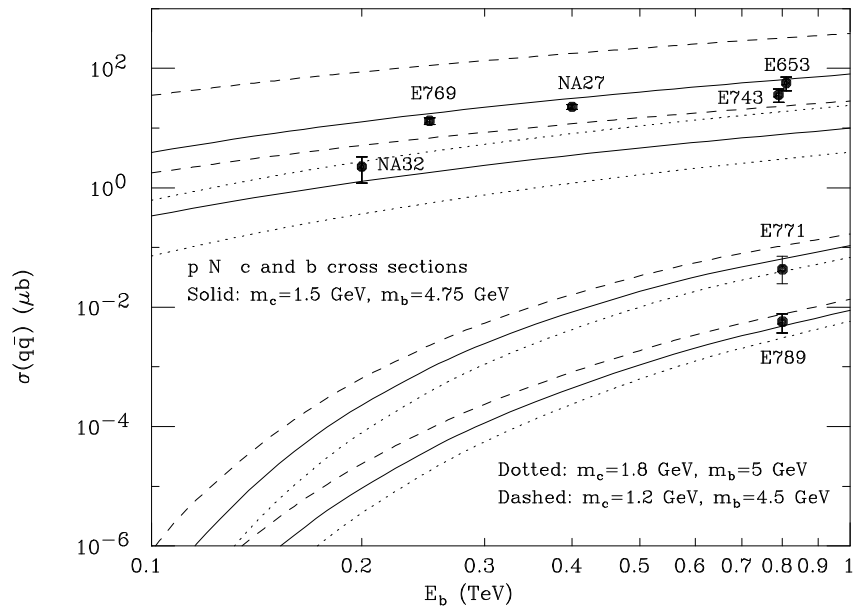


Fig. 27: Charm and bottom production cross sections in proton-proton collisions at fixed target energies

Quantitative Particle Physics, Cargese, 20 Jul-1 Aug 1992.

- [4] O. V. Tarasov, A. A. Vladimirov and A. Y. Zharkov, , *Phys. Lett.* **B93** (1980) 429–432.
- [5] T. van Ritbergen, J. A. M. Vermaseren and S. A. Larin, , *Phys. Lett.* **B400** (1997) 379–384, [hep-ph/9701390].
- [6] S. A. Larin, T. van Ritbergen and J. A. M. Vermaseren, , *Nucl. Phys.* **B438** (1995) 278–306, [hep-ph/9411260].
- [7] S. G. Gorishnii, A. L. Kataev and S. A. Larin, , *Phys. Lett.* **B212** (1988) 238–244.
- [8] S. G. Gorishnii, A. L. Kataev and S. A. Larin, , *Phys. Lett.* **B259** (1991) 144–150.
- [9] L. R. Surguladze and M. A. Samuel, , *Phys. Rev. Lett.* **66** (1991) 560–563.
- [10] E. Braaten, S. Narison and A. Pich, , *Nucl. Phys.* **B373** (1992) 581–612.
- [11] S. Bethke, , *J. Phys.* **G26** (2000) R27, [hep-ex/0004021].
- [12] T. Kinoshita, , *J. Math. Phys.* **3** (1962) 650–677.
- [13] T. D. Lee and M. Nauenberg, , *Phys. Rev.* **133** (1964) B1549–B1562.
- [14] G. Sterman and S. Weinberg, , *Phys. Rev. Lett.* **39** (1977) 1436.
- [15] T. Sjostrand, , *Comput. Phys. Commun.* **82** (1994) 74–90.
- [16] L. Lonnblad, , *Comput. Phys. Commun.* **71** (1992) 15–31.
- [17] G. Marchesini *et. al.*, , *Comput. Phys. Commun.* **67** (1992) 465–508.
- [18] **JADE** Collaboration, W. Bartel *et. al.*, , *Z. Phys.* **C33** (1986) 23.
- [19] R. K. Ellis, D. A. Ross and A. E. Terrano, , *Nucl. Phys.* **B178** (1981) 421.

- [20] K. Fabricius, I. Schmitt, G. Kramer and G. Schierholz, , *Zeit. Phys.* **C11** (1981) 315.
- [21] Z. Kunszt, P. Nason, G. Marchesini and B. R. Webber, , Proceedings of the 1989 LEP Physics Workshop, Geneva, Switzerland, Feb 20, 1989, published in *Lep Physics*, v.1:373-453 (QCD161:L39:1989).
- [22] G. Rodrigo, M. Bilenky and A. Santamaria, , *Nucl. Phys.* **B554** (1999) 257–297, [hep-ph/9905276].
- [23] A. Brandenburg and P. Uwer, , *Nucl. Phys.* **B515** (1998) 279–320, [hep-ph/9708350].
- [24] P. Nason and C. Oleari, , *Nucl. Phys.* **B521** (1998) 237–273, [hep-ph/9709360].
- [25] L. J. Dixon and A. Signer, , *Phys. Rev.* **D56** (1997) 4031–4038, [hep-ph/9706285].
- [26] Z. Nagy and Z. Trocsanyi, , *Phys. Rev. Lett.* **79** (1997) 3604–3607, [hep-ph/9707309].
- [27] J. M. Campbell, M. A. Cullen and E. W. N. Glover, , *Eur. Phys. J.* **C9** (1999) 245–265, [hep-ph/9809429].
- [28] S. Weinzierl and D. A. Kosower, , *Phys. Rev.* **D60** (1999) 054028, [hep-ph/9901277].
- [29] **OPAL** Collaboration, G. Abbiendi *et. al.*, , *Eur. Phys. J.* **C20** (2001) 601–615, [hep-ex/0101044].
- [30] **ALEPH** Collaboration, , ALEPH 2001-042, CONF 2001-026, July 5, 2001, contributed paper to this conference.
- [31] S. Catani, G. Turnock, B. R. Webber and L. Trentadue, , *Phys. Lett.* **B263** (1991) 491–497.
- [32] S. Catani, Y. L. Dokshitzer, M. Olsson, G. Turnock and B. R. Webber, , *Phys. Lett.* **B269** (1991) 432–438.
- [33] S. Catani, L. Trentadue, G. Turnock and B. R. Webber, , *Nucl. Phys.* **B407** (1993) 3–42.
- [34] Y. L. Dokshitzer, G. Marchesini and B. R. Webber, , *Nucl. Phys.* **B469** (1996) 93–142, [hep-ph/9512336].
- [35] P. A. Movilla Fernandez, S. Bethke, O. Biebel and S. Kluth, , hep-ex/0105059.
- [36] **DELPHI** Collaboration, P. Abreu *et. al.*, , *Z. Phys.* **C54** (1992) 55–74.
- [37] G. Altarelli and G. Parisi, , *Nucl. Phys.* **B126** (1977) 298.
- [38] G. Curci, W. Furmanski and R. Petronzio, , *Nucl. Phys.* **B175** (1980) 27.
- [39] W. Furmanski and R. Petronzio, , *Phys. Lett.* **B97** (1980) 437.
- [40] R. K. Ellis, H. Georgi, M. Machacek, H. D. Politzer and G. G. Ross, , *Phys. Lett.* **B78** (1978) 281.
- [41] W. L. van Neerven and A. Vogt, , *Phys. Lett.* **B490** (2000) 111–118, [hep-ph/0007362].
- [42] S. A. Larin, P. Nogueira, T. van Ritbergen and J. A. M. Vermaseren, , *Nucl. Phys.* **B492** (1997) 338–378, [hep-ph/9605317].
- [43] A. Retey and J. A. M. Vermaseren, , *Nucl. Phys.* **B604** (2001) 281–311, [hep-ph/0007294].
- [44] S. Moch, J. A. M. Vermaseren and M. Zhou, , hep-ph/0108033.

- [45] M. L. Mangano, P. Nason and G. Ridolfi, , *Nucl. Phys.* **B373** (1992) 295–345.
- [46] G. Altarelli, R. K. Ellis and G. Martinelli, , *Nucl. Phys.* **B143** (1978) 521.
- [47] G. Altarelli, R. K. Ellis and G. Martinelli, , *Nucl. Phys.* **B157** (1979) 461.
- [48] J. Kubar-Andre and F. E. Paige, , *Phys. Rev.* **D19** (1979) 221.
- [49] W. W. Lindsay, D. A. Ross and C. T. Sachrajda, , *Nucl. Phys.* **B222** (1983) 189.
- [50] W. W. Lindsay, D. A. Ross and C. T. Sachrajda, , *Nucl. Phys.* **B214** (1983) 61.
- [51] W. W. Lindsay, D. A. Ross and C. T. Sachrajda, , *Phys. Lett.* **B117** (1982) 105.
- [52] J. C. Collins, D. E. Soper and G. Sterman, , *Adv. Ser. Direct. High Energy Phys.* **5** (1989) 1–91.
- [53] J. H. Kim *et. al.*, , *Phys. Rev. Lett.* **81** (1998) 3595–3598,
[<http://arXiv.org/abs/hep-ex/9808015>].
- [54] S. A. Larin and J. A. M. Vermaseren, , *Phys. Lett.* **B259** (1991) 345–352.
- [55] **CCFR** Collaboration, W. G. Seligman *et. al.*, , <http://arXiv.org/abs/hep-ex/9701017>.
- [56] A. L. Kataev, G. Parente and A. V. Sidorov, , *Nucl. Phys.* **B573** (2000) 405–433,
[[hep-ph/9905310](http://arXiv.org/abs/hep-ph/9905310)].
- [57] J. Santiago and F. J. Yndurain, , *Nucl. Phys.* **B563** (1999) 45–62, [[hep-ph/9904344](http://arXiv.org/abs/hep-ph/9904344)].
- [58] A. D. Martin, R. G. Roberts, W. J. Stirling and R. S. Thorne, , *Eur. Phys. J.* **C4** (1998) 463–496,
[<http://arXiv.org/abs/hep-ph/9803445>].
- [59] R. K. Ellis and W. G. Scott, , *Adv. Ser. Direct. High Energy Phys.* **4** (1989) 131–175.
- [60] **D0** Collaboration, B. Abbott *et. al.*, , *Phys. Rev. Lett.* **86** (2001) 1707–1712, [[hep-ex/0011036](http://arXiv.org/abs/hep-ex/0011036)].
- [61] W. T. Giele, E. W. N. Glover and D. A. Kosower, , *Phys. Rev. Lett.* **73** (1994) 2019–2022,
[[hep-ph/9403347](http://arXiv.org/abs/hep-ph/9403347)].
- [62] H. L. Lai *et. al.*, , *Phys. Rev.* **D55** (1997) 1280–1296, [[hep-ph/9606399](http://arXiv.org/abs/hep-ph/9606399)].
- [63] **CDF** Collaboration, T. Affolder *et. al.*, , *Phys. Rev.* **D64** (2001) 012001, [[hep-ex/0012013](http://arXiv.org/abs/hep-ex/0012013)].
- [64] **CDF** Collaboration, T. Affolder *et. al.*, , *Phys. Rev.* **D64** (2001) 032001, [[hep-ph/0102074](http://arXiv.org/abs/hep-ph/0102074)].
- [65] R. Hamberg, W. L. van Neerven and T. Matsuura, , *Nucl. Phys.* **B359** (1991) 343–405.
- [66] W. L. van Neerven and E. B. Zijlstra, , *Nucl. Phys.* **B382** (1992) 11–62.
- [67] **CDF and D0** Collaboration, F. Lehner, , To be published in the proceedings of 4th Rencontres du Vietnam: International Conference on Physics at Extreme Energies (Particle Physics and Astrophysics), Hanoi, Vietnam, 19-25 Jul 2000.
- [68] S. Frixione, M. L. Mangano, P. Nason and G. Ridolfi, *Heavy Flavours II*, pp. 609 – 706. World Scientific, 1998. [hep-ph/9702287](http://arXiv.org/abs/hep-ph/9702287).
- [69] R. Bonciani, S. Catani, M. L. Mangano and P. Nason, , *Nucl. Phys.* **B529** (1998) 424–450,
[[hep-ph/9801375](http://arXiv.org/abs/hep-ph/9801375)].